Preliminary Propulsion System Design and Integration for a Box-Wing Aircraft Configuration

A Knowledge Based Engineering Approach

P. Proesmans

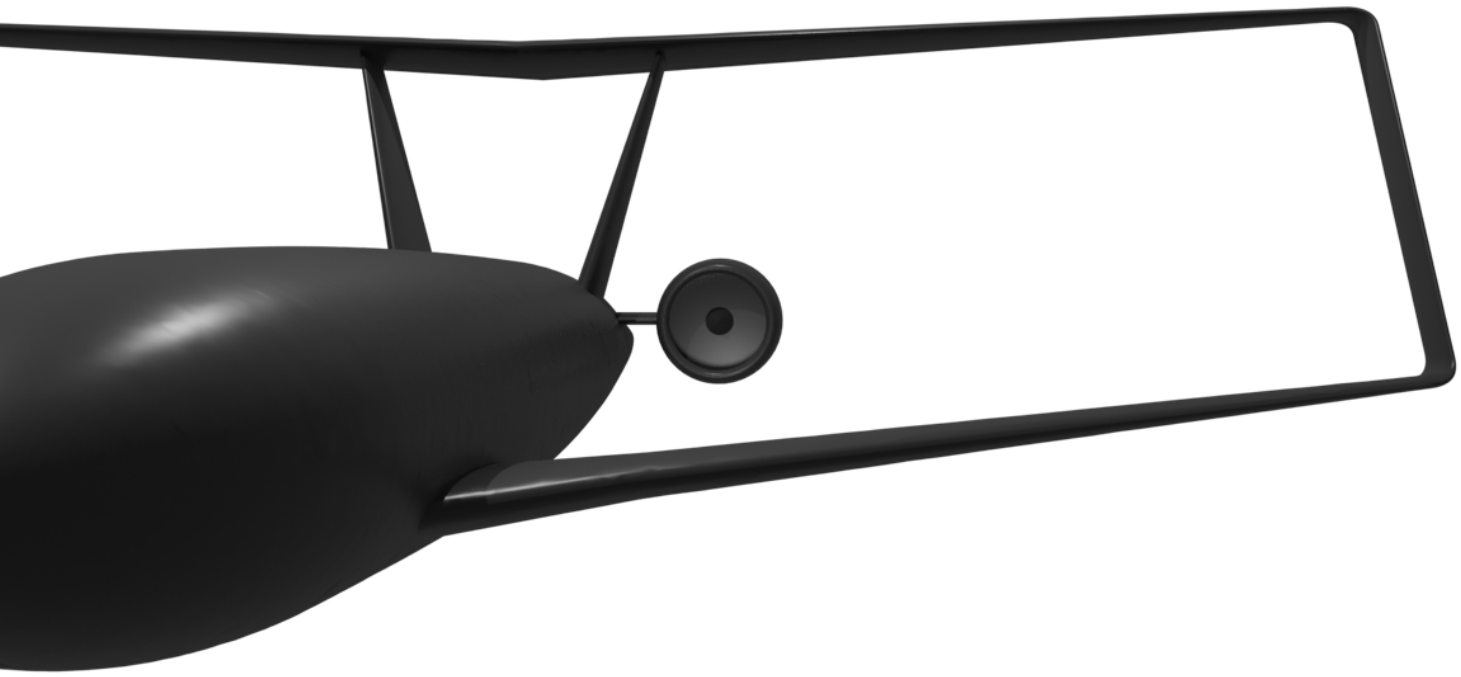

TU Delft Delft University of Technology

PARSIFAL PROJECT

Preliminary Propulsion System Design and Integration for a Box-Wing Aircraft Configuration

A Knowledge Based Engineering Approach

by

P. Proesmans

To obtain the degree of

Master of Science
in Aerospace Engineering

at the Delft University of Technology,

to be defended publicly on Friday December 13, 2019 at 13:30.

Student number:	4275063	
Project duration:	September 2018 – December 2019	
Thesis committee:	Prof.dr.ir. L.L.M. Veldhuis,	TU Delft, committee chair
	Dr.ir. G. La Rocca,	TU Delft, supervisor
	ir. R.J.M. Elmendorp,	TU Delft, supervisor
	Dr.ir. A.H. van Zuijlen,	TU Delft

TU Delft

An electronic version of this thesis is available at http://repository.tudelft.nl/.

Foreword

This report concludes the Master Thesis research focused on preliminary propulsion system design and integration. A Knowledge Based Engineering platform is employed to efficiently store engineering rules and to extend the aircraft geometry with tailored turbofan engines and nacelles. Although the new methods and tools are applied to the box-wing configuration examined by the PARSIFAL project, they are developed with a broader range of applications in mind. I hope that the newly created tools can be employed in future aircraft design projects to consider the propulsion discipline in early design stages.

I would like to thank my supervisors Gianfranco La Rocca and Reno Elmendorp for the interesting Thesis topic and the critical discussions. Special thanks to the PhD candidates Anne-Liza, Akshay and Carmine for helping me where necessary in building and testing the tools developed during this Thesis. I especially appreciate the fact that you were always prepared to help me with software related issues. I am convinced that one day I'll be able to merge repository branches without any help.

I am especially grateful to my parents, Linda and Jan, who have given me the opportunity to study in the Netherlands and Australia, while always having a five-star hotel-like service ready at home. Together with my entire family, they have always supported me, and I think a single Foreword cannot express how grateful I am. Finally, I would to thank my friends in Delft and abroad for their support and the entertaining evenings in the past years.

Pieter-Jan Proesmans
Delft, December 2019

Executive Summary

In several aircraft design projects the integration of a suitable propulsion system has proven to be an interesting challenge. Installing podded engines can have a driving impact on the aerodynamics, balance and overall flight characteristics of the aeroplane. The objective of the project described in this report is to employ a Knowledge Based Engineering approach towards aero engine design, installation on the aircraft and evaluation of this integration. In particular, the design and integration of the propulsion system for the box-wing aircraft studied by the PARSIFAL project is of interest.

To achieve this objective of engine design and integration, a new preliminary engine design tool, called GTpy, is introduced which allows to model various engine cycles through a component-based definition. The inputs and outputs are stored in the CPACS data model. This facilitates straightforward communication with other tools, such as the in-house Multi-Model Generator and PHALANX tools for example in multi-disciplinary design routines. GTpy is coupled to the Gas turbine Simulation Program to carry out off-design simulations of the engine system. Engineering rules are implemented to preliminary size the aero engine and to estimate the weight.

The engine geometry obtained through the sizing process is employed to automatically design a short-ducted nacelle. Once the engines are positioned with respect to the airframe, pylons are automatically lofted to connect the nacelles with the fuselage or wings. This completes the installation. Subsequently, the meshing strategy currently in place to carry out aerodynamic analyses with VSAERO is extended to include the nacelles and pylons. The rule-based design and geometry manipulations are facilitated by ParaPy, the Knowledge Based Engineering platform utilised by the Flight Performance and Propulsion department. The analysis with VSAERO is validated with the NASA Common Research Model. In addition, the Multi-Model generator can provide the necessary inputs for other work packages in the PARSIFAL project, such as noise prediction.

These applications are employed in three experiments to test their capabilities and suggest an engine and its integration for the PARSIFAL Prandtlplane. Firstly, the effect of the turbofan overall pressure ratio and bypass ratio on the thrust specific fuel consumption and installation weight is studied. It is observed that increasing both design variables affects the fuel consumption in a similar fashion, while the weight penalty is more sensitive to the bypass ratio. In the second experiment, the same engine is installed first on the rear wing, and subsequently on the aft fuselage section of the Prandtlplane to compare the effect on the aerodynamic forces and moments. Although both installations decrease the lift and increase the moment coefficient with respect to the aircraft without engines, these effects are enlarged for the on-wing installation since the flow around this wing is strongly disturbed.

In the third experiment, the effect of changing engine design variables on the aircraft aerodynamics is investigated. To do so, the routine GTpy - Multi-Model Generator - VSAERO is run for 42 combinations of overall pressure ratio and bypass ratio. Although the nacelle geometry is adapted accordingly, the results produced by VSAERO show irregularities. Hence, the effect of increasing nacelle diameter, for example, does not show a consistent trend in lift or moment coefficients. The behaviour of the drag coefficient is unrealistic, and therefore empirical correlations or higher fidelity aerodynamic analysis are advised to estimate the drag of the engine components instead. Although suggestions are made to eliminate the noise from the results, the root cause has not been identified. Therefore, care should be taken that uncertainties in the aerodynamic data do not propagate in other results when disciplines are added to this workflow of disciplines.

The observations from these tests are employed to recommend an engine design and installation on the current PARSIFAL configuration. A net thrust of 33 kN in cruise (h =11 000 m and Mach=0.79) and 180 kN in take-off (sea-level-static) is considered per engine in a two-engine configuration. The resulting aero engines feature a bypass ratio of 11, an overall pressure ratio of 57 and a fan pressure ratio and turbine inlet temperature adapted to minimise specific fuel consumption and installation weight. The nacelles are installed on the rear of the fuselage section such that the engine centre of gravity is aligned with the rear spars of the vertical tails. It is expected that this location minimises the interference with the complex wing system.

Contents

List of Figures

List of Tables

Nomenclature

Roman Symbols

$\dot{m}$	Mass Flow	[kg/s]
A	Cross-sectional Area	[m^2]
B_i	Bernstein Coefficient	[-]
C_D	Aircraft Total Drag Coefficient	[-]
C_P	Specific Heat at Constant Pressure	[J/(kgK)]
C_p	Pressure Coefficient	[-]
C_{D_0}	Zero Lift Drag Coefficient	[-]
C_{D_i}	Induced Drag Coefficient	[-]
C_L	Aircraft Lift Coefficient	[-]
C_M	Aircraft Pitching Moment Coefficient	[-]
D	Diameter	[m]
e	Span Efficiency Factor	[-]
e_0	Oswald Factor	[-]
FG	Gross Thrust	[N]
FN	Net Thrust	[N]
g	Constraint	[-]
h	Specific Enthalpy	[J/kg]
L	Length	[m]
P	Power	[W]
p	Pressure	[Pa]
R	Radius	[m]
T	Temperature	[K]
U	Radial Velocity	[m/s]
v	Axial Velocity	[m/s]
V_∞	Freestream Velocity	[m/s]

Greek Symbols

α	Angle of Attack	[deg]
ΔT_{ISA}	Difference in Ambient Temperature at Sea Level with Respect to Standard Value of 288.15 K	[K]
η_{comb}	Combustion Efficiency	[-]
η_{pol}	Polytropic Efficiency	[-]
λ	Load Coefficient	[-]

ϕ	Flow Coefficient or Velocity Potential	[-]
Π	Total Pressure Ratio	[-]
ψ	Head Coefficient	[-]
ρ	Density	[kg^3/m]
φ	Normalised x-abscissa	[-]
ξ	Normalised y-ordinate	[-]

Subscripts

i	Arbitrary Engine Station Number
amb	Ambient Value
cooling	Value for Cooling Flows
core	Value for the Core of a Turbofan
des	Value at Design Point
fuel	Value for Fuel Flow
h	Value Specified at Hub of Cross-section
id	Ideal, Fully Expanded Exhaust Flow
T	Total Value of Enthalpy, Temperature or Pressure
t	Value Specified at Tip of Cross-section
thr	Value at the Throat Section of a Nozzle

1 Introduction

The integration of the propulsion system is known to be one of the most interesting challenges in aircraft design [12]. Engine and aircraft manufacturers have to work closely together to, first of all, develop a power solution which is able to meet all operating requirements of the mission in an efficient manner, and secondly, to install this system on the aircraft without negatively affecting the flight characteristics. A fascinating case illustrating this puzzle is the recent redesign of the Boeing 737 aircraft, where a larger bypass ratio (BPR) was preferred to decrease the fuel consumption, leading to a larger engine, forcing the designers to reconsider the integration with the airframe [22].

Also for new aircraft designs, a suitable combination of engine cycle and installation has to be found. A specific research topic of interest is the propulsion system integration on the box-wing aircraft investigated in the PARSIFAL project [2]. This configuration, also known as a Prandtlplane or closed-wing aircraft, was initially considered the "Best Wing System" by Ludwig Prandtl in 1924 [23] and has always been an extraordinary idea in aerospace engineering because of its theoretically minimum induced drag. PARSIFAL reconsiders this configuration since it offers both aerodynamic and non-aerodynamic benefits and opportunities.

The specific aircraft studied in the PARSIFAL programme aims at offering the payload capacity of an Airbus A330 or Boeing 767, with the range and wingspan of an Airbus A320 or Boeing 737 type aircraft. This requires the selection of suitable turbofan engine which has to be tailored such that the top level requirements (TLR) of this aircraft can be met. Additionally, the challenges and opportunities of engine integration on a closed-wing design are to be explored.

To be able to capture the effects of the propulsion system on other disciplines such as aerodynamics, weight, flight mechanics and noise, it is advised to develop physics-based turbofan design and analysis tools which allow to rapidly, yet accurately react to changes in top level requirements. These methods must be independent of the aircraft configuration. Furthermore, they are required to operate in an automated manner such that they can be included in multi-disciplinary analysis and optimisation (MDAO) frameworks.

To achieve this, a Knowledge Based Engineering (KBE) approach is taken which facilitates the automation of rule-based sizing processes and other design steps, such as meshing, through the implementation of smart software applications to size components and manipulate geometries [24]. The in-house application featuring this technology is called the Multi-Model Generator (MMG), which will be elaborated upon in the following chapters. Overall, it is expected that the KBE technology saves time and brings more knowledge to earlier design stages. Especially the latter aspect is important in the study of new and unconventional aircraft configurations, where the technical risk level is high, tempering further developments.

Aim and Scope

The engine integration poses a challenging problem in the early design stages of a new configuration where a lot of options are to be explored, leading to possibly unexpected influences on the propulsion system design itself, or even the overall aircraft performance. For new aircraft architectures, the development risk is high for an aircraft manufacturer and it is desired to have as much knowledge about the new concept as early as possible, before proceeding with the costly detailed design. Especially in the case of a box-wing configuration,

limited research has been conducted to study the various engine integration opportunities with sufficient accuracy.

The current Thesis project aims at capturing the multi-disciplinary complexity of the propulsion integration problem in a set of computer-based tools, and to employ these tools to recommend the best propulsion system integration for the exotic Prandtlplane architecture proposed by the PARSIFAL project. The research objective is to *design, integrate and evaluate a turbofan-based propulsion system for a Prandtl-Plane configuration by modelling the system in a Knowledge Based Engineering application.*

A Knowledge Based Engineering approach is selected since it allows to address the multi-disciplinary nature of the problem at hand in a flexible and time efficient manner [13]. Although the final objective is the specific study of the Prandtlplane configuration, the goal of this Thesis is to set up the methods and tools as general as possible such that they can also be used for other configurations. In this way, the validation of the methods is facilitated by the availability of data for conventional aircraft, and a comparison can be made between box-wing configurations and conventional designs in the future.

In the current project, only podded turbofan engines are considered because of two reasons: firstly, to compare the performance of box-wing aircraft with existing configurations, it has been decided to study engine technology which is currently being employed or further developed. Secondly, introducing new engine or integration concepts would further increase the development risks, which have to be minimised for a market introduction in 2035. Nevertheless, restrictions to the location of the podded installations should be limited.

The following set of three main research questions are to be answered in order to achieve this research goal:

RQ1 What methods can be employed to evaluate the impact of the podded turbofan integration on the performance of the aircraft from aerodynamic, flight mechanics and acoustic perspectives?

RQ2 Considering the top level requirements provided by the PARSIFAL project for a medium sized commercial aircraft, what is the recommended integration employing turbofan engines?

RQ3 What is the effect of varying aircraft top level requirements on the integration of podded turbofan engines on a Prandtlplane configuration?

To guide the development of the tools and build a robust software application, the following supporting questions are posed:

- What knowledge and techniques have to be implemented to preliminary design and analyse an aero engine in an automatic manner to consider the propulsion discipline in multi-disciplinary analysis and, potentially, optimisation routines?
- Which parameterisation and design rules allow to automate the creation of the nacelle and pylon geometries?

Thesis Outline

This report starts with an overview of the existing research considering engine design and installation in general, and specifically for the box-wing aircraft architecture in Chapter 2. Subsequently, the role of the propulsion discipline in multi-disciplinary analysis and optimisation (MDAO) framework is discussed in Chapter 3. Furthermore, this chapter introduces the different software packages and their connections.

Subsequently, the developed methodology is elaborated upon in the three subsequent chapters, following the "define, integrate and analyse" steps as stated in the research objective. Chapter 4 describes the design of the aero engine, including the required procedures and the implemented engineering knowledge. In Chapter 5, the integration with the airframe and thus the geometrical design of the nacelles and pylons is treated. Chapter 6 considers the multi-disciplinary evaluation of the propulsion system, focusing on the aerodynamics and noise disciplines.

In Chapters 7 and 8 the newly developed tools are tested and employed to explore the design space for engine development and installation on the PARSIFAL box-wing aircraft. Finally, the most important conclusions are summarised in Chapter 9. This final chapter also suggests recommendations for further research and extensions of the methodology presented in this report.

2

Literature Review

The key objectives of the current research project are to develop an integrated system of tools which allow to define, integrate and evaluate the propulsion system, and to employ this system to propose a suitable integration for the PARSIFAL concept. These objectives are defined based on a review of the state-of-the-art work regarding engine design and installation. This chapter provides a summary of the completed literature review. Additionally, the use of advanced design methodologies in aircraft model development is studied.

This chapter is structured as follows: first of all, the motivation and goals of the PARSIFAL project are discussed. Secondly, previous research into the propulsion system integration on box-wing aircraft is examined. However, the idea is to develop methods which are independent of aircraft configuration, and hence the general approaches towards engine design and integration are studied in Sections 2.3 to 2.5. Subsequently, an overview is provided of advanced methodologies, such as Knowledge Based Engineering, considering the opportunities they offer to tackle multi-disciplinary design problems. Finally, the findings are summarised in Section 2.7.

2.1. PARSIFAL Project

The need for new research regarding propulsion system integration on a Prandtlplane follows from the European PARSIFAL project which was launched in May 2017 [1]. PARSIFAL, or "Prandtlplane ARchitecture for the Sustainable Improvement of Future AirpLanes", aims at introducing the innovative box-wing aircraft configuration to advance the future of aviation. In this section the background and goals of the project are summarised. The task to design and integrate the propulsion system is one of the main work packages, as discussed in Section 2.1.3.

2.1.1. Aircraft Market Position and Project Goals

The need for new aircraft designs, conventional or exotic, arises from the continuously expanding demand for air traffic. Market analysis conducted by Airbus [25] predicts that 92% of passenger aircraft (>100 passengers) to be introduced in the coming 20 years should be of the small and medium range categories. This trend is rather similar for all regions, amounting to approximately 33638 new aircraft in total in these classes. Simultaneously, national governments and international authorities are suggesting stricter rules and goals to reduce the negative impact of aviation on the environment while raising the standards for safety and reliability [26].

Although extraordinary aircraft designs may be able to meet all of the requirements arising from the above considerations, current airport facilities and operational procedures may be limiting the level of innovation. Many large airports can become congested in the following years, as indicated in Figure 2.1. Building new airports requires an enormous financial investment and time. Therefore, it would be beneficial if existing airports could handle more passengers with limited changes to the current facilities, such as runways and terminals.

[1] URL `https://cordis.europa.eu/project/rcn/209709_en.html` [Accessed on 27 September 2018]

Figure 2.1: Evaluation of airport capacity between 2017 and 2027 [1]

Taking all these aspect into consideration, PARSIFAL proposes to study the introduction of a box-wing aircraft, targeting short to medium range flights with an increased number of passengers. In fact, it is currently expected that, due to the particularities of the closed-wing design discussed in Section 2.1.2, the PARSIFAL aircraft could enter a new market segment by offering a higher payload capacity for a given range compared to current competitors, as indicated in Figure 2.2.

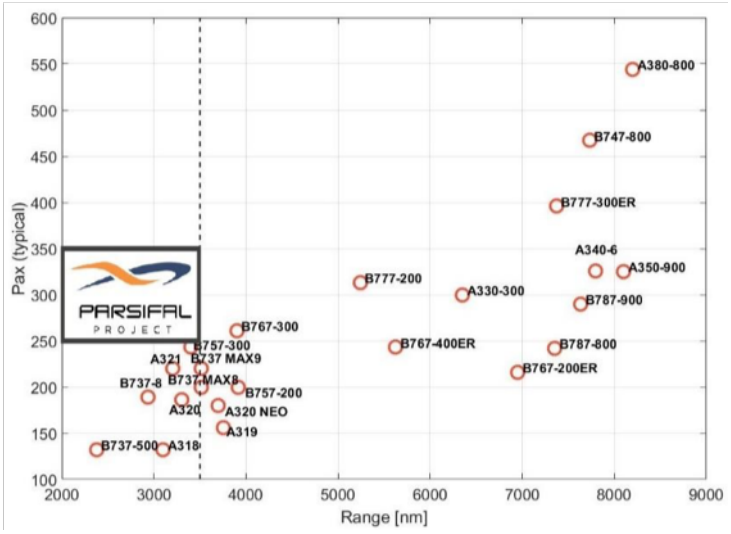

Figure 2.2: PARSIFAL market positioning [2]

From the preceding considerations, the PARSIFAL project defined the top level aircraft requirements for a new aircraft on which the research focuses. These TLR's are summarised in Table 2.1 [2]. The underlying idea is to develop a plane which has the same operational range, span and ground handling characteristics as an Airbus A320 or Boeing 737, while offering the payload capacity of an Airbus A330 or Boeing 767. Although limiting the total fuel consumption to that of an Airbus A320 or Boeing 737 is unrealistic at this stage, an improvement in fuel consumption and payload, and thus payload-range efficiency (PRE) is targeted [2]. An additional requirement is to reduce the turn-around time at airports compared to aircraft with similar payload potential.

[2] URL `https://www.schiphol.nl/en/you-and-schiphol/page/five-questions-about-aircraft/` [Accessed on 23 November 2019]

Table 2.1: PARSIFAL top level aircraft requirements [2] compared to those of the Airbus A320neo and Airbus A330-300 [27, 28]

Requirement	**PARSIFAL**	**Airbus A320**	**Airbus A330**
Number of passengers	250 to 330	150 to 180	250 to 290
Range [km]	≤ 4000	6300	11750
Maximum Take-Off Weight [kg]	7000 to 136000	79000	242000
Cruise Mach number	≥ 0.78	0.78	0.82
Initial cruise altitude [m]	11000	11280	11280
Max. operating altitude [m]	11735	12130	13137
ICAO aerodrome reference code	4C	4C	4E
Wake turbulence category	M	M	H

Although the box-wing configuration is expected to be well suited for this set of TLR's, as discussed in the next section, the configuration may or may not offer an improved performance for different mission types. This is why a main objective of the PARSIFAL project is to develop the design and analysis tools necessary to explore box-wing aircraft of various sizes and different sets of TLR's. Having such methods in place allows to quickly evaluate different designs with appropriate fidelity such that their performance can be compared to competitors or other non-conventional layouts. This objective closely relates to the vision laid out in Flightpath 2050 where *"Multi-disciplinary design and development tools are used routinely and co-operatively to support a high level of integrated system design."* [26]

2.1.2. Prandtlplane Benefits and Conceptual Design

Considering the above requirements, the PARSIFAL programme opted to research the Prandtlplane concept further since it is expected to offer several aerodynamic, structural and operational benefits when compared to a tube-and-wing design. In this section these particularities of the closed-wing concept are highlighted and coupled to the conceptual PARSIFAL design.

Aerodynamics Already in 1924, Ludwig Prandtl identified the closed-wing configuration, i.e. two staggered wings connected by vertical sections at the wing tips, as the "Best Wing System". The architecture was given this name since it theoretically minimises the lift induced drag generated by the main lifting surfaces, i.e. the wing(s) [23], for a given wingspan and lift. The box-wing configuration aims at minimising the lift induced drag coefficient, C_{D_i}. This drag component is created by the vorticity shed behind a three-dimensional lifting system, such as a wing. This vorticity is typically shed at the tips of a wing due to difference in pressure between the lower and upper surfaces of the wing. As flows escapes from the pressure side of the wing over the wing tip, a tip vortex is created. These vortices, characterised by cross-flow (downwash and a spanwise components), extract kinetic energy from the freestream flow, resulting in drag.

This drag contribution can be represented in simplified form of an aircraft drag polar, formulated in Equations (2.1) and (2.2). While the first formulation assumes that only one drag component is dependent on the lift coefficient, the latter considers two terms being dependent on the lift. In Equation (2.1) it is assumed that the vortex drag is the only component dependent on the lift coefficient, while all other elements are captured by C_{D_0}. In Equation (2.1), the $C_{D_2} \cdot {C_L}^2$ term represents the profile drag component which is susceptible to changes in lift coefficient. In either formulation, the box-wing architecture focuses on reducing the last term.

$$C_D = C_{D_0} + C_{D_i} = C_{D_0} + \frac{{C_L}^2}{\pi \cdot A \cdot e_0} \tag{2.1}$$

$$C_D = C_{D_0} + C_{D_2} \cdot {C_L}^2 + \frac{{C_L}^2}{\pi \cdot A \cdot e} \tag{2.2}$$

Assuming the lift coefficient C_L is fixed for a given flight condition and weight, the induced drag term can be minimised by increasing the aspect ratio A, and/or the Oswald factor e_0 in Equation (2.1) or the span efficiency factor e in Equation (2.2). The aspect ratio can be altered by changing the ratio between the span and average chord of the wing planform. Although they are not equal, the Oswald and span efficiency factors are related and vary according to the overall shape and local twist of the wing system.

Both factors, e_0 and e, are influenced if a non-planar wing planform is selected. In Figure 2.3 the span efficiency factors for different non-planar wing layouts are gathered. From the figure it can be seen that the box-wing concept has the highest span efficiency factor, effectively minimising the induced drag.

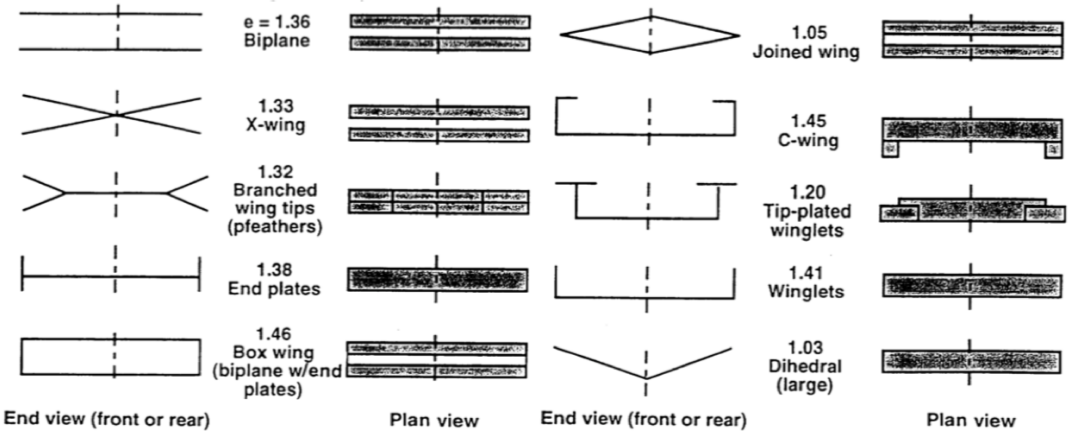

Figure 2.3: Span efficiency factors for non-planar wing planforms, adapted from [3]

Even if the lift distributions on both wings are not equal, the induced drag is minimised by this configuration as long as the lift distribution over the vertical elements is adapted accordingly [29]. Furthermore, Munk's theorem [23] ensures that longitudinal stagger or sweep angles do not affect the Best Wing System solution, and allow to alter the wing planform for high Mach regimes, such as transonic flight.

Lowering the induced drag reduces the overall drag assuming other drag components are not affected, improving the lift-to-drag coefficient (L/D) in various flight phases, and decreasing the thrust required. The latter in turn has a positive effect on the fuel consumption, emissions and overall noise level, especially in take-off and landing [30]. Alternatively, this wing system allows to carry more payload for a given span, which is the objective of the aircraft suggested in the PARSIFAL project. However, this is valid under the assumption that other drag components, such as friction drag, do not increase.

Flight Mechanics and Control In addition to the aerodynamic potential, the configuration offers several advantages and opportunities in the field of flight mechanics. The two relatively large wings, producing both positive lift, provide pitch control through pure couple, which is more efficient and safer than a regular configuration with one large wing and horizontal stabiliser [30]. Additionally, direct lift control (DLC) measures can be applied and implemented in the control system. This would allow to make subtle, yet effective adjustment to the lift produced by the wings without having to change the angle of attack through pitch control. DLC can potentially improve manoeuvring precision during landings and allow for more effective reaction to gust loads.

The two large wings and the vertical connecting elements expand the design space for high lift devices and control surfaces. Possibly, the functions of these movable surfaces can be combined in a single system, similar to flaperons or elevons. However, a clear advantage is that control systems, such as ailerons, can be placed on both wings increasing the overall redundancy and boost flight safety. This large design freedom allows to enhance passenger comfort and to improve stall behaviour.

Structures Since both wings produce positive lift, the fuselage is effectively "supported" at two points, closer to the nose and tail. This situation alleviates the loading throughout the fuselage, allowing to save structural weight in the fuselage. Nonetheless this weight reduction has to be compared to the possible weight increase due to the complicated wing system.

Operations and Handling Keeping the requirements from Section 2.1.1 in mind, the above benefits allow to carry more payload for a given wingspan. Hence, the Prandtlplane with the payload of a Boeing 767 or Airbus A330 can make use of gates which are too small for these two conventional aircraft. Thus, smaller airports all over the world can expand their passenger and freight capacity without having to adapt (all) facilities for larger aircraft.

The current PARSIFAL design of the Prandtlplane features a wide cabin with a twin aisle configuration and three large doors on each side. This arrangement allows to reduce boarding and deboarding times at airports and, as a result, decrease the turn-around-time. An operator might opt to plan more flights with a single aircraft for example. Also airports can make use of this reduced ground time. Moreover, since the roots of the wings are positioned at the front of the fuselage and on the tail, one continuous cargo deck can be implemented. This further reduces the time required for ground operations since the luggage or other freight can simultaneously be loaded from the front and unloaded from the back, or vice versa.

One significant benefit of this configuration is that all these advantages can be achieved with no changes to the conventional cabin services or emergency exit procedures. Hence, it is expected that the configuration can help tackle the challenges of the near future aviation while the flying experience from the operator or passenger perspective does not have to change.

2.1.3. Propulsion System Design

The need for new research follows directly from the objectives stated in Work Package 7 "Analysis and design of the propulsion system" which is coordinated by Delft University of Technology. This Work Package consists of two objectives:

WP7.1 Definition of a propulsion system, based on state-of-the-art technologies:

- Determination of number and position of engines on airframe
- Engine sizing and steady state performance analysis at all relevant flight conditions and throttle setting
- Engine-airframe integration studies
- Fuel system design (wing/fuselage tanks placement and fuel transfer effect on weight and balance)

WP7.2 Feasibility of Very Large Bypass Ratio turbofan engines installation:

- Preliminary design of turbofan engines with very large bypass ratio
- Study on the potential aircraft performance benefits of very large bypass ratio turbofan engines compared to conventional turbofan engines

It is mentioned in the first objective that the propulsion system has to employ state-of-the-art technologies. Therefore, in the new research project, only podded turbofan engines are considered. This includes modifications to the standard engine architecture, such as a geared fan or a bleedless configuration. However, ducted fans, open rotor or propeller concepts are out of scope. Also special integration options, such as boundary layer ingestion, are outside the scope of this research.

Although this somehow limits the level of innovation introduced in the PARSIFAL Prandtlplane, the current technology standard is selected for two reasons. Firstly, using state-of-the-art turbofan technologies allows to compare the box-wing aircraft directly to conventional configurations with the same top level requirements and propulsion systems. Secondly, since the expected introduction is already in 2035, the technical development risk has to be minimised. This is ensured by considering current or near-future propulsion technologies.

Nevertheless, the box-wing concept offers more engine installation opportunities because of the configuration with a low wing in the front and a high aft wing. Especially this high wing allows to consider ultra high bypass engines because the ground clearance constraint does not necessarily limit the fan diameter, while this is the case in conventional, underwing installations. Hence, the rules employed to create the nacelle and pylon geometries should be general enough such that the engines can be installed (almost) anywhere on the aircraft. This requirement is taken into account in Chapter 5.

2.2. Engine Integration on Box-Wing Aircraft

A first step towards the definition of the new research is the investigation of engine integration examples in other box-wing research projects. This section gives an overview of similar studies with the aim to find the rationale behind engine placement on a Prandtlplane and to explore the challenges of installing engines on this configuration. The propulsion integration on a 300-passenger Prandtlplane was investigated in detail by de Klerk at Delft University of Technology in 2010. This work is reviewed in Section 2.2.1. Alternative box-wing designs are discussed in Section 2.2.2.

2.2.1. Propulsion System Design and Integration on a 300-Passenger Prandtlplane

In 2010 de Klerk studied the design and integration of a propulsion system on a Prandtlplane [4]. His research focused on a Prandtlplane for 300 passengers with a range of 6000 nautical miles (11 000 km). This section provides a summary of the research process followed by de Klerk and highlights the differences with the new research presented in this report. A significant amount of aircraft design had already been performed prior to his work, so the geometry of the aircraft without engines was fixed. The research methodology employed by de Klerk can be summarised as follows:

1. Select the ideal engine type, the number of engines and their location
2. Optimise the engine cycle and dimensions, which includes estimating the weight
3. Analyse the aerodynamics of the aircraft-engine combination
4. Evaluate the flight mechanics and mission performance of the complete configuration

In the following paragraphs these steps are discussed to highlight the findings and methods which can be transferred to the new research, as well as to identify possible differences.

Propulsion Selection and Positioning Firstly several engine types, cycles and installations are compared, ranging from the standard turbofan to more exotic cycles such as intercooled recuperated engines and installations such as distributed propulsion. To select the appropriate combination a trade-off is made based on fuel burn, emissions, noise, Prandtlplane compatibility, design risk, and acquisition and maintenance costs. The best concept was shown to be a bleedless turbofan architecture, also known as a More Electric Engine (MEE).

The geared turbofan was suggested as another viable option once it had been further developed. In 2016, the first Pratt & Whitney PW1100G geared turbofan entered into service [31] and further developments are taking place, for example, in the Rolls-Royce UltraFan project [3]. Hence the geared turbofan can potentially be reconsidered in a trade-off with a reduced risk factor, especially when VHBPR are studied.

Based on the trend seen on the latest long-haul aircraft such as the Boeing 787 and the Airbus A350, the number of engines is set to two since this allows to install larger, more efficient engines while the number of parts is minimised. The same general considerations apply to the new research, albeit that depending on the top level requirements more engines might be required. Eight possible engine locations are compared, as presented in Figure 2.4. All positions are evaluated taking into account the aspects included in Table 2.2. Based on this trade-off, de Klerk concludes that positioning the engines at the rear of the fuselage, configuration C in Figure 2.4, is the best option.

Table 2.2: Engine position aspects considered by de Klerk [4]

Required landing gear length	Structural weight	Centre of gravity location
Aerodynamic interference	Pitching moment	Accessibility
One engine out moment	Engine burst safety	Cabin noise vibrations
Local structural stiffness	Engine inlet air quality	Noise shielding to ground

[3] URL `https://www.rolls-royce.com/products-and-services/civil-aerospace/future-products.aspx` [Accessed on 21 September 2018]

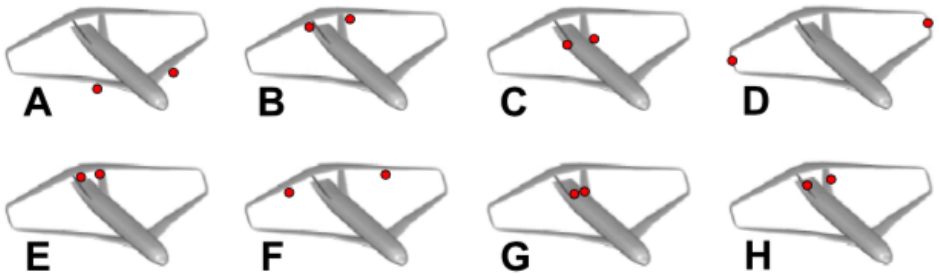

Figure 2.4: Possible engine positions suggested by de Klerk [4]

Engine Sizing and Cycle Optimisation With the engine type selected, the sizing of the aero engine is initiated by deriving the propulsion requirements from several mission phases such as take-off, climb and cruise. Especially the condition where one engine is inoperative during take-off appeared to be critical. To design, optimise and analyse the turbofan engine, de Klerk employed the Gas Turbine Simulation (GTS) tool developed by de Kok [32]. This MATLAB based tool can analyse the performance of an aero engine and also includes an empirical weight estimation method. Although GTS allows to design turbofan of different sizes, the architecture is fixed to a three-spool configuration.

Aerodynamic Design and Analysis The aerodynamic analysis of the aircraft without engine was already considered before de Klerk's research. In de Klerk's study, the nacelles and pylons are added to the airframe and the complete configuration is analysed with the linear potential flow solver VSAERO. To model the engines in VSAERO, an axisymmetric nacelle geometry is developed by considering the inlet shape of the JT9D engine which was already modelled in VSAERO, and the approximate outer shape of the Rolls-Royce Trent 1000. Since the basic engine dimensions (diameter and length) are provided by GTS, assumptions are made towards the dimensions of the nacelle: the maximum nacelle diameter is assumed to be 5% larger than the fan diameter, and the nacelle length is set to 110% of the bare engine length. As discussed further in Section 2.4, a more flexible definition of the nacelle is preferred which suits the aero engine geometry.

Flight Mechanics Analysis Using the performance results from GTS and VSAERO, de Klerk evaluates the flight dynamics of the complete aircraft throughout its mission profile using the multi-fidelity Flight Mechanics Model, currently known as PHALANX. It was found that installing the engines on the rear section of the fuselage had a positive effect on the static stability and the phugoid dynamic behaviour. Only the Dutch roll and one engine inoperative conditions posed problems which would require a redesign of the vertical tail surface and rudder.

2.2.2. Alternative Box-Wing Designs

De Klerk defined the engine integration for a specific case, being a 300-passenger Prandtlplane. To create a more complete picture, the engine installation for different cases is studied. This section therefore provides an overview of different box-wing research projects which considered the engine integration.

In 1974 the Lockheed-Georgia Company, as a contractor for NACA, completed a preliminary design study of a transonic box-wing aircraft for 400 passengers and a range of 5500 nautical miles [5]. The concept is shown in Figure 2.5. Here it is decided to install the jet engines with a bypass ratio of 5 under the forward wing at semi-span points and at the tips. The engine location is partially driven by the requirement to have a smooth area distribution to minimise wave drag. However, it is found that this positioning is not optimal from a flutter perspective and thus engines mounted on the fuselage are considered. Nevertheless, the low wave drag requirement appears to be critical due to the cruise Mach number of 0.95.

Another investigation into the box-wing concept was conducted by Schiktanz and Scholz in 2011 [6]. For a reference mission with a payload of 20 tons (approximately 150 passengers) and a range of 1550 NM, they opted for a propulsion system based on turbofan or turbojet engines (the exact type is not mentioned) located close to the centre of the fuselage, as displayed in Figures 2.6 and 2.7. According to Schiktanz and Scholz, the

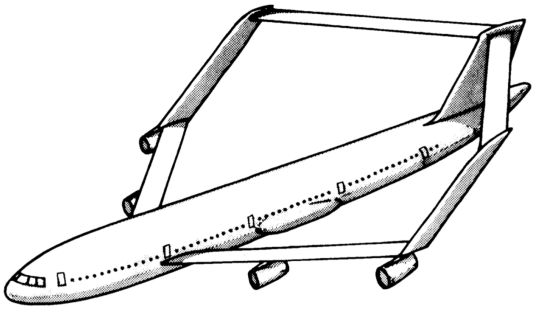

Figure 2.5: Box-wing concept studied by Lockheed-Georgia Company in 1974 [5]

rationale behind this engine placement is that the relatively heavy powerplants should be placed close to the centre of gravity (CG) such that the shift in CG during loading is minimal. They state that the wings are not suitable positions to place the engines since they violate this CG related requirement. Although positioning the engines close to the suspected CG location is appropriate, the paper does not consider other aspects of the engine installation.

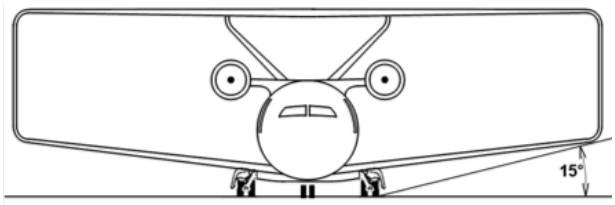

Figure 2.6: Bow-wing aircraft design by Schiktanz and Scholz [6], front view

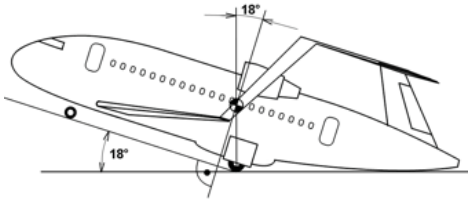

Figure 2.7: Box-wing aircraft design by Schiktanz and Scholz [6], side view

Several internet articles mention the development of a future box-wing aircraft by Lockheed Martin [7, 33] with ultra high bypass engines mounted under the aft wings, as is shown in Figure 2.8. Lockheed Martin suggested this design in 2012 with Rolls-Royce Ultrafan Engines, offering a 22% decrease in specific fuel consumption [34]. Although not specifically stated, a reasonable explanation for this engine position would be the large fan diameter of the ultra high bypass engines. The high position of the aft wing provides enough ground clearance for this type of engine.

Figure 2.8: Lockheed Martin's advanced vehicle concept [7]

Other box-wing design studies concentrate on the aerodynamic design, the structural issues and/or challenges related to the flight dynamics. In the conceptual design research conducted by Jemitola and Fielding [35] in 2012, the engines are considered in the optimisation loop, with the number of engines being a design parameter. However, it seems that they are fixed at the rear of the fuselage, similar to the position suggested by de Klerk. The nacelles and pylons are not taken into account in the aerodynamic analysis. The engine performance is taken into account by considering the thrust as a function of Mach number, altitude and throttle setting.

In the multidisciplinary optimisation performed by Andrews and Perez in 2018 the engines are again positioned on the sides of the fuselage, but the axial location of the inlet along the fuselage is considered a design parameter [36]. Also the sea level thrust of the engines is a variable in the optimisation process, while the bypass ratio is kept constant. To evaluate the available thrust and SFC as functions of the Mach number and altitude, an engine model by Bartel and Young [37] was employed. The details and applicability of this model are discussed in Sections 2.3.2 and 4.5.2.

The optimisation by Andrews and Perez also considers the fuel volume required and a constraint is imposed stating that all fuel should fit in the wings. This constraint is critical, and when removed, the box-wing aircraft shows a more superior performance compared to a conventional design. However, the additional fuel has to be stored in the fuselage. A similar result was found by de Klerk [4].

From these different Prandtlplane concepts it can be concluded that almost no other research reaches the level of detail provided by de Klerk, from an engine integration perspective. A multi-disciplinary approach towards the engine integration is often missing. Therefore, it is suggested to consider the study and results of de Klerk as the foundation for the research introduced in this report. It is recommended to consider the general approach to engine integration used for conventional aircraft projects. Literature on engine design and integration is therefore reviewed in the following sections.

2.3. Preliminary Aero Engine Design

When a new aircraft design is initiated, potential engine manufacturers are usually involved early in the development process. Initially, a statistics-based approach can be employed using a database of existing turbofan engines, as suggested by Svoboda [38]. Although statistical methods are fast, they do not always allow to consider the current advancements in technology. Additionally, such methods are already implemented in the in-house conceptual aircraft synthesis tool, Initiator. However, a more profound engine design approach is preferred to gain more knowledge about this system.

The book by Mattingly et al. [8] is often referenced in engine design research. The process from this book is depicted in Figure 2.9. The approach starts with a complete aircraft mission analysis, followed by a parametric analysis of the design point, also called the reference point. Subsequently, a complete engine performance analysis is carried out to estimate the engine operation throughout the flight envelope. As can be seen in Figure 2.9, this is an iterative process which is required to ensure the engine minimises the fuel consumption while ensuring all conditions can be met.

Considering the flowchart in Figure 2.9, the research described in this report start at the engine cycle analysis step. The initial constraint and mission analysis are carried out by the Initiator tool, which provides inputs for the procedure described in Chapter 4. Other engine research projects, as for example conducted by Reitenbach et al. [39], employ similar steps. Therefore, these steps are briefly reviewed individually in the following sections. However, in this research the objective is to develop the engine model to support the aircraft design process. Hence, the product under consideration is the aircraft and not the aero engine itself.

2.3.1. Thermodynamic Cycle Design

Although the underlying physics of gas turbine systems remain the same, different approaches exist towards cycle selection. While Mattingly et al., for example, present a more elaborate approach towards selecting and analysing the performance, the technique suggested by TASOPT [19] is component-based. This section discusses several methods to determine the thermodynamic cycle which suits the required aircraft performance, and highlights their advantages and limitations.

Aircraft Engine Design Book The book by Mattingly et al. [8] presents a thorough approach to aero engine design for various architectures based on the gas turbine engine, including turbojets, turbofans and turboprops. The cycle is simulated as a one-dimensional flow of perfect gas, while component efficiencies are introduced to model the non-ideal component processes. The parametric analysis considers a reference point (in other literature often called the design point) and sizes the engine for this point. Also bleed air and cooling requirements are accounted for. A sweep of the design parameters is studied for different flight conditions

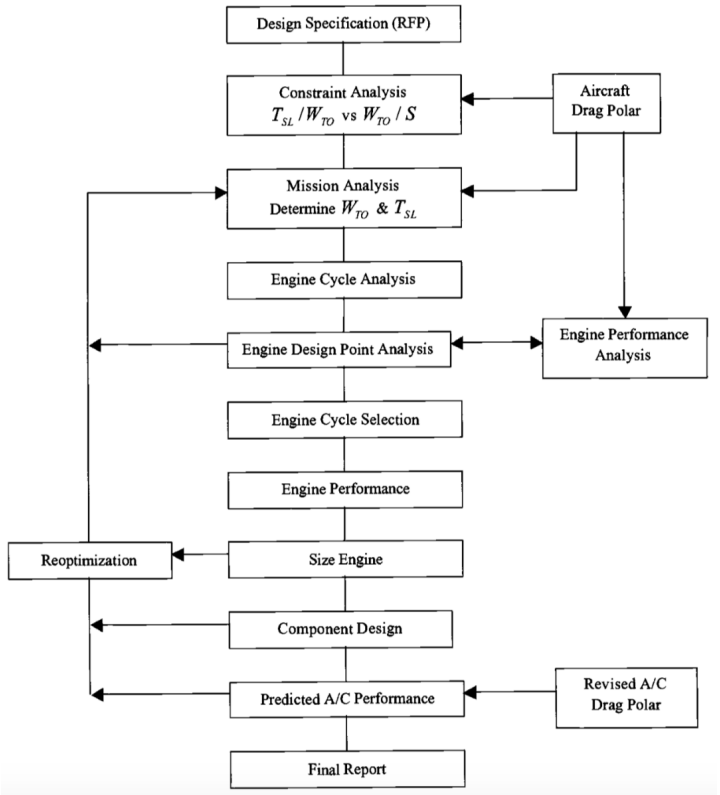

Figure 2.9: Preliminary engine design sequence suggested by Mattingly et al. [8]

and a successful combination is selected. Possibly, an optimisation can be carried out to minimise the cruise specific fuel consumption, for example.

Based on the set or range of design parameters, the steady state performance of the cycle in different operating conditions and for different flight Mach numbers, altitudes and throttle settings can be tested. This analysis is carried out through Newtonian iterations of the (mixer) bypass ratio, core entrance Mach number and the engine mass flow rate. For detailed steps, the reader is referred to Chapter 5 in the book by Mattingly et al. No component maps are required in this approach since the component efficiencies are assumed constant, which simplifies the off-design analysis. Although not entirely correct, Mattingly et al. claim that this assumption provides reliable results for the considered design stage.

Although the methods presented by Mattingly et al. are complete and robust, they are developed separately for every type of engine cycle. Hence, a model has to be constructed individually for two-shaft and three-shaft turbofan architectures, for example. When implemented in a software application, this does facilitate the straightforward addition of new elements or higher fidelity models in the future. Furthermore, the structure of the input variables would have to be made specific for every cycle. Therefore, a more general modelling of the individual components may be preferred.

TASOPT Transport Aircraft System Optimization, TASOPT, is a scheme which relies on low-order physics-based models to preliminary size and optimise new aircraft configurations and corresponding engines [40]. Especially the suggested component-based turbofan modelling techniques are of interest in the current research project since they allow to model several engine configurations, e.g. two versus three spools, using the same building blocks. Hence, for example, turbine elements model the process where a change in enthalpy is prescribed. Depending on the number of shafts, this process has to be repeated two or three times in the engine cycle. Instead of developing separate processes for all possible engine architecture, this approach allows to model various configurations by creating instances of pre-defined blocks.

The approach allows to consider novel turbofan architectures such as geared fans and is general enough to work with different fuel types. It is concluded that the TASOPT methods are quite flexible, making them powerful in a preliminary design stage of different concepts. However, it is required to use (preliminary) fan and compressor maps and to scale them accordingly to determine the off-design performance. Although Greitzer et al. [19] present methods to approximate these maps, the approximations still have to be calibrated with existing maps or experimental results.

TASOPT Signomial Programming A new approach introduced by York et al. [21] is to take the first principles methods from TASOPT and to optimise all parameters by specifying the gas turbine model as a signomial program problem. In order to do so, all physical relations must be written as posynomial inequality constraints or monomial equality constraints. This allows to solve all equations via convex optimisation (geometric programming) or through sequential convex programming. Although the engine modelling approach developed in TASOPT is applied, some of the relations are re-formulated to fit the standard form of a monomial, posynomial or signomial.

This signomial programming technique does not lose any of the capabilities of the TASOPT methods, such as cooling air, power offtake, and the possibility to model geared turbofans. Furthermore, it does not consider the design and off-design points separately. The operational points of interest such as cruise, top of climb and take-off are specified as combinations of Mach number, altitude and required thrust. These points act as constraints, and if one becomes active it is taken into account in the optimisation.

Potential advantages of this concept are that the computation is fast because of the mathematical formulation, sensitivities are easily computed and no separate analysis for design and off-design conditions has to take place. The signomial technique can be implemented using dedicated packages in Python. Disadvantages include the fact that the implementation of the actual signomial programming is expected to require more time than conventional methods if the same component-based flexibility is desired. Furthermore, similar to the regular TASOPT methods, preliminary fan and compressor maps have to be provided.

2.3.2. Off-design Performance Analysis

As included in the design process introduced in Figure 2.9, an off-design or performance analysis of the engine is required to ensure it can operate in all flight conditions the aircraft may encounter. Therefore, the steady-state variation in thrust and thrust specific fuel consumption with flight Mach number, altitude and throttle setting is of interest. Three options are considered to obtain this off-design operation of an engine:

1. Build a dedicated tool to solve for the steady-state operation which employs Newton iterations, as for example suggested by the TASOPT research [19]. However, the implementation time for a robust solver is expected to be too long.

2. Empirical relations can be used as discussed by Bartel and Young [37]. Although these calculations are faster than numerical methods, accurate solutions ($\pm 1\%$) are only possible if the relations are calibrated using performance data of existing engines. Data of existing engines is often not publicly available and might not be appropriate for future engines.

3. The most accurate option is to employ commercial software, such as GSP[4], GasTurb[5] or PROOSIS[6]. Such programs offer high accuracy and flexibility in terms of engine architecture, by combining 0D and 1D models. However, they are more complex, require more inputs, and possibly need manual interaction in a design routine.

As discussed in Section 4.3, the third option is selected because it offers the most accurate solution and since such software can model various engine cycles. Moreover, the software can also be utilised to further developed engine simulations in the future. The model provided by Bartel and Young is also implemented for validation and comparison purposes.

[4] URL `https://www.gspteam.com` [Accessed on 7 November 2018]
[5] URL `http://www.gasturb.de` [Accessed on 7 November 2018]
[6] URL `https://www.ecosimpro.com` [Accessed on 7 November 2018]

2.3.3. Sizing Methods

Although statistical relations can be used to estimate the dimensions, it is preferred to determine the size of the engine based on the outcome of the thermodynamic cycle design, as much as possible. Several research projects appear to employ the same method to preliminary determine the diameters of the components by assuming local axial Mach numbers and hub-to-tip ratios at the in- and outlets of the components [19, 41]. To estimate the length of the components, it is advised to carry out a simple meanline design for turbomachinery components [41] and to still employ statistical relations for other components [42, 18] from earlier engine designs. Since these methods have been implemented successfully in earlier research projects and since the rules can be tailored to each component type, they are applied in this research. The exact working principles are laid out in Section 4.4.

2.3.4. Weight Estimation

A preliminary estimate of the aero engine weight has to be made to determine the impact on the entire aircraft weight and the balance of the aircraft. This is often a challenging task on a component level since actual component weights of existing engines are well kept secrets in industry. Additionally, since the trend is to further increase the bypass ratio in the coming years, impacting the mechanical design of the engines, the use of statistical relationships is to be avoided since these are often calibrated with low bypass engines.

Lolis et al. [43] provide a recent overview of the existing preliminary weight estimation methods for aero engines. Two approaches are identified: whole engine-based or component-based. The first category estimates the weight of the entire engine (or fan and core structures separately), while the latter aims at estimating the weight of individual engine components or modules.

Examples of a whole engine-based methods are the relations provided in aircraft design books written by for example Torenbeek, Raymer and Jenkinson et al. Although these relations allow for a rapid evaluation, the problem is that they often rely on publicly available data of old engines (1940 to 1980), making them unsuitable for future high bypass, potentially geared turbofan engines. Furthermore, they only capture the effect of a couple design parameters, such as net thrust, bypass ratio, overall pressure ratio or fan diameter, and not their interrelated effects.

Component-based methods are typically physics-based, but can still rely on statistical relations for smaller scale elements. Although the accuracy of these methods is higher in general, they require more knowledge about the geometry of the engine, which translates into more inputs. However, in the preliminary design stage of a new engine, several input parameters might be unknown. Examples of such methods are WATE (and its later versions) developed by NASA and Boeing, and WeiCo created through a collaboration between Chalmers University and Stuttgart University [43].

Based on a test set of 56 engines, Torenbeek's method requiring four inputs resulted in the smallest error (± 25%) of the whole engine-based methods according to Lolis et al. [43]. The component-based WATE model was able to reach an error of less than 10%, although it required more knowledge. From a comparative analysis Lolis et al. concluded that a hybrid method would yield the best of both approaches in a preliminary design stage: it is faster and requires less inputs, while at the same time it does not (completely) rely on available engine data.

TASOPT [19] considers the engine weight as a function of the core mass flow, BPR and OPR. However, several relations are suggested to estimate the engine weight employing these parameters. First, the function can be derived from existing turbofan engines. In this case, Equation (2.3) can possibly be used [40]. It is logical that the weight of the fan scales with the bypass ratio, the structural weight varies with the highest pressure obtained inside the core, and that the whole engine weight is related to the ingested mass flow.

$$W_{eng} = \left(\frac{\dot{m}_{core}}{\dot{m}_{ref}}\right)^{b_0} \left[W_0 + W_{fan}\left(\frac{BPR}{BPR_{ref}}\right)^{b_1} + W_{case}\left(\frac{OPR}{OPR_{ref}}\right)^{b_2} \right] \tag{2.3}$$

For the above equation, Drela suggests to calculate the coefficients and exponents through non-linear regression using the complete weight of existing engines. However, this does not correspond to the basic idea of the TASOPT approach, which is physics-based. A more advanced method is provided in Appendix H of the report

by Greitzer et al.. There it is decided to utilise an advanced version of WATE, called WATE++, to estimate the weight of single components.

WATE++ is first calibrated using the data from seven existing engines, which required detailed input from the engine manufacturers. Based upon this calibration, and rather than running the WATE++ program in the TASOPT routine, several hundred engine designs are simulated using various large ranges of BPR, OPR and $\dot{m}$. Using this outcome, correlations are developed using again the three variables from above. The basic relation is provided in Equation (2.4), where a, b and c are functions of the bypass ratio.

$$W_{eng} = a\left(\frac{\dot{m}_{core}}{100\,[lbs/s]}\right)^{b}\left(\frac{OPR}{40}\right)^{c} \tag{2.4}$$

2.4. Nacelle and Pylon Design

A strong interaction is present between the engine and aircraft design. An unconstrained optimisation of the engine cycle will most likely try to increase the bypass ratio and fan diameter for improved uninstalled efficiency. However, this is not without installation challenges such as increased nacelle weight and drag. The explicit need to consider the engine integration early in the development of novel aircraft was expressed by Hoheisel in 1997 [44]. In this section and the following, several aspects of the integration of the engine with the airframe are treated.

Several approaches can be taken to determine the external shape of the nacelle. The simplest models do not consider the size of the bare engine separately, but provide equations to derive the nacelle dimensions, as shown in Figures 2.10 and 2.11, based on engine performance data. Jenkinson et al. [9] for example suggest relations considering existing installations and requires the fan diameter, BPR, OPR, inlet mass flow and maximum operating Mach number as inputs. Depending on whether the exhaust gases are mixed or not, different sizing relations have to be used.

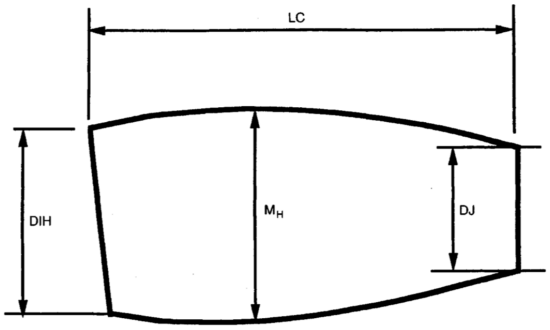

Figure 2.10: Dimensions of a nacelle with mixed exhaust according to Jenkinson et al. [9]

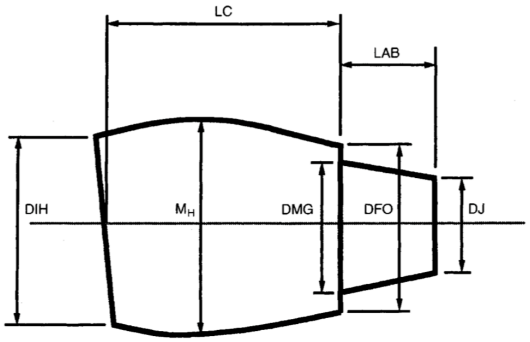

Figure 2.11: Dimensions of a nacelle with separate jets according to Jenkinson et al. [9]

Although this method allows to quickly estimate the basic dimensions of the nacelle, it relies on relatively old, unpublished data and it does not describe the exact aerodynamic shape of the outer cowlings. Since the approximate size of the engine is known from preliminary aero engine design, it is advised to consider this as an input rather than only the performance parameters specified above. Additionally, to create the geometry in for example ParaPy (see Chapter 3) or Computer-Aided Design (CAD) software, more details about the geometry have to be known.

An assessment of the aerodynamic interference between the engines and the aircraft for a Flying-V configuration is carried out by Rubio Pascual [45]. In this study the axisymmetric nacelle is parameterised using Class Shape Transformation (CST) curves. This approach is established from studies by Heidebrecht et al. [10] and by Christie et al. [46] where the CST parameterisation is employed to construct the individual curves defining the nacelle while ensuring a smooth aerodynamic shape. For such a parameterisation, a fourth-, fifth-, or sixth-order system of equations can be solved to find the appropriate Bernstein coefficients when an intuitive parameterisation is employed, as for example shown in Figure 2.12. This parameterisation allows to easily alter the nacelle design and various shapes can be considered by adapting only a few variables.

This is an interesting approach since the intuitive parameters can be derived from the aero engine geometry through engineering rules. Furthermore, the parameterisation can possibly even be extended to model more complex, non-axisymmetric nacelle shapes.

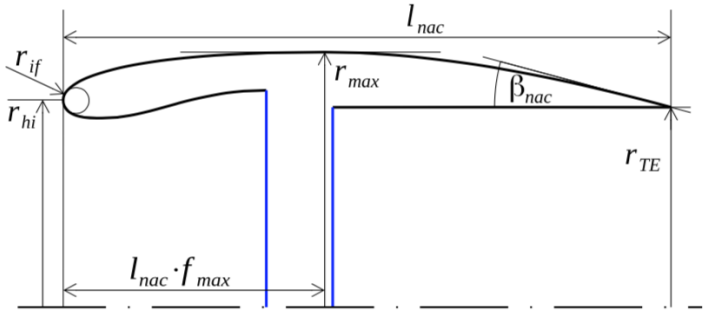

Figure 2.12: Nacelle parameterisation by CST curves [10]

The geometry of the pylon is created after the nacelle has been positioned and the correct orientation has been selected. Oliveira et al. [47] advise to first determine the shape and position of the leading and trailing edges of the pylon respectively, and to then create the actual fairing by a process called “pylon lofting". The thickness and shape of the fairing can be defined using inviscid aerodynamic analysis. De Klerk [4] decided to model the pylon using a NACA 0006 airfoil shape. Alternatively, different standard airfoil shapes or CST curves can be used to develop the pylon shape.

2.5. Evaluation of the Engine Installation

As mentioned earlier, the installation of podded engines can have a considerable impact on the aircraft performance, especially if the fan diameter continues to increase. In this section, several aspects are elaborated upon which should be taken into account when positioning the engines and iterating on the integration.

2.5.1. Aerodynamic Considerations

The aerodynamic effects of propulsion integration are characterised by several issues. These issues differ depending on the location of the engine, e.g. under the wing or at the tail of the fuselage. Oliveira et al. [47] focus on underwing engine installation and indicate that mainly the convergence channel between the nacelle, pylon and wing can lead to a loss in lift and vortex drag penalties due to the increased flow velocity on the lower wing surface. A shock wave at this location can lead to flow separation when interacting with the boundary layer. Additional aerodynamic aspects which are considered in the paper are:

- The gully depth and penetration, which represent the vertical distance and horizontal overlap between the engine and wing affect the interference drag. These distances are indicated in Figure 2.13 by dz and dx respectively.
- The pitch and toe angles of the nacelle should be adapted to the inlet flow during cruise and the impingement of hot exhaust gases on lift or control devices.
- The pylon design can be altered to avoid shock waves and prevent boundary layer separation.
- The ground clearance should be tailored to prevent possible ingestion of debris and the formation of ground vertices.
- The direction of the flux of the thrust reversal should be selected such that the flow does not greatly influence the aerodynamics of other components and movables. Also, the flow should not be re-ingested by the engine.
- The use of vortex generators on the nacelle has to be considered to control the flow in high angle of attack situations.

Oliveira et al. suggest to employ mainly (inviscid) 3D panel methods to position and orient the nacelles, as well as analyse the outer shape of the pylon and any local wing modifications. However, to examine the details of the jet plume or the influence of thrust reversal, higher fidelity Reynolds-Averaged Navier-Stokes (RANS) simulations are recommended. However, the latter are considered out of scope in this study since the large scale effects of engine integration are of main interest in the current design stage.

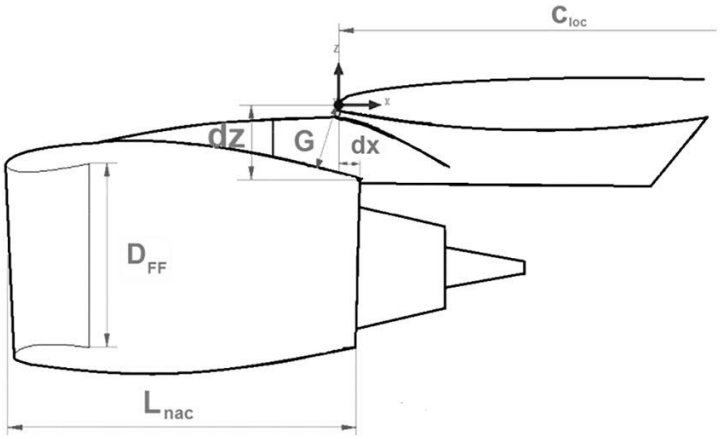

Figure 2.13: Sketch of nacelle installation parameters [11]

Berry [12] provides a general overview of the aerodynamic issues and how they were considered in the engine integration of the Boeing 777. An overview of the aerodynamic effects is provided in Figure 2.14. Similarly, a combination of aerodynamic tools is employed to analyse the installation, first considering the isolated nacelle, followed by an analysis of the installed configuration. Both Oliveira et al. [47] and Berry [12] describe the use of wind tunnel experiments to verify the complete design. In this research this is not considered since the objective is to build the computational tools required to assess the integration in an early, creative design stage.

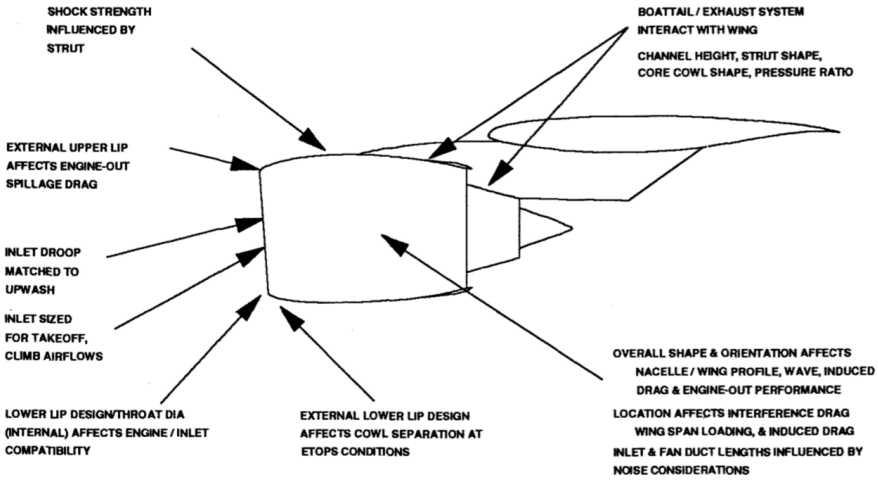

Figure 2.14: Aerodynamic factors influencing nacelle installation [12]

Following the discussion above, the use of a 3D panel code appears to be appropriate in the current development stage of the PARSIFAL aircraft. VSAERO analyses software is selected in this research for several reasons. As Groot [48] indicated, VSAERO offers a balance between computational time and accuracy. Hence, it allows to study the complete aircraft with movables in a timely manner with an acceptable accuracy. And although VSAERO is not expected to provide the same fidelity as RANS or higher fidelity simulations, the potential flow solver has been proven to give insight in aerodynamics of nacelle integration studies in the past [49, 50]. Several types of analysis are possible, from a relatively simple flow through nacelle, to a full aircraft integration where the engine inflow and jet exhaust are modelled.

It should be noted that while other research projects focused on the detailed analysis of nacelle aerodynamics [11, 51], it is not considered to be of interest in the research project discussed in this report. As discussed in Chapter 1, the main objective is to recommend a preliminary propulsion system integration for the PrandtlPlane, rather than studying the specific aspects of the local aerodynamic effects.

2.5.2. Non-Aerodynamic Considerations

Besides the effect the engines have on local aerodynamics, several non-aerodynamic constraints or aspects follow from other disciplines, such as flight mechanics, acoustics, structures and maintenance [12, 47]. A multi-disciplinary analysis may also consider these aspects since they can directly influence the design, although not all of them can be accounted for in a straightforward quantitative manner. A short overview of each of these aspects is provided in this section.

The flight mechanics of the aircraft can be impacted by the engine integration in several ways: firstly, the engine installations typically constitute approximately 8% (jet engines) up to 12% (turboprops) [17] of the maximum take-off weight of transport aircraft. Hence, moving this mass longitudinally and laterally has an effect on the balance and inertia of the aeroplane. Secondly, the location and orientation of the thrust vector(s) with respect to the aircraft centre of gravity can affect the force and moment balance. Thirdly, the latter balance is also altered by the aerodynamic forces acting the nacelle surfaces. Hence, considering these effects, the control system allocation may also be different for the aircraft with and without engines.

The engines perform a rather dominant role in noise production of the entire aircraft, especially during take-off [52]. The noise generated can be reduced through appropriate engine cycle selection and acoustic liners inside the ducts. Additionally, the noise level can be further decreased by placing the engines over the wing for example, effectively shielding the observers on the ground [53]. For the sake of passenger comfort, cabin noise has to be limited. Especially engines directly connected to the fuselage, close to the cabin, can increase this noise level [4]. An assessment of the complete aircraft noise is also targeted in a different work package of the PARSIFAL project. Since specialised models are required to assess the acoustics of the engines on an aircraft level, the necessary inputs are provided to the respective PARSIFAL partner, as discussed in Section 6.2.

Also the effect of the engine location on the structural weight has to be taken into account. Although the detailed design of, for example, the pylon and thrust links is outside the scope of this research, a qualitative analysis can be made. Placing the engines more outboard on the wing, for example, will relieve the bending stress in the wing. For engines attached to the fuselage, it is advised to place them close to other load bearing structures. Additionally, due to their weight, the location of the engines also affects the flutter characteristics, especially if they are located on the wing. Berry [12] indicates that particularly the fore/aft position of the engines with respect to the wing can affect the flutter characteristics.

From an airliner's perspective, installed maintenance of the engines performs an important role. Easy access to the engine and its subsystems reduces the time required for maintenance and thus saves money. Engines placed between vertical fins or on high positions with respect to the ground, for example, make maintenance activities more difficult. Additionally, producing and acquiring the machinery required to gain access to the engines in unusual locations can potentially increase the cost of aircraft operations. However, this aspect is difficult to quantify in early design stages.

From a safety and regulations point of view, Berry devotes a separate section to the following measures which, among others, affect the size, location and orientation of the engines:

- Ground, runway, and taxi light clearances and airport gate compatibility
- Roll clearance in case of crosswind landing or flat tires
- Safe distance between the engine and emergency escape slide from passenger doors
- Ground clearance in case of a collapsed landing gear
- Turbine disk burst zones without critical control systems
- Water spray ingestion, which may be different from a conventional configuration

All these interactions between the propulsion system indicate how multi-disciplinary the engine design and integration problem is. However, not all disciplines can be considered in a single research project with the

same level of detail. Hence, in the project described in this report, it is decided to focus on the aerodynamic aspect since it directly influences other disciplines such as flight mechanics and structures. Moreover, the necessary preparations are made for the flight mechanics and acoustic aspects. Nevertheless, for the specific PARSIFAL case, several of these disciplines are covered by different work packages, which can employ the results from this research and possibly provide feedback.

2.6. Multi-Disciplinary Design Methodologies

The reason for examining more advanced design methods in this literature review is threefold: firstly, one of the recommendations of de Klerk is to include the developed methods in the design routine called the Design and Engineering Engine (DEE) as introduced by La Rocca and van Tooren [13]. This technology is further elaborated upon below. Secondly, Early [54] identified in 2000 the need from an industry perspective for advanced and flexible engine integration tools which "*... provide the ability to react quickly to inevitable design changes, driven by constantly changing requirements, during the product development cycle.*". However, the implementation of such methods for engine integration studies appears to be limited. Finally, the usage of multi-disciplinary development application is highlighted in the Flightpath 2050 objectives for future aviation [26].

The concept of the DEE framework for aircraft design, as mentioned by de Klerk, is introduced by La Rocca and van Tooren [13] and schematically shown in Figure 2.15. The aim of this framework is to provide a multi-disciplinary approach towards aircraft design. Knowledge Based Engineering technology is employed to support this routine where the so-called Multi-Model Generator performs an important role.

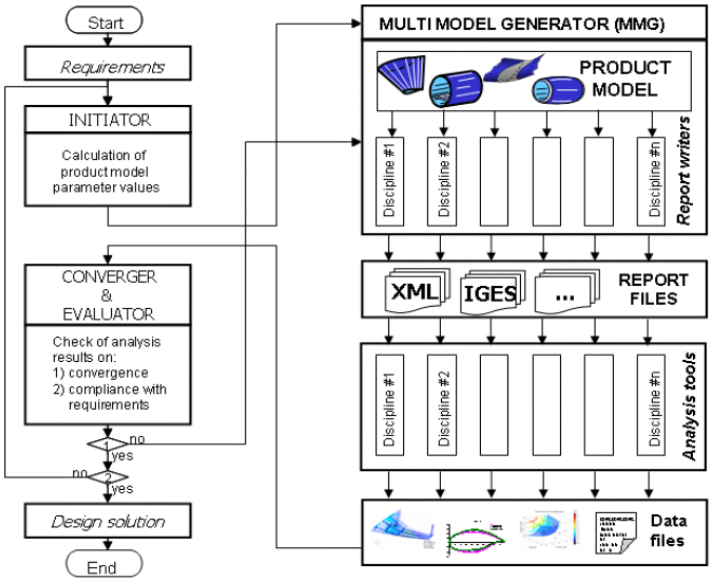

Figure 2.15: Design and Engineering Engine [13]

The framework in Figure 2.15 works as follows: first an initial, conceptual aircraft model in generated from the specified top level aircraft requirement. Subsequently, the aircraft geometry is further developed in the Multi-Model generator by making use of High Level Primitives (HLP's), or "building blocks" such as wings, fuselages, connecting elements, etc., which together make up the aircraft product model. This step is made possible through object-oriented programming and makes the MMG flexible and generic such that different aircraft configurations can be modelled employing instances of component classes, such as `Wing` and `Fuselage`.

Thirdly, the product model has to be transformed into a format which can be interpreted by commercial or academic analysis tools targeting a certain discipline. These analysis tools are not necessarily adjusted for this design routine. This step in which the model is "translated", is carried out according to programmed rules and produces the report files as indicated in Figure 2.15. Finally, the results from various disciplines can be gathered, and iterated upon if required.

One of the advantages of employing such a Multi-Model Generator is that external tools (i.e. not inherent to the routine) of variable fidelity can be employed. Hence, higher fidelity aerodynamic or structural tools can be included in an automatic design routine. Repetitive tasks such as meshing or making small geometrical changes can be carried out by the MMG, reducing the time required for these non-creative tasks. This is supported by KBE technology which allows to efficiently evaluate expert knowledge implemented as rules, combined with the power of Computer Aided Design (CAD) operations to easily manipulate the product geometry. The latter are facilitated by ParaPy software, which provides the functionalities needed to build rule-based applications, including the geometry modelling and integration with analysis tools [7].

Additionally, by incorporating several disciplines in the framework and automating their execution, more knowledge about the design can be gathered in the early design stages. Hence, by constructing Multi-Disciplinary Analysis and Optimisation (MDAO) routines, the results from one discipline can be utilised to review certain design choices and immediately evaluate the effect on other disciplines.

Currently, the in-house MMG is capable of preparing the geometry of conventional and box-wing aircraft and translating that geometry in a mesh which can be interpreted by the VSAERO aerodynamics software. This MMG can be further extended with an engine HLP to consider the effect on the aircraft performance, as indeed suggested by de Klerk. A higher fidelity view of the engine performance and influence is currently not implemented, but would pave the way to a more complete analysis of new aircraft systems.

One, publicly available application of KBE techniques in the aero engine industry is presented by Cedar et al. [55]. Here, KBE technology is employed in the so-called “Intelligent Master Model" to simplify adaptions to the engine configuration and automate component definitions. This allows to easily study new technological developments and to react rapidly to customer requirements. Such an application of KBE is also of interest in this research. Additionally, a similar process can bring the engine together with the airframe to automate the definition of components such as nacelles and pylons.

2.7. Literature Review Conclusions

The objective of this section is to shortly highlight the most important results from the literature review, and to clearly identify the gap in existing research. It can be concluded that, except for de Klerk’s Thesis, research dedicated to the integration of turbofan engines on the PrandtlPlane configuration is minimal. Although several box-wings concepts have been further developed, the rationale behind the engine placement is not in all cases studied in detail. Hence a different approach has to be found such that podded turbofan engines can be sized and installed on a PrandtlPlane of any size by considering several disciplines.

Furthermore, the use of advanced design methods for automated propulsion systems design and integration on a preliminary level is limited. In the current aircraft product in the in-house Multi-Model Generator, the engines are not yet taken into account. Hence, to further augment the study of aircraft performance, it would be beneficial to study how the propulsion discipline can be implemented, providing higher fidelity than currently available.

The review also revealed methods which can be applied in the new research. Also various installation aspects are identified. However, it should be noted that some sources are relatively old. Although this does not make them invalid, newer insights should be used when possible. Especially when statistical relations are suggested, the applicability of the available data to a new design problem has to be evaluated critically. It is therefore preferred to implement physics-based approaches since it would allow the methods to be applied independent of the aircraft configuration and independent of the top-level requirements.

Since the research by de Klerk, several new technologies and/or methods are developed. One example is the introduction of larger bypass ratios, potentially with a geared fan architecture. Secondly, the CST curves parameterisation allows for a more flexible and more detailed modelling of the nacelle. Finally, the use of a KBE approach is facilitated by recent software developments. An example of this is ParaPy, the Knowledge Based Engineering platform currently in use at the Flight Performance and Propulsion department. This software allows to build rule-based engineering applications in Python, including the geometry modelling and integration with discipline specific analysis tools.

[7] URL `https://www.parapy.nl` [Accessed on 7 November 2019]

3

The Propulsion Discipline in a Multidisciplinary Design Framework

As introduced in Chapter 1, the first goal of this new research is to develop a set of methods and tools to design and analyse the integration of a turbofan based propulsion system on any aircraft configuration. These methods focus on the propulsion discipline in the overall aircraft design, and should be able to operate in MDAO frameworks currently under development in the Flight Performance and Propulsion research group of Delft University of Technology. Although the formulation of such a complete framework is not within the scope of this research, this chapter aims at clarifying how the propulsion discipline developed in the following chapters, fits in a larger MDAO framework. Furthermore, the connections between the different software packages are introduced and the inclusion of the engines in the Multi-Model Generator is considered.

Considering the aircraft as the product under consideration, and not only the turbofan engine, the design and analysis framework is presented in Figure 3.1. This framework is adapted from DEE presented in Figure 2.15 [13]. The uncoloured blocks represent tools and methods which were already developed prior to this research. The blue filled elements indicate functionalities which are implemented or upgraded in the current research.

The workflow starts with an initial, conceptual design of the aircraft created by the Initiator based on top level requirements (TLR) and certain design variables [56]. It provides an estimation of the aircraft mass, aerodynamic performance and geometry. The latter is finalised in the MMG. Since the Initiator currently employs empirical relations to estimate propulsion-related parameters, an additional preliminary engine design tool is implemented which utilises a physics-based approach. Such an approach is preferred since it allows to model engines with varying bypass ratio and technology levels with improved fidelity.

This engine design tool, currently called GTpy, is set up in Python with the help of ParaPy functionalities and provides the basic geometry of the bare aero engine as input to the MMG. This engine sizing process is elaborated upon in Chapter 4. The MMG is capable of modelling the geometry of various aircraft configurations by combining instances of `Wing` and `Fuselage` classes. In this research, the MMG capabilities are extended to include the nacelles and pylons, which are automatically designed around the engine geometry, as discussed in Chapter 5.

Once the geometry of the complete aircraft is generated, the Multi-Model Generator can prepare the reports needed for discipline specific analyses. In the case studied here, only three disciplines are shown, but this can vary. Other aspects may for example include structural, aero-elastic and/or cost analyses. For the propulsion discipline, the off-design analysis is conducted by the Gas Turbine Simulation Program (GSP), for which an XML input file has to be created. Although Figure 3.1 shows this reporting as a function of the MMG, it can also be executed from the engine preliminary design tool. The integration with GSP and its specific use-cases are also treated in Chapter 4.

The second report includes the mesh generation for aerodynamic analysis. In the current research the commercial VSAERO software is selected to perform an analysis of the complete aircraft. Since VSAERO is based on a 3D panel method, a mesh is required over the exterior surface of the model. This mesh can be automatically generated by the MMG and exported to the format which can be interpreted by VSAERO. The latter operations are facilitated by ParaPy built-in functions. This research makes use of these functions to extend

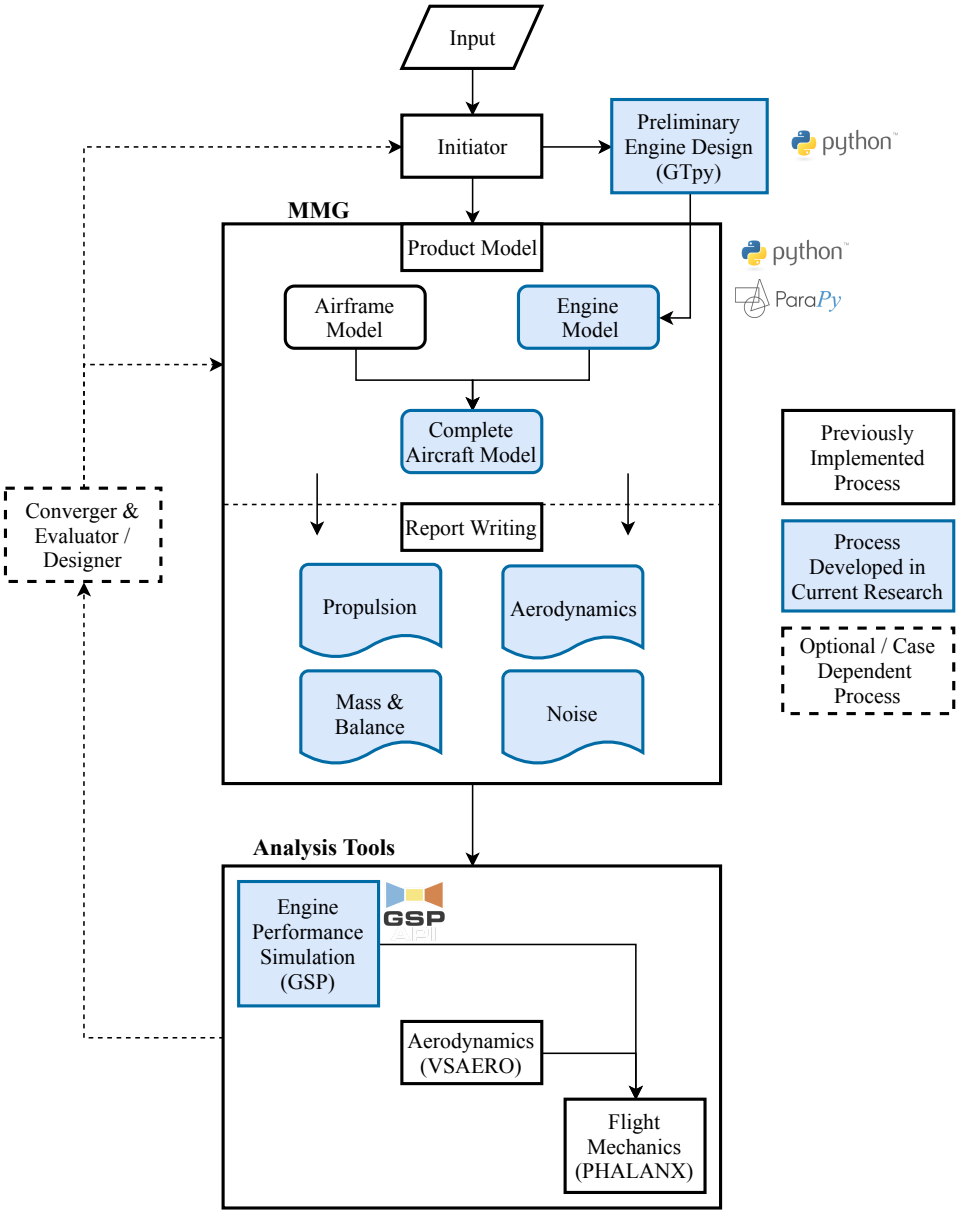

Figure 3.1: Design and analysis framework, including the employed software packages

the existing aircraft meshing strategy [48] to include the nacelles. This strategy and the specifics of modelling the turbofan engines in a 3D panel code are considered in Chapter 6.

The results from the engine off-design and aerodynamic analyses can be used to evaluate the flight mechanics of the aircraft. This discipline is studied by PHALANX, a multi-fidelity flight mechanics tool developed at the Flight Performance and Propulsion research group. Depending on the MDAO problem formulation, PHALANX can be employed to investigate the control and stability derivatives of the aircraft, to size the control surfaces or to consider a complete mission analysis.

The last discipline specific input prepared by the MMG is that of the noise analysis. Since the engines perform a rather dominant role in noise production of the entire aircraft, especially during take-off [52], it is recommended to include them in the preliminary noise analyses. In the PARSIFAL project, a different partner is studying the perceived noise around the aircraft in various flight conditions. The current propulsion integration tool allows to produce the necessary inputs for the noise models by Heidmann [57] (fan and compressor noise) and Stone [58] (jet noise) which are implemented by the PARSIFAL partner.

The workflow presented above also suggests an iterative loop with a converger and evaluator block, ensuring that the aircraft design meets all top level requirements and is consistent. This is only one example of a MDAO problem formulation. The framework may include an optimiser, or disciplines can be left out or added for the specific problem at hand. In this research, the propulsion, aerodynamic and flight mechanics disciplines are of main interest for a specific airframe configuration. The use of the Initiator module and optimisations are considered out of scope.

A proposed multi-disciplinary workflow is shown in Figure 3.2. This workflow is developed with the help of a PhD candidate, employing the KADMOS software [59]. For a fixed aircraft configuration and engine location, the design thrust (FN_{des}) and the engine geometry can be iterated upon employing results from a flight mechanics analysis. Starting with an initial design thrust, the engine is designed by GTpy. Then, the aircraft geometry including nacelles can be generated in the MMG. This shape is also meshed by the MMG and subsequently analysed with VSAERO.

During the GTpy execution, also an engine deck is created where the available thrust for certain points in the flight envelope is determined. Combining this engine deck with the results from VSAERO, the aircraft can be balanced and the trim conditions can be computed by PHALANX. From this analysis, the trim drag can be calculated, which is fed back to the Converger module, which in turn provides an updated design thrust (FN_{des}) to GTpy. This allows to walk again through all disciplines, until the design thrust has converged.

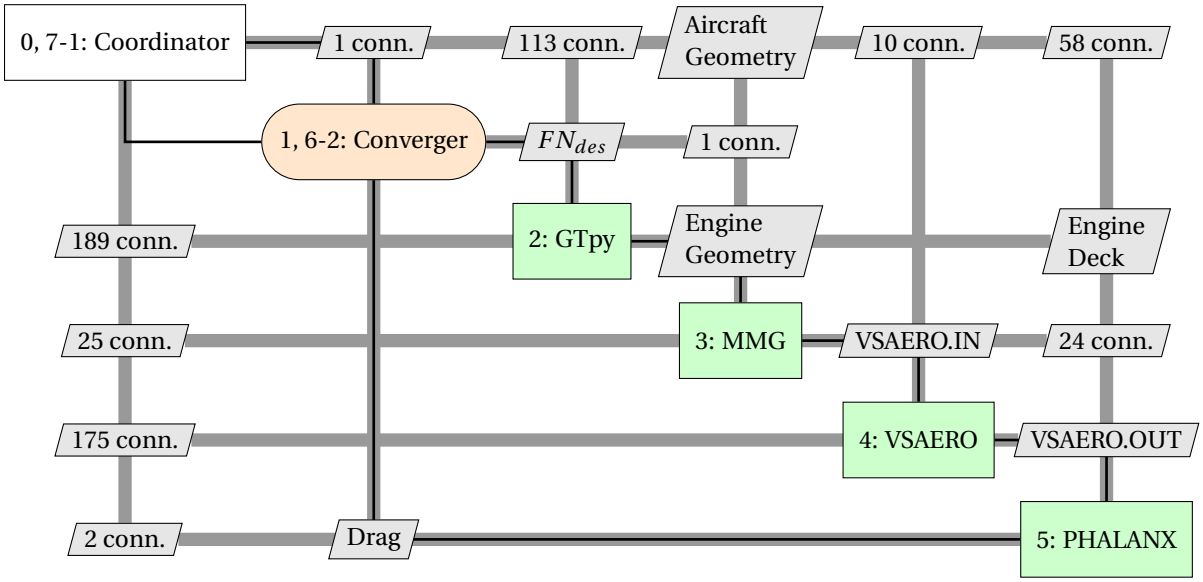

Figure 3.2: Example of a multi-disciplinary analysis workflow to iterate on the design thrust of the engines

This is just one example of what can be done when multiple disciplines are combined in a design framework. Important to note is that the tools developed in the following chapters are developed while taken such multi-disciplinary frameworks and the associated data handling into account. Hence, certain design steps are automated using engineering knowledge from literature such that the number of inputs can be reduced, although all inputs can still be altered manually. Additionally, a consistent communication format between the tools is established making use of the CPACS data model [60]. The implementation of this data structure is elaborated upon in Section 4.1 and Appendix A.

4

Preliminary Aero Engine Design

In this chapter, the preliminary design and analysis of the aero engine are studied. The process which is typically followed has been thoroughly studied before by Mattingly et al. [8] and applied in recent research by Reitenbach et al. [39]. The steps, as applied in this research, are presented in Figure 4.1. From an initial aircraft sizing, as completed by the Initiator for example, the basic requirements for the engine can be derived. These typically include stringent thrust and power levels at characteristic points in the flight envelope. Based on these requirements, an engine concept can be selected. Subsequently the thermodynamic cycle at the design point is fixed and used to analyse the performance in off-design conditions. Employing the results from these two types of analysis, an estimate of the aero engine geometry can be created. These four individual steps are discussed in Sections 4.1 to 4.4. In Section 4.5 the verification and validation steps are elaborated upon.

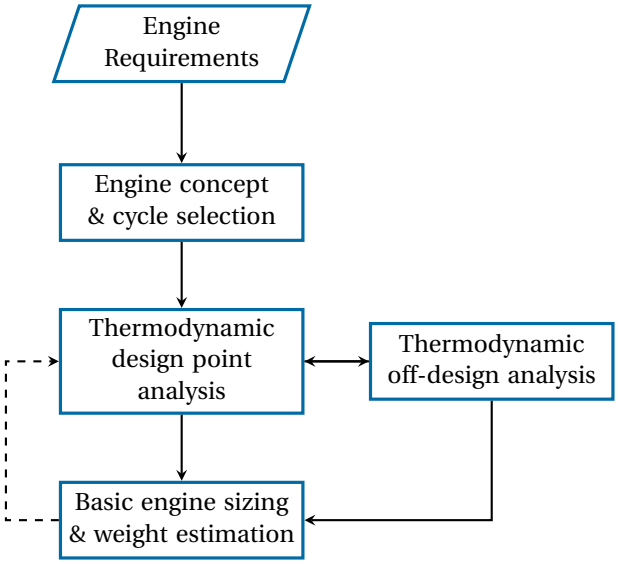

Figure 4.1: Preliminary design process for gas turbine engines

The requirements element in Figure 4.1 refers to requirements specifically for the engine, and not the aircraft. Hence, they include the net thrust at specific operating conditions in the flight envelope, the power and bleed air required by other aircraft systems, and possibly temperature limits in the turbines. Methods to estimate these values are not implemented in this research. Thrust values for example are expected to follow from early mission analysis, as for example completed by the Initiator.

One could argue that one step is missing in Figure 4.1, being the selection of an in-service engine. In certain study cases, an existing engine may already satisfy all requirements. The developed application does not search automatically through an engine database, and therefore it is advised to complete this step manually. Nevertheless, if a suitable engine is identified, the details of the thermodynamic cycle and the exact size are often not publicly available. Hence, the tools treated in this chapter can also be employed to model existing engines based on the available inputs, as done for the validation case in Section 4.5 for example.

4.1. Engine Architecture Selection

Similarly to the aircraft definition employed in the MMG, the engine model is considered in an object-oriented, component-based manner. This means that a gas turbine can be constructed as a combination of individual components, each type of component having its own class. This structure is illustrated by the Unified Modelling Language (UML) diagram in Figure 4.2. Each component complements firstly models the 0D thermodynamic process that is associated to it using the approach presented in TASOPT research [19]. Secondly, it contains the engineering rules to size the component at a conceptual level. Both aspects are discussed in the following sections.

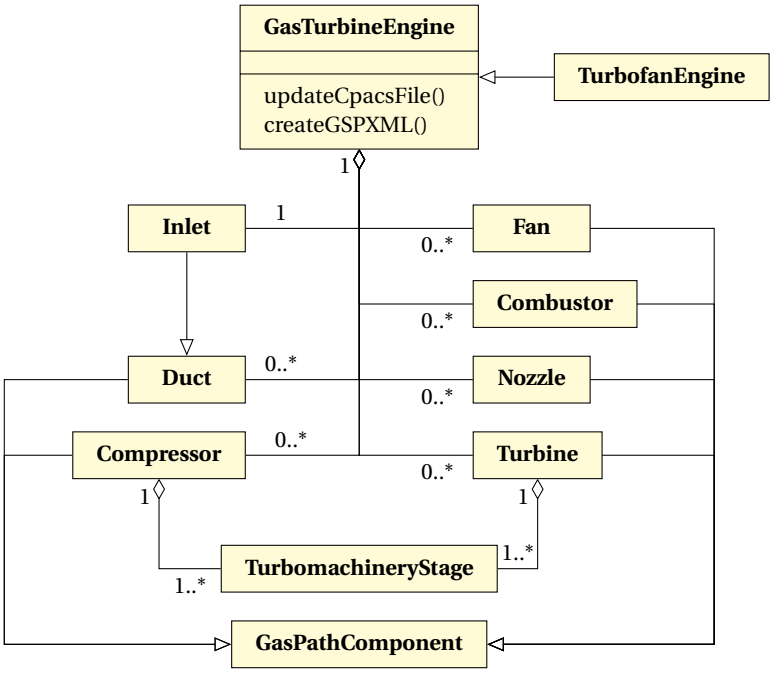

Figure 4.2: Simplified class diagram showing the component-based definition of gas turbine engines in GTpy

This object-oriented programming paradigm is implemented since it provides flexibility in engine cycle (e.g. turbojet and turbofan) and architecture (e.g. two- vs three-shaft) selection. Additionally, this format facilitates the implementation of new components in the future, such as electric motors or maybe propeller elements. Furthermore, the Gas turbine Simulation Programme (GSP) utilised in this research makes use of a similar object-oriented structure [61], and thus the communication between the Python-based application and GSP is simplified.

As can be seen in Figure 4.2, also `GasPathComponent` and `TurbomachineryStage` classes are implemented. The first class forms the basis for all other components, by modelling parameters such as inlet and outlet mass flows, temperature and pressure values which are required in all components. This ensures consistency between the classes, reduces the amount of code and paves the way for further developments. The `TurbomachineryStage` class represents a single stage of turbomachinery, typically a rotor-stator combination for compressors, and stator-rotor for turbines. Although no individual blades are currently modelled, this class assists in the axial length estimation of compressors and turbines, as is further elaborated upon in Section 4.4.1.

Although the `GasTurbineEngine` class allows to build different cycles, the remainder of this report focuses on the turbofan configuration since it is of main interest in the PARSIFAL project. This can be supported by studying Figure 4-1 in the book by Torenbeek [17], which shows that for a flight Mach number of 0.78-0.79 [2], a turbofan will result in the minimum fuel consumption compared to other cycles. As a consequence, also the knowledge included in the individual classes is mostly related to the turbofan configuration, especially in the `TurbofanEngine` specialisation, although the engineering rules are kept as general as possible.

To standardise the communication with other disciplines, the CPACS [60] data format is employed for all input and output files of GTpy. A new toolspecific section is added to the default CPACS format to support

the component-based definition of the engines in GTpy, as presented in Appendix A. Information needed by other tools, such as engine mass and performance maps, is stored in the preallocated engine slots of the CPACS format under the vehicles/engines/engine element. Hence the use of the toolspecific format is only necessary for the engine architecture selection and sizing in GTpy. However, in the author's opinion it would be helpful to include a component-based definition of engines in the standard CPACS format, similar to the setup for complete aircraft.

Although engineering rules are implemented to minimise the number of required inputs and to automate the design process, most of the computed variables can be overwritten by the user through the input file. This may be of interest when values of an in-service component are known and can be used to adapt the model.

4.2. Design Point Analysis

Once an engine layout is selected through the CPACS input file, the thermodynamic performance at the selected design point has to be evaluated before proceeding with further analyses. Although this research focuses on turbofan engines, the procedure presented in the following paragraphs is still considered to be valid for other gas turbine based cycles which are to be sized for a combination of thrust and power. Only for highly innovative configurations, such as for example hybrid-electric engines, a revised strategy is required.

The main inputs for this procedure are, in case of a turbofan engine, the bypass ratio (BPR), the fan pressure ratio (FPR), the overall pressure ratio (OPR) and the turbine inlet temperature (TIT), which is here considered to be the total temperature of the flow at the outlet of the combustor before any cooling is added. Furthermore, a design operating point, defined by net thrust, altitude and flight Mach number, has to be provided. For a turbofan engine, this is typically the top-of-climb (TOC) or cruise condition where the corrected mass flow is at its maximum and the momentum drag is high for high bypass engines [14, 52].

Although the BPR and FPR can be set independently for a turbofan configuration, keeping all other inputs constant, an optimum FPR can be found for a selected BPR (or vice-versa) which minimises the thrust specific fuel consumption at the design point [62]. This effect is experimentally shown in Figure 4.3 for a fixed OPR and TIT. The condition for this "optimum" can be derived analytically for a turbofan configuration, and this point occurs when the ratio between the ideal (fully expanded) bypass jet velocity ($v_{19,\mathrm{id}}$) and the ideal core velocity ($v_{9,\mathrm{id}}$) is equal to the transfer efficiency of the fan drive, as expressed in Equation (4.1) [62]. In this equation, the efficiencies represent the losses which occur through the fan and low pressure turbine (LPT) themselves as well as the losses in the subsequent ducts and nozzles.

$$\frac{v_{19,\mathrm{id}}}{v_{9,\mathrm{id}}} = \eta_{\mathrm{transfer}} = \eta_{\mathrm{LPT}} \cdot \eta_{\mathrm{Fan}} \tag{4.1}$$

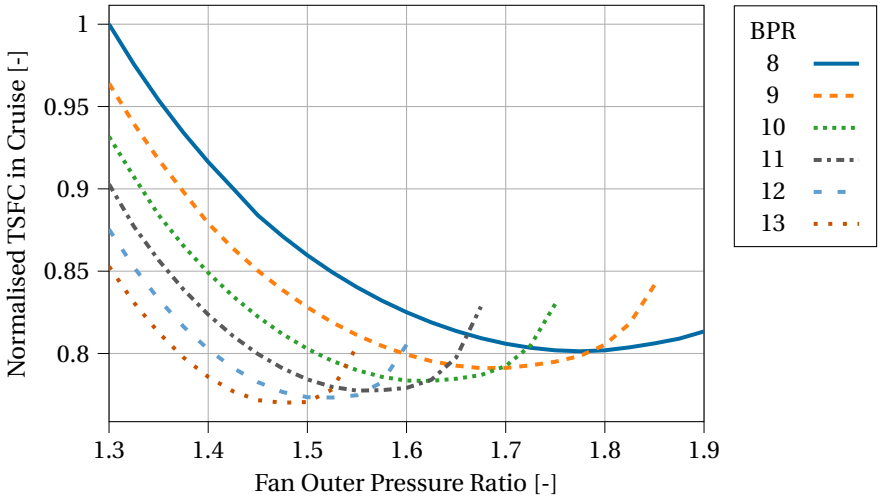

Figure 4.3: Variation of TSFC (normalised to 1.8756×10^{-5} kg/(Ns)) in cruise for varying FPR and BPR, keeping OPR (40) and TIT (1400 K) constant

Considering that such an optimum exists, only the BPR or the FPR has to be provided to the tool such that the other variable (FPR or BPR) can be adapted freely. Hence, if for example the BPR is provided as an input, the FPR is optimised such that the condition specified in Equation (4.1) is met. The objective of this small optimisation is thus to minimise the difference between the ratio of expanded exhaust velocities, and the transfer efficiency. If instead the FPR is fixed, the bypass ratio is varied to achieve the same condition. This optimum fan pressure ratio for a provided bypass ratio also maximises the specific thrust at design point [14].

Once the thermodynamic cycle is established, with or without TSFC minimisation subroutine, the required inlet mass flow at the design point ($\dot{m}_{0,\text{des}}$) can be computed to obtain the desired net thrust level, FN_{des}. This is done through the `gtpy_size` function which manages the iterations to achieve the required mass flow according to the process presented in Figure 4.4. Also the iterations to obtain the correct cooling flow ratios are carried out by this function. These ratios, which are inputs for every compressor, can be determined based on temperature limits in the turbines provided in the input file, although these iterations are optional. Additionally, since the turbomachinery components drive the geometry of the flowpath, the shape of the ducts connecting these components can be iterated upon in this function.

Before the mass flow and cooling flow iterations are initiated, an instance of the `TurbofanEngine` class is created which is altered throughout the iterations and finally provided as an output. The design points analysis and cooling estimation are considered to be converged once the absolute error between current and required thrust and temperature levels is smaller than a user set value, which by default is $1 \cdot 10^{-3}$.

The thermodynamic calculations of the individual components follow the approach presented by Greitzer et al. [19] in the large scale TASOPT research. Small modifications are implemented to simplify the overall modelling, while also certain rules and assumptions are included to minimise the number of inputs. Therefore, in the following paragraphs the thermodynamic calculations of all components are briefly discussed.

A variable specific heat $C_p(T)$ is implemented to account for the effect of temperature variations and for the changing gas composition through the combustor on C_p. The specific heat is assumed to be a polynomial function of the local temperature, where the coefficients of the polynomial depend on the gas composition (air or air-kerosene mixture) and the fuel-to-air ratio, if applicable (Formulae 3.23 and 3.24 by Walsh and Fletcher [14]). This relatively simple function improves the prediction of the total parameters at each of the component inlet and exits. It forms the basis for all basic thermodynamic calculations described in the following paragraphs.

GasPathComponent This general component does not model any thermodynamic process but defines attributes and methods which are required in all other classes and therefore do not have to be repeated. For example, all components require an inlet mass flow, total pressure and temperature, axial Mach number, type of gas and fuel-to-air ratio. It also ensures the mass flow is conserved, although this property is reconfigured in specialisations such as compressors where a fraction of the air flow may be extracted for bleed or cooling mass flows.

Fan and Compressor Although both components require similar inputs and model the same process, two separate classes are created to simplify the implementation in Python since in the case of a fan, the flow is split into two by a prescribed bypass ratio. Both components require pressure ratios and polytropic efficiencies as input variables to be able to determine the total conditions at the outlet. The use of polytropic efficiency, instead of isentropic efficiency, is preferred to model the non-isentropic process since it does not vary with pressure ratio, and hence values based on technology level can be assumed. The relation modelling the compression process is included in Equation (4.2), where indices 1 and 2 refer to the inlet and outlet conditions of a process respectively.

$$\Pi = \frac{p_{T2}}{p_{T1}} = \left(\frac{T_{T2}}{T_{T1}}\right)^{\frac{\eta_{\text{pol}} \cdot Cp}{R}} \tag{4.2}$$

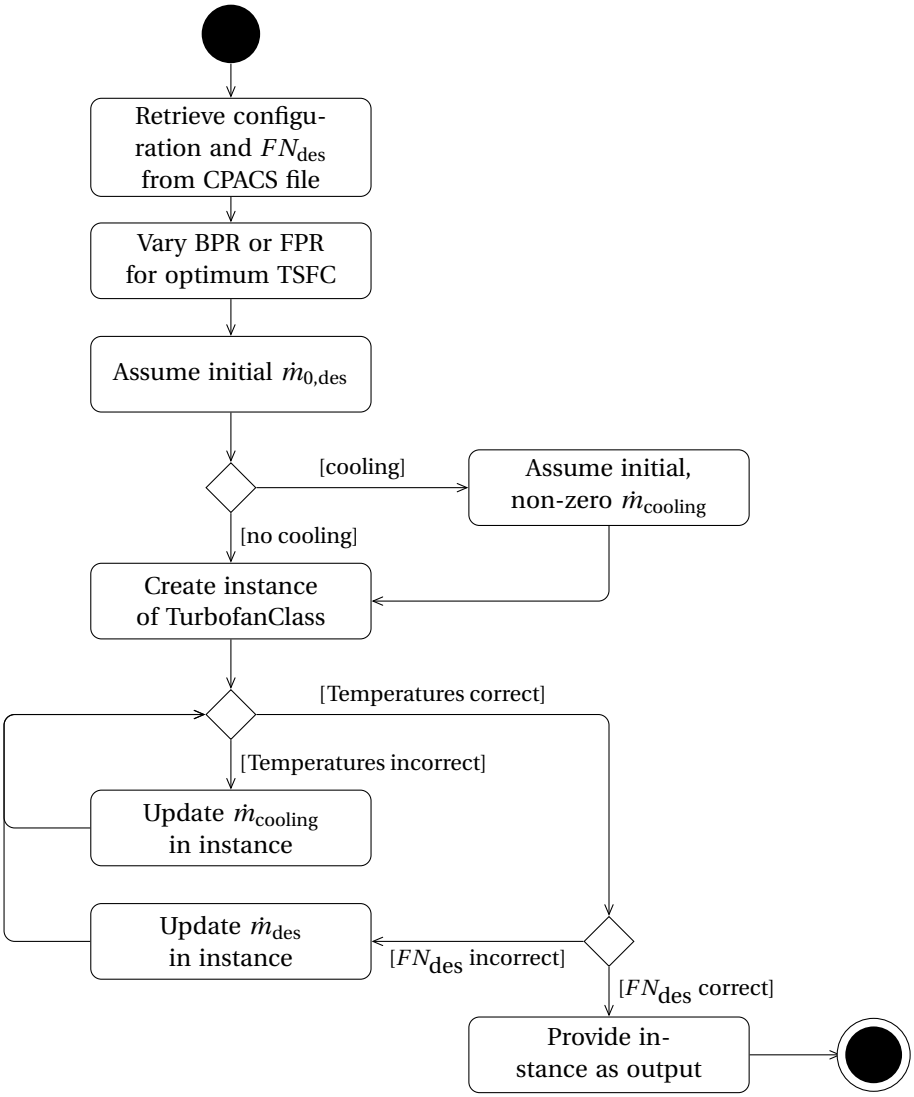

Figure 4.4: Activity diagram of the gtpy_size function which iterates upon the ingested mass flow, and optionally the cooling flows, to achieve the correct net thrust at the design point

However, it is decided to utilise a variable specific heat $C_p(T)$ to improve the accuracy, as described above. Hence, the temperature ratio cannot be calculated in a straightforward manner, but rather has to be solved through iterations. Without going into the specific of the implementation, the iterations are set up by defining $\sigma(T)$, the entropy-complement function of the gas as follows [19]:

$$\sigma(T) = \int_{T_{\text{ref}}}^{T} \frac{C_p(T)}{T}\,\mathrm{d}T \quad \text{with} \quad T_{\text{ref}} = 298\text{K} \tag{4.3}$$

This function allows Equation (4.2) to be rewritten as Equation (4.4). The latter can be solved through Newton iterations for T_{t2} at the outlet of the compressors, such that the change in C_p is accounted for. As an initial estimate, T_{t2} can be taken to be the value obtained with Equation (4.2) with $C_p(T_1)$.

$$\frac{\sigma(T_2) - \sigma(T_1)}{R} - \frac{\ln \Pi}{\eta_{\text{pol}}} = 0 \tag{4.4}$$

Once T_{t2} is computed, also the power required for the compression can be determined using Equation (4.5) where $\dot{m}_1$ is the mass flow entering the compressor, and $h_t(T_{Ti})$ (=h_{Ti}) is the total specific enthalpy at the

respective station (Equation (4.6)). $\dot{m}_1$ is employed since any air taken from the compressor for bleed or cooling purposes is subtracted from $\dot{m}_1$ at the end of the compressor, $\dot{m}_2 = \dot{m}_1 - \dot{m}_{\text{cooling}} - \dot{m}_{\text{bleed}}$. For the fan component, the total power required is the sum over the core and bypass compression processes.

$$P_{\text{comp}} = \dot{m}_1 \cdot (h_{T2} - h_{T1}) \tag{4.5}$$

$$h(T) = \int_{T_{\text{ref}}}^{T} C_p(T)\,\mathrm{d}T \text{ with } T_{\text{ref}} = 298\text{K} \tag{4.6}$$

Specifically in fans, the total pressure ratio of the core region is lower than the ratio achieved in the bypass zone since the radius in the hub region is smaller, and hence so is the circumferential speed. To model this effect, the empirical rule formulated in Equation (4.7) is included in the `Fan` class [62]. The bypass pressure ratio $\Pi_{\text{fan, bypass}}$ can be defined by the user, or calculated for a given BPR as discussed above.

$$\Pi_{\text{fan, core}} = 1 + 0.8\left(\Pi_{\text{fan, bypass}} - 1\right) \tag{4.7}$$

Combustors At the design point condition, both the inlet conditions and the outlet temperature T_{T2} are known. Hence, the pressure at the outlet p_{T2} and the added fuel flow have to be determined. p_{T2} is smaller than the inlet pressure due to small losses in the combustion process and to avoid hot flows entering the preceding components, usually compressors. Hence, it is assumed that for modern compressors $p_{T2}/p_{T1} = 0.95$ [8].

The fuel mass flow $\dot{m}_{\text{fuel}}$, is obtained through an enthalpy balance over the combustor, as described by Equation (4.8) where η_{comb} is the combustion efficiency. The latter parameter defaults to 0.99 in the application to account modern combustor technology levels [8]. Equation (4.8) also has to be solved iteratively since h_{T2} depends on $C_p(T_2)$, which in turn relies on the fuel-to-air ratio of the gas leaving the combustor and thus the fuel flow $\dot{m}_{\text{fuel}}$.

$$\dot{m}_1 \cdot h_{T1} + \dot{m}_{\text{fuel}} \cdot h_{\text{fuel}} \cdot \eta_{\text{comb}} = (\dot{m}_1 + \dot{m}_{\text{fuel}}) \cdot h_{T2} \tag{4.8}$$

$$\Rightarrow \dot{m}_{\text{fuel}} = \dot{m}_1 \cdot \frac{h_{T2} - h_{T1}}{h_{\text{fuel}} \cdot \eta_{\text{comb}} - h_{T2}} \tag{4.9}$$

Turbines The main inputs for a turbine component are the power it has to deliver, needed to drive compressors or taken to power other systems, the polytropic efficiency and any power added to the turbine, for example by an electric motor. However, before the conditions at the outlet are determined, first any cooling flows calculated by the dedicated loop in Figure 4.4 are added. This is completed by a simplified mixing model where the inlet and cooling mass flows are added and the fuel-to-air ratio of the resulting mixture is updated, assuming no pressure losses occur. Knowing the conditions at the inlet (T_{T1}, p_{T1}, $\dot{m}_1$) and assuming no pressure losses occur in the mixing process, the sum of the inlet and cooling mass flows is then used to determine the pressure drop over the turbine.

The total power to be produced by the turbine, P_{turb}, is given by Equation (4.10), where the first term is the sum over all N compressors relying on the turbine under consideration. From the resulting P_{turb}, a change in specific enthalpy is determined Δh (< 0 for turbines), which in turn is employed to find the temperature and pressure at the outlet of the turbine, T_{T2} and p_{T2} respectively. Similarly to the process for compression, these parameters can be obtained by iteratively solving Equation (4.11) for T_{T2}.

$$P_{\text{turb}} = \sum_{j=1}^{N} P_{\text{comp},j} + P_{\text{offtake}} - P_{\text{added}} = \Delta h \cdot \left(\dot{m}_1 + \dot{m}_{\text{cooling}}\right) \tag{4.10}$$

$$h_{T2} - h_{T1} - \Delta h = 0 \tag{4.11}$$

The current implementation also requires the user to specify mechanical efficiencies for each turbine since also in the GSP model these bearing and windage losses are accounted for in the turbine components. This follows from the assumption that only one turbine can be connected a single shaft, while multiple compressors can be attached to a certain shaft. Although not shown in the above equations, these efficiencies are thus actually attributed to a certain shaft rather than a turbine. As a result, the mechanical efficiency is taken into account in the $P_{\text{comp},j}$ term. For modern turbofan engines, the mechanical efficiency of each shaft is estimated to be equal to 99% [14].

Ducts and Inlets In these components no mechanical work and/or heat is added, nor extracted. Hence, the total temperatures at the inlet (T_{T1}) and outlet (T_{T2}) are equal. Nevertheless, losses in total pressure can occur due to viscous effects and/or inappropriate aerodynamic design. Such losses are modelled by specifying a loss $\Delta p_T = p_{T2}/p_{T1}$. For inlets, Δp_T is assumed to be equal to 0.98 [8], while for other internal ducts this parameter is set to 0.99 by default. The designer can manually overwrite these values in case of non-standard or older designs through the CPACS input file.

Convergent Nozzles In its current implementation, only convergent nozzles are supported. Convergent-divergent nozzles can offer more thrust than a purely convergent exhaust when the nozzle pressure ratio is large enough. However, in case of turbofan engines, this pressure ratio is limited and adding a convergent-divergent nozzle does not lead to a performance improvement which outweighs the increase in weight and length [62]. Nevertheless, a convergent-divergent nozzle class can be added later to study low bypass turbofan or turbojet engines.

For the thermodynamic process, the pressure at the inlet of the nozzle is of importance. This determines whether the throat of the nozzle is choked or not. This condition can be checked by calculating the critical pressure ratio and comparing it to the actual pressure ratio. In case the nozzle is choked, the Mach number in the throat (M_{thr}) will be equal to 1, else the number is less than this value. In either case, the static conditions in the throat can be calculated using the isentropic relationships since the total pressure in the component is known.

From the static conditions, the axial velocity of the gas leaving the nozzle (v_{thr}) and the cross-sectional area of the throat (A_{thr}) can be computed. The gross thrust of the nozzle can be computed for the nozzle employing the relations in Equation (4.12). In case the nozzle is choked, the flow has to further expand outside of the nozzle to reach the ambient static pressure (p_{amb}). This results in an additional thrust component. In either case, a thrust coefficient C_x is employed to take into account any losses in the nozzle due to friction and flow non-uniformity [14]. The relation presented in Chart 5.14 (Figure 4.5) of the book by Walsh and Fletcher [14] is employed to automatically determine this coefficient in the application.

$$\begin{cases} FG = C_x \cdot \dot{m} \cdot v_{\text{thr}} \text{ if } M_{\text{thr}} < 1 \\ FG = C_x \cdot \left[\dot{m} \cdot v_{\text{thr}} + \left(p_{\text{thr}} - p_{\text{amb}}\right) \cdot A_{\text{thr}}\right] \text{ if } M_{\text{thr}} = 1 \end{cases} \tag{4.12}$$

GasTurbineEngine and TurbofanEngine In the high-level classes, instances of the previously described components are combined to construct a single thrust-producing engine cycle. Power balances between compressors and turbines are ensured by these classes, while also system parameters such as total net thrust FN are computed. The general formulation of FN is provided by Equation (4.13), where the gross thrust FG is the sum of the gross thrust forces produced by the individual N nozzles. $\dot{m}_{0,\text{ des}}$ and $v_{0,des}$ are the total ingested mass flow and flight velocity at the design point respectively.

$$FN = FG - \dot{m}_{0,\text{ des}} \cdot v_{0,des} = \sum_{j=1}^{N} FG_j - \dot{m}_{0,\text{ des}} \cdot v_{0,des} \tag{4.13}$$

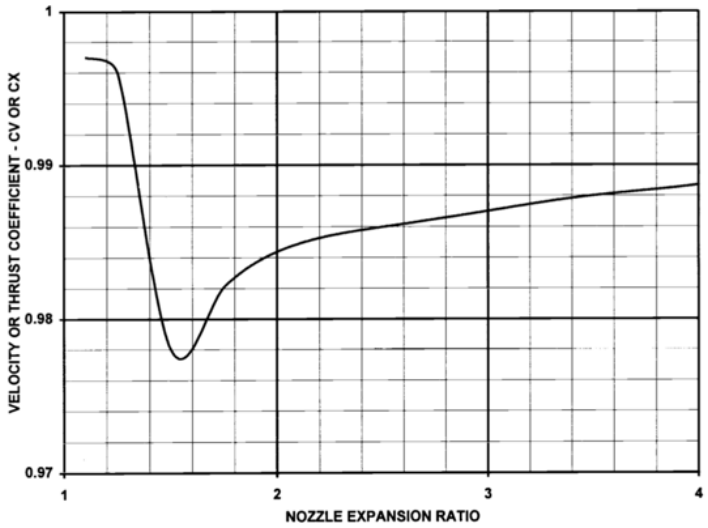

Figure 4.5: Convergent nozzle thrust coefficient as a function of nozzle expansion ratio [14]

4.3. Off-design Point Analysis

The design point analysis, as discussed in the previous section, provides the necessary parameters to trigger the off-design analysis and to evaluate the behaviour of the engine at other operating points of interest, such as take-off, and throughout the entire flight envelope of the aircraft. The data from these two analysis types can in turn be employed in the sizing step of the engine (e.g. for the mass estimation) and allows to perform a complete mission analysis of the aircraft including variations in available thrust and fuel consumption.

The off-design analysis in this research is carried out by GSP [61]. This software is selected since it has been verified and validated for several other projects and because its application programming interface (API) allows to run the models from other programming languages. A new interface between Python and GSP is developed, making use of the predefined API functions such that the GSP calls can be coordinated from the Python based GTpy tool or the ParaPy user interface.

The use of external software aligns with the DEE strategy, i.e. to translate the ParaPy model of the engine to a discipline specific representation which facilitates the use of higher fidelity, external software. To do so, the data from each component instance in Python is mapped onto the XML structure which can be interpreted by GSP. To simplify this process, for each component class a GSP template is prepared which can be filled out by the instances of a class in GTpy. The complete GSP input file is then prepared in the `GasTurbineEngine` or `TurbofanEngine` class by collecting XML elements written by individual classes in one large XML file. This process is schematically shown in Figure 4.6.

The GSP API and error equation elements are automatically added to the XML file to support the two aforementioned analysis types. The GSP API can construct the engine model, without any user interaction, and selects the correct sets of state and error variables needed to simulate the engine system. The error equation component ensures that a given engine variable, such as the net thrust or rotational speed, is equal to a value specified by the user in the off-design analysis. Advanced engine control components (e.g. for bleed flow or temperature limits) are not included in this research.

The analysis with GSP requires component maps for the fan, compressors and turbines such that the component pressure ratio and mass flow can be related to the rotational speed and the efficiency. Since these maps cannot be constructed at this design stage, they are taken from literature [63, 64, 65] and from the GSP built-in map library. The selection of correct low speed or high speed map for compressors and turbines is based on the relative location of the component in the flowpath and the pressure ratio compared to other instances of the same component type.

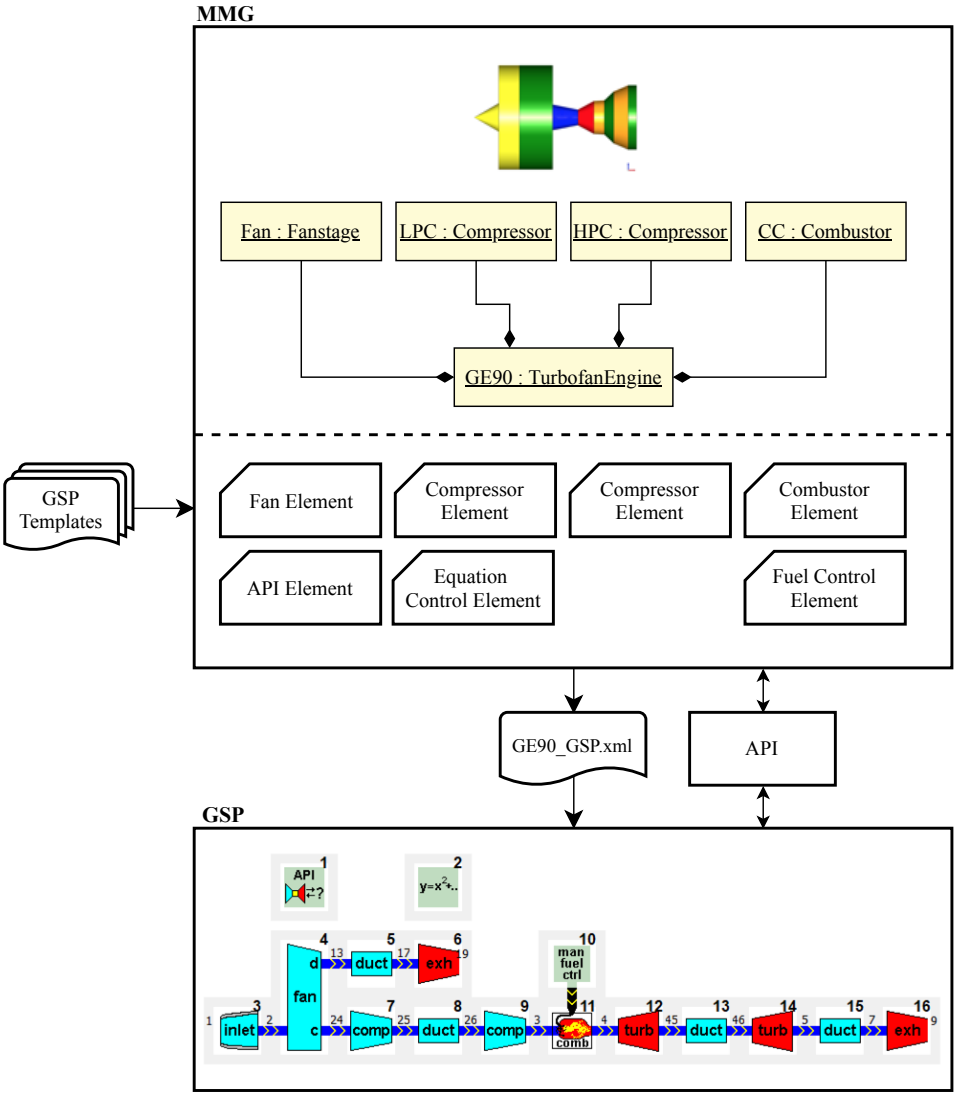

Figure 4.6: Diagram showing the connections between the MMG (Python) and the Gas turbine Simulation Program (GSP). Certain components such as ducts, turbines and exhausts are omitted in the MMG model for clarity.

For the first type of analysis, for example when the engine characteristics at take-off are unknown, the required thrust and flight conditions have to be provided to the API. For take-off, the latter can be set sea level static conditions. An error equation component is automatically added to the GSP model in order to converge to the required thrust. Through multi-variable Newton-Raphson iterations, the error variables are minimised by finding the correct values for the set of state variables. For a general two-spool turbofan engine, the latter set typically includes the corrected mass flow, spool speeds, pressure ratios, and bypass ratio [61]. In addition to the error equation for the thrust, error variables are selected by the program to imply power and mass flow balances.

To create a performance deck of the engine, the net thrust is not explicitly specified, but rather controlled by a thrust setting. In this research, the speed of the first spool, typically the fan spool, specified as a percentage of the design speed (N1%), is selected as control variable because it correlates directly to ingested mass flow, which in turn is proportional to the produced net thrust [66]. For each point in a specified set of flight conditions, N1% can be varied in a range between e.g. 20 and 100%, depending on the operational conditions, to obtain the net thrust and fuel consumption throughout the flight envelope. From this outcome, also the thrust lapse rate can be computed.

4.4. Size and Weight Estimation

The results from the design and off-design analyses are utilised to preliminary size the engine flowpath and estimate the bare engine weight. In this research the selected reference point (i.e. TOC or cruise) will be used for both thermodynamic as well as basic mechanical design of the turbofan engine. Although the design of different components is normally driven by different operating conditions, in the early design stages one operating condition is considered to be sufficient to size the components and the flowpath [14, 41]. Furthermore, since this research focuses on the engine integration, the outer geometry and basic flowpath are of main importance, and hence the more detailed design of components is deemed out of scope.

4.4.1. Geometry

The flowpath of the aero engine, defined by local diameters and component lengths, is to be constructed since it allows to build a nacelle suited to the specific engine in later stages. An example of such a flowpath is shown in Figure 4.7 for a two-spool turbofan, where each type of component is drawn using a different colour. The general rule is that outlet of a component defines the inlet of the subsequent component, although exceptions can be made by introducing ducts. Additionally, the calculation of the axial length is distinct for every component. Therefore, an overview of the implemented sizing rules is provided in this section.

A preliminary flowpath geometry can be constructed by assuming local axial Mach numbers at component in- and outlets, and by carrying out a basic meanline design of the turbomachinery components [14, 41]. The Mach number and isentropic relations are employed to calculate the local static pressures and temperatures at the inlet and outlet of the components when the total counterparts are known from the design point analysis. From the static values, the local density and axial velocity of the flow can be determined, allowing to compute the cross-sectional area (A_i in Figure 4.8) since the mass flow is known. If a local hub-to-tip ratio ($R_{h,i}/R_{t,i}$) is provided or if an annulus type is selected from Figure 4.9, the circular cross-section is defined by its hub and tip radii, $R_{h,i}$ and $R_{t,i}$respectively. This calculation is valid for all currently components currently modelled in GTpy.

Fan The diameter of the fan is determined by the design mass flow calculated with the procedure from Figure 4.4, and an axial Mach number of 0.6 at the inlet [67]. Additionally, a hub-to-tip ratio of 0.3 is specified at this station. This maximum diameter is constant for the fan component. At the outlet the mass flow is split into two, according to the bypass ratio: one portion will pass through a bypass duct, while the other part continues its path through the core of the engine. The cross-sectional areas at the end of the fan are computed based on the static conditions at this location where the Mach number is assumed to be between 0.4 and 0.5.

The hub radius of the bypass outlet is found from the maximum diameter and the respective outlet area. Then a small splitter wedge is added, with a height equal 3% to the inlet tip radius, and a length of 20% of the total

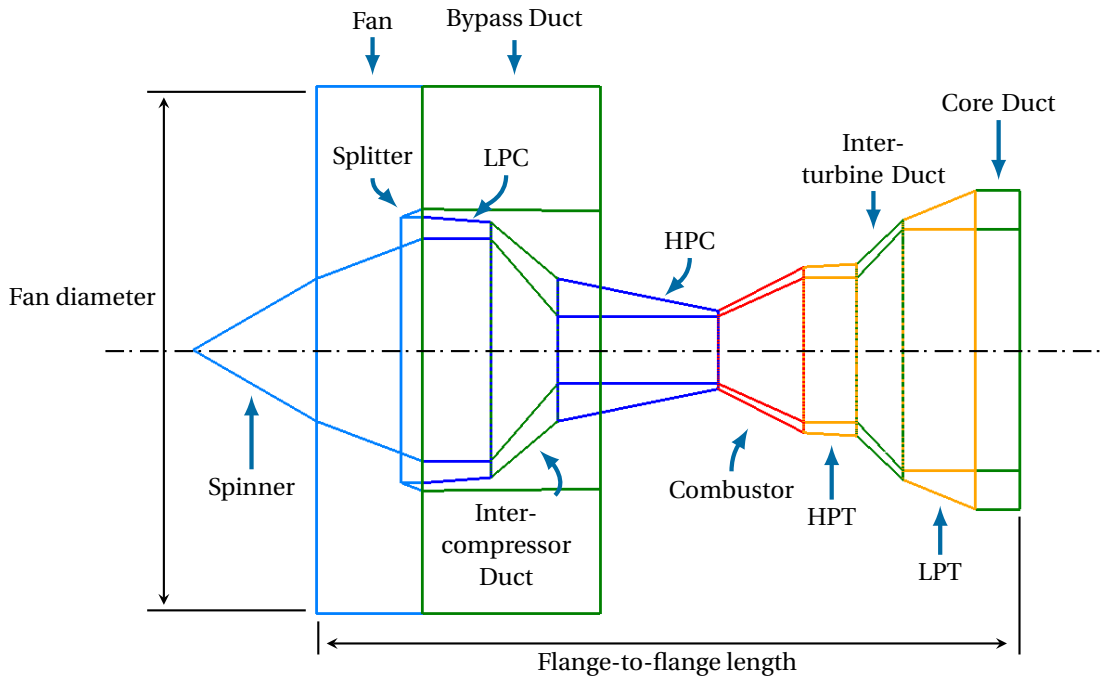

Figure 4.7: Cross-section of the aero engine flowpath generated by GTpy. Each colour represents a different component type.

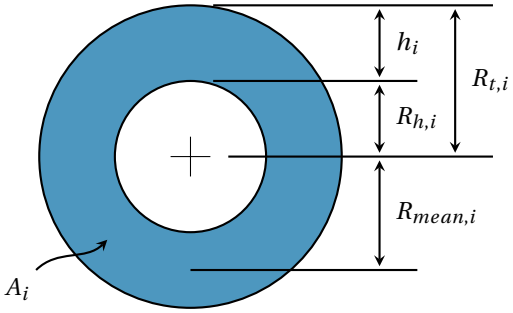

Figure 4.8: Cross-section of arbitrary station i between two subsequent components

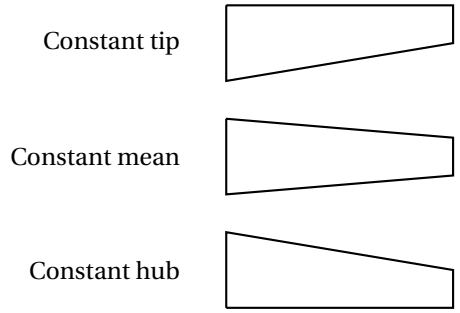

Figure 4.9: Three annulus types options which can be specified to automatically determine the hub-to-tip ratio of the outlet

fan component length, as estimated from publicly available engine diagrams [68, 15]. Subsequently the hub radius of the core exit is retrieved from the core side cross-sectional area. Although the assumed parameters generally result in an outlet hub radius which is larger than the inlet hub radius, care should be taken that this inequality is not reversed. The increase in hub radius exerts a force on the fluid required to increase the pressure ratio of the core side.

The axial length of the fan component is estimated by preliminary sizing the fan blades. The axial chord is found by multiplying the approximated height of the fan blades (retrieved from the hub and tip radii) with an aspect ratio of 2.73 [18]. This axial chord length is multiplied by 1.5 to account for clearances and the splitter to find the total axial length.

As discussed further in the following paragraph, the fan drives the rotational velocity of the connected shaft at the design point, $N1_{\text{des}}$. This velocity is calculated based on the maximum relative tip Mach number of the fan blades (currently set to 1.6 [14]), and the tip radius of the fan blades.

Compressors and Turbines Both of these turbomachinery components follow a similar mean line design procedure. The rotational speed performs an important role in the mean line design, and has to be assumed or calculated for each shaft. Although this speed is typically a trade-off between the performance and mechanical stresses in each of the components attached to a single shaft, in this research only one of the com-

ponents is accepted to drive the speed. This component can be specified by the user or is taken to be the first component in the flowpath lying on a certain shaft. In the case of a two-spool turbofan, the fan and high pressure compressor are assumed to drive the speed of the respective shafts, while the other components are considered to follow the rotational speed prescribed by these components.

Whether the component drives the speed or not, use is made of non-dimensional parameters including the flow ϕ and load λ coefficients to determine the component dimensions. However, first the number of stages has to be estimated such that the work per stage is known. For both component types, the user can manually specify the number of stages or the number can be estimated through iterations. First the automated design strategy for compressors is elaborated upon, followed by the approach for turbines.

Since the pressure ratio a single compressor stage can deliver is limited, and since the high pressure ratio is achieved in the first stage, the number of stages is increased until the pressure ratio over the first stage is below the maximum value of 1.6 [18]. Here it is assumed that each stage performs an equal amount of work, Δh_s. This method does however take into account variable inlet guide vanes which may have to be added in front of the other stages.

For the turbine two approaches can be taken: or a maximum diameter can be imposed, or a specific speed N_s can be targeted. For the first approach, the work per stage (Δh_s) is equal to the total turbine power divided by the estimated number of stages. Then the mean radial velocity U_{mean} can be determined using the definition of the load coefficients, as shown in Equation (4.14). For a modern turbine, the load coefficient λ is assumed to be 4 [69]. Then the maximum tip radius of the turbine can be calculated from the mean radius R_{mean}, rotational velocity ω and outlet area of the turbine A_{out}, following the procedure from Equations (4.15) to (4.17). Once $R_{\text{t, out}}$ is less than the desired maximum diameter, the correct number of stages is found.

$$U_{\text{mean}} = \sqrt{\frac{2\Delta h_s}{\lambda}} \tag{4.14}$$

$$R_{\text{mean}} = \frac{U_{\text{mean}}}{\omega} \tag{4.15}$$

$$h_{\text{out}} = \frac{A_{\text{out}}}{2\pi R_{\text{mean}}} \tag{4.16}$$

$$R_{\text{t, out}} = R_{\text{mean}} + \frac{h_{\text{out}}}{2} \tag{4.17}$$

Alternatively, a certain specific speed N_s based on load and flow coefficient from literature, defined by Equation (4.18), can be achieved by varying the number of stages and thus Δh_s. The optimum flow coefficient ϕ for a given load coefficient can be selected employing Equation (4.19) [69]. The first approach is for example preferred when designing a low pressure turbine for a turbofan engine. This ensures that the turbine does extend into the bypass duct. The second approach however proves to be more useful for smaller high pressure turbines in turbofan engines.

$$N_s = \frac{\phi^{\frac{1}{2}}}{\psi^{\frac{3}{4}}} = \frac{\omega \cdot Q^{\frac{1}{2}}}{\Delta h_s^{\frac{3}{4}}} \text{ with } \psi = \frac{\lambda}{2} \text{ and } Q = \frac{\rho}{\dot{m}} \tag{4.18}$$

$$\phi = \sqrt{\frac{\psi^2 - 1}{4}} \tag{4.19}$$

Once the number of stages is known, either for a compressor or a turbine, the length can be approximated. Onat and Klees [18] suggest an approach where the aspect ratio of the blades at the start and end of the component are roughly known from reference engines, and the aspect ratios of the blades in between can be evaluated by simple linear interpolation. Since the annulus height at the inlet and outlet are known from

simple sizing with Mach number and hub-to-tip ratio, the axial chord length can be found by calculating the height at intermediate stages and multiplying the height by the estimated local aspect ratio.

Aspect ratios for the compressor and turbines are gathered in Section 4.4.1. Note that a compressor with ten stages in fact has twenty blade rows, neglecting potential variable inlet guide vanes. To determine the height and lengths of the individual stages, instances of the `TurbomachineryStage` are employed. These instances do not model the actual blade geometries, but rather account for their presence. In addition to the chord lengths, a relative blade spacing of 17% per blade is assumed. The complete length is then sum of the individual stage chord lengths plus a small blade spacing per blade row.

Table 4.1: Assumed blade aspect ratios for the length calculation of turbomachinery stages [18]

		Inlet	**Outlet**
Compressor	LP	4.0	3.0
	HP	3.0	1.5
Turbine	LP	2.0	4.0
	HP	1.5	1.5

Ducts The geometry creation of ducts is rather straightforward. Since ducts have to be placed behind another component, the duct inlet is aligned and sized with the outlet of this preceding component. The user can then control the axial length and the hub-to-tip ratio and axial Mach number at the outlet. If these are not provided manually, the same parameters as at the inlet station are taken and only a drop in total pressure can slightly modify the exit cross-section. The length is then assumed to be equal to the length of the previous component.

A different automated design strategy can be selected when the ducts are placed between turbomachinery components. If compressors or turbines are automatically sized as described above and the diameters at the inlet and outlet are known, these geometries can drive the change in radial cross-section of the intermediate ducts. Hence, the ducts are adapted to provide a logical transition between more dominant components. In this case the axial length of the duct is assumed to be equal to the change in radial height.

Combustors Similarly to ducts, a combustor is modelled by specifying hub-to-tip ratios and Mach numbers at the exit plane, or it can be adapted to turbomachinery components enclosing the combustion chamber. However, differently from ducts, the axial Mach number is typically lower in the combustion chamber than in the rest of the flowpath [14], according to the specific flow and cooling requirements. Hence, the outlet Mach number of the combustor is by default set to 0.1 [19]. This low Mach number together with a tailored residence time, here assumed to be equal 3 ms [14], drive the axial length of the combustor. The average axial flow velocity between the inlet and outlet stations is multiplied by this residence time to obtain the length of the burner component.

As can be seen in Figure 4.7, the combustor appears to be quite thin when compared to other engine diagrams. This is because the component is merely modelled as a narrow trapezium, while in an actual application this component is wider because the flow is split into primary, secondary and tertiary flows. However, the overall engine dimensions, normally determined by components such as the fan and the turbines, are of main interest in this research, and thus a more detailed design of the combustor is out of scope.

Inlets In the current modelling process of GTpy the thermodynamic process of inlets is considered to be part of the engine performance analysis. However, the geometry creation of the inlet is a part of the nacelle design process. Therefore, the inlet design rules are discussed in Section 5.1.2.

Spinner The spinner (nose cone) at the start of engine is modelled as a simple cone following an angle of 30 degrees pointed in the forward direction. The base of the radius of the cone is equal to the hub radius of the first non-inlet. For the engine configuration shown in Figure 4.7, the spinner base radius is derived from the fan radius.

4.4.2. Weight Estimation

The total weight of the bare engine is estimated using correlations developed for the TASOPT routine [19]. The analytical correlations are based on simulations by the more detailed WATE++ aero engine mass estimation software. This program employs a component-based weight prediction method and thus develops the engine mechanical design in more detail. Using seven currently available engines, the WATE++ model was calibrated and used to simulate hundreds of engines with varying BPR, OPR and inlet mass flow. The resulting relations are able to estimate the masses of the calibration engines within ±10% of the published data, except for the CFM56-7B27 engine. Note the mass in this section refers to the mass of the bare aero engine, hence including component casings and accessories, but excluding structural elements such as thrust links, pylons and nacelles.

The weight of turbofan engine can be assessed using Equation (4.20), where a, b and c are polynomial functions of the bypass ratio. These polynomials are presented in Equations (4.21) to (4.23) for a direct drive engine with current technology levels. Other polynomials, with varying multipliers, are available to represent cases with new technology infusion, leading to a weight reduction as well as engines with a geared fan. For an engine without a geared fan, the relations are based on simulations with bypass ratios varying between 4 and 20, and overall pressure ratios between 25 and 60. In the simulations with a geared fan, the maximum bypass ratio tested was 50.

$$W_{\text{eng}}[\text{lbs}] = a \cdot \left(\frac{\dot{m}_{\text{core}}[\text{lb/s}]}{100} \right)^{b} \cdot \left(\frac{OPR}{40} \right)^{c} \tag{4.20}$$

$$a = 18.09 \cdot BPR^2 + \left(4.769 \cdot 10^{2}\right) \cdot BPR + 701.3 \tag{4.21}$$

$$b = \left(1.077 \cdot 10^{-3}\right) \cdot BPR^2 - \left(3.716 \cdot 10^{-2}\right) \cdot BPR + 1.190 \tag{4.22}$$

$$c = \left(-1.058 \cdot 10^{-2}\right) \cdot BPR + 0.232 \tag{4.23}$$

This weight estimation method is selected at this stage since it is simple to implement and since it allows for fast evaluation. Furthermore, the chosen variables, $\dot{m}_{\text{core}}$, BPR and OPR, are well suited since they capture the effects both thrust and technology level have on the engine mass. It is necessary to use the performance values at take-off for this relation since these are employed to calibrate the above relationship. Hence, an off-design analysis with GSP has to be completed prior to the weight estimation.

Based on the data provided in the TASOPT research report, constant weight fractions are assumed for the components of a two-spool turbofan. These are gathered in Table 4.2 and can be employed to predict the location of the centre of gravity of a two-spool turbofan engine along its centre line. This approach however does not work for engine architectures with three shafts or variables nozzles, and therefore it is recommended to replace this correlation based method with a complete component-based weight estimation as described by Onat and Klees [18].

Table 4.2: Average weight fractions of main components for a general two-spool turbofan engine [19]

Component	**Weight fraction of total engine weight [%]**
Fan	26.00
Low Pressure Compressor	5.92
High Pressure Compressor	10.78
Combustor	4.83
High Pressure Turbine	10.13
Low Pressure Turbine	23.5
Accessories & Other Components	18.84

4.5. Verification and Validation

As described in the previous sections, the design routine of the propulsion system is programmed in Python, while the GSP software provides off-design analysis capabilities. To ensure that all individual blocks of code and the connections work correctly, the General Electric GE90 engine, powering the Boeing 777 aircraft, is selected as a verification and validation case. This engine is chosen since a relatively large amount of information about the design is publicly available. The design data employed to model this engine, is gathered in Table B.2 [21, 19, 20]. The cruise phase is considered as the reference point, while take-off is considered an off-design operating condition. The requirements defining these points are summarised in Table B.1.

4.5.1. Design Point Performance Verification

Since the design point analysis is executed by GTpy (Python), the calculation of thermodynamic parameters (pressure, temperature, enthalpy, etc.) is verified with a GSP model of the GE90 engine to ensure that all physical relationships are correctly implemented in Python. The input parameters utilised in both the GTpy and GSP models are summarised in Table B.2. This is an important step since this analysis in GTpy forms the basis for all other design steps. A subset of the results of this verification are shown in Table 4.3, where the subscripts indicate the corresponding station according to ARP 755A station numbering [14]. The close agreement between the two tools indicates that the analysis is carried out accurately. Minor differences can be explained due to a different model for the change in specific heat (at constant pressure) as a function of temperature, $C_p(T)$.

Table 4.3: Verification of the design point analysis in GTpy (Python)

Parameter	**GTpy**	**GSP**	**Difference [%]**
T_{T3} [K]	306.34	306.17	+0.06
P_{T3} [Pa]	70906	70884	+0.03
A_9 [m^2]	0.75022	0.74798	+0.30
A_{19} [m^2]	3.9944	3.9950	-0.02
$\dot{m}_{\text{fuel}}$ [kg/s]	1.2104	1.2136	-0.26
TSFC [kg/(N s)]	1.5548×10^{-5}	1.5588×10^{-5}	-0.26
FN [N]	77850	77857	-0.01
FG [N]	219222	219182	+0.02

4.5.2. Off-Design Analysis Validation

To obtain an accurate prediction of the engine performance throughout the flight envelope, the capabilities of GSP are employed. An engine deck of the GE90 is created and compared to data provided in Appendix J of Nicolai and Carichner [70] and to the empirical model proposed by Bartel and Young [37]. The results are presented in Figures 4.10 and 4.11 for the thrust specific fuel consumption and net thrust at 100% N1% respectively. The values are normalised with respect to the sea-level-static value of the data set by Nicolai and Carichner.

As can be seen in the plots, the results produced by GTpy and GSP correspond relatively well to data provided by Nicolai and Carichner [70]. However, at low Mach number and altitude, a difference of approximately 10% is present between the GSP model and the data published by Nicolai and Carichner. A logical explanation is that certain variants of the GE90 are rated at more than 100% N1% in these conditions, allowing for more thrust for a short period of time. When N1% is increased by 5%, the GSP analysis intersects with the available data. Additionally, minor discrepancies are expected because the input and validation data may not be available for the exact same GE90 type.

The model by Bartel and Young [37] appears to work well in the take-off regime, but overestimates the thrust in other flight conditions. Especially for h = 5000 ft and h = 10000 ft, the lines show a trend which is more alike to turbojets or low-bypass turbofans [14]. Furthermore, the empirical model is only capable of predicting the TSFC accurately in the cruise regime, while GSP produces a more reliable model throughout the entire flight

envelope. Nevertheless, the empirical model requires less computational time, and thus may be of interest when only the cruise phase is considered.

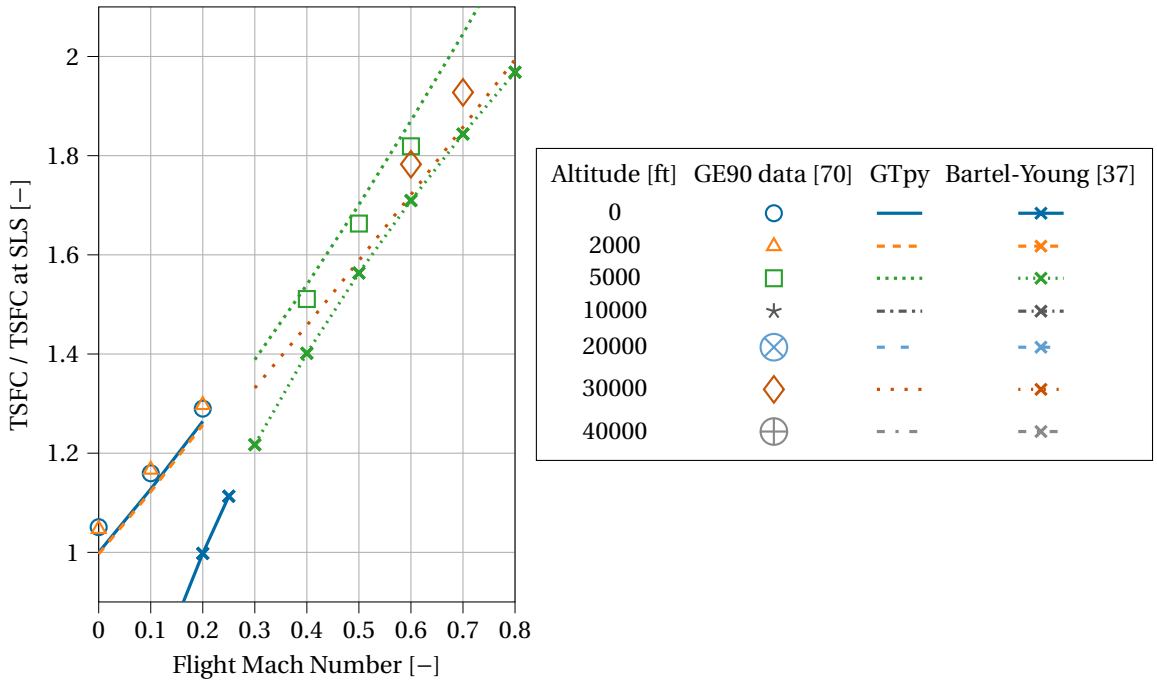

Figure 4.10: Validation of TSFC calculation throughout the flight envelope with GTpy and GSP, compared to GE90 engine data [70, Appendix J] and the empirical model presented by Bartel and Young [37]

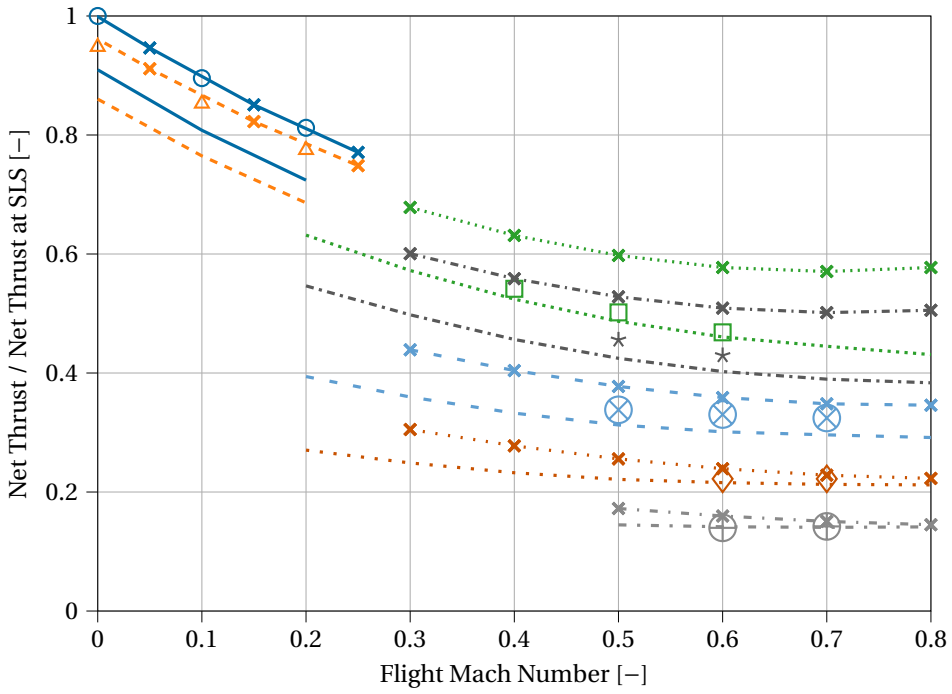

Figure 4.11: Validation of net thrust calculation throughout the flight envelope (N1% = 100%) with GTpy and GSP, compared to GE90 engine data [70, Appendix J] and the empirical model presented by Bartel and Young [37]

4.5.3. Size and Weight Validation

In Table 4.4 a limited set of dimensions and the estimated mass obtained with GTpy are compared to actual GE90 data [20]. It can be seen that the error in the fan diameter and the weight are relatively small. Also the difference in predicted number of turbomachinery stages appears to be limited. However, although GTpy overestimates the number of stages, the overall flange-to-flange length of the engine is underestimated by approximately 12%. Although the difference in mass is rather small, it is expected since the GE90 engine was employed to calibrate the simulations completed to create Equation (4.20).

Table 4.4: Validation of the engine sizing and weight estimation in GTpy [20]. Dimensions are indicated in Figure 4.7

Parameter	**GTpy**	**Data**	**Difference**
Fan diameter [m]	3.22	3.40	-5.29 %
Flange-to-flange length [m]	4.30	4.90	-12.24 %
Number of LPC stages	4	3	+1
Number of HPC stages	10	10	0
Number of HPT stages	3	2	+1
Number of LPT stages	6	6	0
Bare engine mass [kg]	7809	7825	-0.20 %

By comparing the cross-section produced by GTpy with an actual one taken from literature Figure 4.12, it can be seen that although the lengths of the fan, LPC and turbines appear to be well estimated, especially the axial lengths of the inter-compressor duct and the high pressure compressor are underestimated. Although not confirmed, it is expected that more space is required for structural elements in the duct. Additionally, the variable inlet guide vane present in front of the GE90 HPC is not accounted for in GTpy.

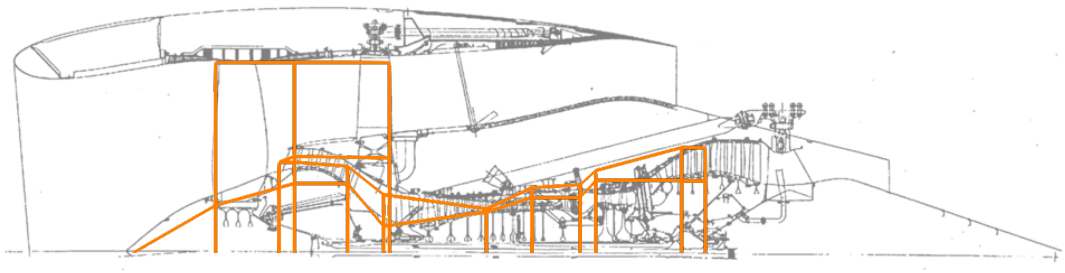

Figure 4.12: Cross-section of GTpy GE90 model (in orange) placed on top of the actual cross-section [15]

Furthermore, it should be noted that the differences obtained in this validation step are expected to vary with the chosen reference engine. If an automated design of the CFM56-7B is carried out, the length and fan diameter differ only by -0.62% and -3.64% respectively from the values provided by Jane's Aero-Engines [68]. However, as pointed out by Greitzer et al. [19], Equation (4.20) does not allow to predict the mass of the CFM56-7B engine as well as that of the GE90. It can be concluded that engine manufacturers make distinct design decisions and trade-offs, and that these decisions cannot be fully captured with the assumptions made in this research. Hence, it is advised to further examine how the mechanical design can be implemented in the GTpy application.

5

Airframe Integration

Once the geometry of the aero engine is known, the installation on the aircraft can be completed. Since this research only considers podded turbofan engines, the creation of nacelle and pylon geometries is required. This chapter describes the extension of the aircraft model in the Multi-Model Generator to include the engines and nacelles.

Considering the object-oriented structure of the Multi-Model Generator, a separate class is created for the nacelle. This class can be instantiated from user inputs or from attributes of a `TurbofanEngine` instance. The engine and nacelle instances are combined in a class called `EngineInstallation` which is considered at the same level as other High Level Primitives such as Wings and Fuselages, as illustrated by Figure 5.1. Instantiating the nacelle and engine in another class instead of creating the geometries separately in the `Aircraft` class allows to consider the installation in itself without the need of an `Aircraft` instance, and allows to implement certain rules which are dependent on both the nacelle and the engine without cluttering the aircraft class. Hence, the creation of the `EngineInstallation` class is mainly driven by implementation convenience.

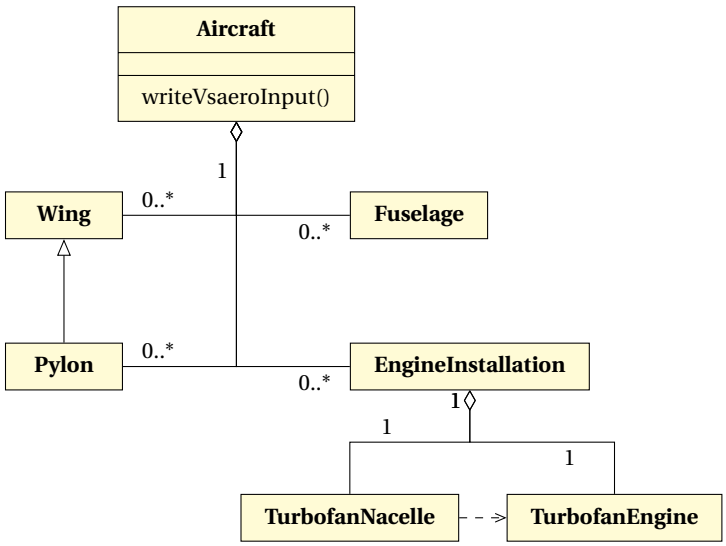

Figure 5.1: Class diagram of the High Level Primitives in the MMG

A separate `TurbofanNacelle` class is built specifically for high bypass turbofan engines. Hence, this class can for example not be used for turbojet, turboprop, or mixed-exhaust turbofan engines. The reason for this is that attributes of the specialised `TurbofanEngine` are used to size the turbofan nacelle, and these attributes and the associated design rules are different for other engines. Nevertheless, the methodology and the underlying curve classes (as treated in Section 5.1) can be employed to define other nacelle types.

As can also be seen from the diagram, the pylon is a specialisation of the existing Wing class (`WingFromRails`) in the current implementation of the MMG. This allows to make use of existing rules facilitating the geometric

intersections with the fuselage and the meshing of the aircraft. Nevertheless, this imposes some restrictions on the pylon design, which are discussed in Section 5.2. Nevertheless, the pylon is currently independent of the engine type and can potentially be employed for the installation of turboprop or turbojet engines.

5.1. Nacelle Design

The nacelle shape follows from various requirements, the driving ones being the structural fairing to the engine and the reduction of aerodynamic drag of the podded installation. Kozaczuk [71] researched the requirements following from operator and certification perspectives, resulting in the following short list of functions of the nacelle which have to be considered, while minimising the weight:

- allow for efficient airflow into and out of the engine throughout the entire flight envelope
- provide structural strength to sustain inertial and pressure loads
- minimise noise propagation
- provide fire containment
- prevent ice accumulation on engine parts
- provide thrust reversal functionality
- allow for easy access to the engine for maintenance purposes

This research focuses on the aerodynamic aspect of the nacelle design since it can have direct impact on the flight mechanics. Before discussing the implemented design rules in Section 5.1.2, the parameterisation of the nacelle geometry is introduced in Section 5.1.1. Only short duct nacelles are considered in this research since they are preferred over long duct nacelles for high-bypass ratio engines. The inherent increase in nacelle diameter with engine bypass ratio already enlarges the nacelle weight and drag. A long bypass duct would reinforce these penalties, not outweighing the engine performance (in case of mixing), thrust reversal and noise benefits [71, 62].

5.1.1. Nacelle Parameterisation

A convenient and robust parameterisation of the nacelle is required to be able to easily alter the geometry in case of a multi-disciplinary analysis or optimisation routine, while the parameter choice also has to offer enough flexibility. The intuitive parameterisation suggested by Bartoli et al. [72] consists of seventeen parameters defining key points and local slopes on the nacelle, which is assumed to be axisymmetric. However, these parameters do not fully describe the actual, aerodynamically-shaped contour of the nacelle. Furthermore, in order to add droop to the inlet, as is often done in practice, the nacelle has to be made non-axisymmetric.

Therefore, it is decided to combine the convenient parameter selection of Bartoli et al. [72] with a Class Shape Transformation (CST) representation of individual curves constructing the nacelle shape. Such a representation automatically leads to a continuous curve which has a smooth aerodynamic shape [46, 51]. This is considered a valuable combination since it allows the designer to locally control the nacelle profile without having to specify each individual point on the surface.

Furthermore, the CST parameterisation is defined by polynomials which can be easily differentiated and manipulated to include key geometrical features. In normalised form, the CST parameterisation prescribes the y-ordinate (ξ) as a function of the abscissa (φ) as follows [46, 73]:

$$\xi(\varphi) = C_{N2}^{N1}(\varphi) \cdot S(\varphi) + \varphi \cdot \Delta\xi_{TE} \text{ with } \xi = \frac{y}{L} \text{ and } \varphi = \frac{x}{L} \tag{5.1}$$

where $\varphi \in [0,1]$, L is the axial length of the curve in x-direction and $\Delta\xi_{TE}$ is the offset in ξ at the end of the curve [46]. The class function is provided by Equation (5.2). The exponents $N1$ and $N2$ determine the basic class of the geometry. The shape function $S(\varphi)$ of order n, defined by Equation (5.3), is a sum of $n+1$ Bernstein polynomials weighted by Bernstein coefficients B_i.

$$C_{N2}^{N1}(\varphi) = \varphi^{N1} \cdot (1-\varphi)^{N2} \tag{5.2}$$

$$S(\varphi) = \sum_{i=0}^{n} B_i \cdot \binom{n}{i} \cdot \varphi^i \cdot (1-\varphi)^{n-i} \tag{5.3}$$

The Bernstein coefficients are however not directly related to a physical distance or angle, and hence the physics-based parameterisation of Bartoli et al. [72] has to be translated to a set of Bernstein coefficients. This transformation can be performed by applying a set of constraints and/or boundary conditions to the curve, each one formulated as in Equation (5.4). The constraints can be applied to include certain points on the curve and to fix the local first or second derivative. The first and the last Bernstein coefficients are known from $N1$, $N2$ and the boundary conditions. The complete set of Bernstein coefficients can be obtained by solving a system of equations constructed from an arbitrary number of constraints, as long they are consistent with the selected class exponents.

$$\xi^{(k)}(\varphi) = \left[C_{N2}^{N1}(\varphi) \cdot S(\varphi) + \varphi \cdot \Delta\xi_{TE}\right]^{(k)} \text{ for k = 0, 1 or 2} \tag{5.4}$$

This approach of translating physical parameters into Bernstein coefficients and drawing the according curve is implemented in a specialisation of ParaPy's native `FittedCurve` class, which is called `CstContrainedCurve`. Three specialisations of the `CstContrainedCurve` are created to define the individual curves defining the longitudinal cross-section of the nacelle, as shown in Figure 5.3, being the `CowlCurve`, `InletCurve` and `ExhaustDuct`. This structure is clarified by the UML diagram in Figure 5.2.

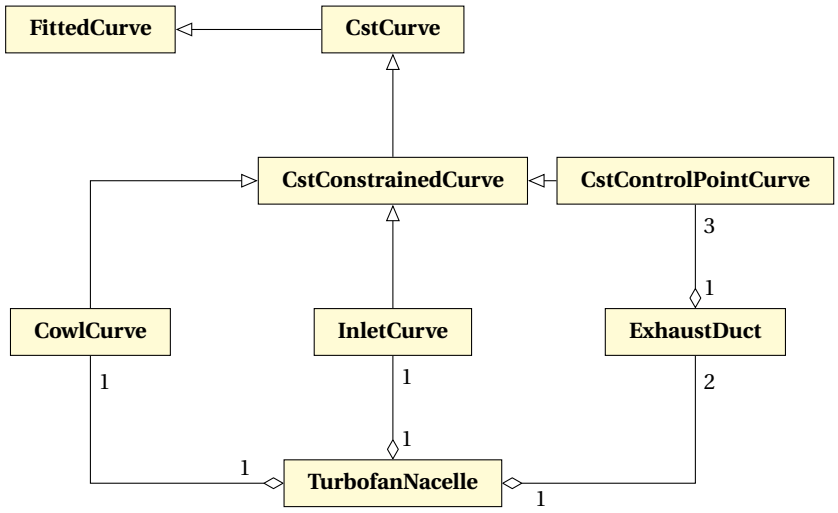

Figure 5.2: Class diagram of the specialisations of the `FittedCurve` class employed to define the nacelle geometry

These classes take the intuitive parameters as an input and translate them into constraints, which in turn are employed to construct a system of linear equations. The `CowlCurve` and `InletCurve` classes assume a shape similar to airfoils, setting the class function exponents $N1$ and $N2$ to 0.5 and 1 respectively. Each `ExhaustDuct` is built from three curves with a shape transformation of a basic curve with $N1 = N2 = 0$.

In case of the fan cowl shape, the `CowlCurve` class constructs the curve automatically from the parameters shown in Figure 5.4: the leading edge nose radius (R_{nose}), the length in x-direction (L), the tail angle (β) and the relative axial and radial positions of the crest (f_{crest} and R_{crest}/L). Additionally, an offset of the tail with respect to the highlight point, $R_{\text{TE}} - R_{\text{hi}}$, can be included. In the case of the cowling, the boundary conditions and constraints (g_i) are formulated in Equation (5.5). These four constraints, leading to four Bernstein coefficients, result in a CST curve of order three. B_1 and B_2 can be found be rewriting g_1 and g_2 in the format of Equation (5.4) and solving the system of two equations for its two unknowns B_1 and B_2.

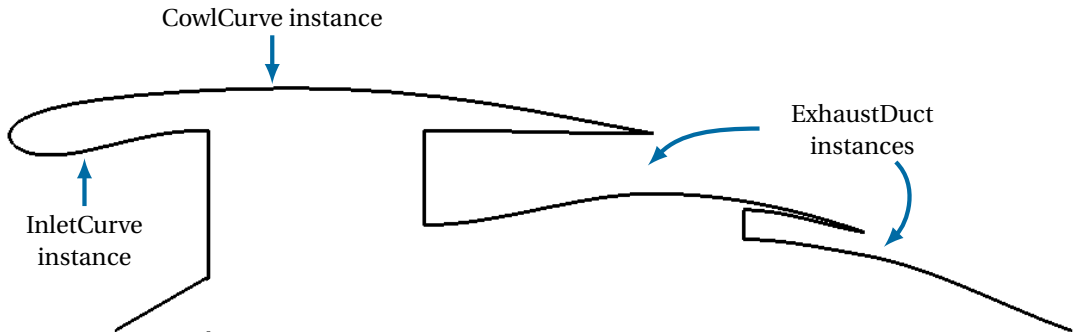

Figure 5.3: Longitudinal cross-section of the upper half of the nacelle

$$\begin{cases} B_0 = \sqrt{\frac{2 \cdot R_{\text{nose}}}{L}} \\ B_3 = -\tan\beta + \frac{R_{\text{TE}} - R_{\text{hi}}}{L} \\ g_1 : \xi\left(\varphi = f_{\text{crest}}\right) = \frac{R_{\text{crest}}}{L} \\ g_2 : \xi'\left(\varphi = f_{\text{crest}}\right) = 0 \end{cases} \tag{5.5}$$

The inlet curve is constructed using the same format as the cowl curve, except that the sign of $\xi(\varphi)$ is reversed. The working principle of the curves modelling the exhaust ducts is different: instead of specifying a fixed set of variables, an arbitrary number of control points ($N_{\text{CP}} > 2$) is used to define the curve shape, as displayed in Figure 5.5. For each control point, its abscissa φ, its ordinate $\xi(\varphi)$ and the local slope $\xi'(\varphi)$ have to be specified. These control points are derived from the aero engine geometry and assumed design rules, as discussed in the following section. This parameterisation is preferred for exhaust ducts because it allows for more flexible duct shapes with any number of control parameters [46]. Although not considered in this research, this flexible parameterisation can be useful when optimising the duct shapes using higher fidelity aerodynamic analysis. Again, these control points are translated into constraints (Equation (5.6)) and transformed to Bernstein polynomials.

$$\begin{cases} B_0 = 0 \\ B_5 = \frac{R_{\text{CP}_2} - R_{\text{CP}_0}}{L} \\ g_1 : \xi'\left(\varphi = 0\right) = 0 \\ g_2 : \xi'\left(\varphi = 1\right) = 0 \\ g_3 : \xi\left(\varphi = f_{\text{CP}_1}\right) = \frac{R_{\text{CP}_1}}{L} \\ g_4 : \xi'\left(\varphi = f_{\text{CP}_1}\right) = \tan\beta \end{cases} \tag{5.6}$$

Once all the curves have been constructed, the 3D geometry of the nacelle can be created. For the exhausts, the `ExhaustDuct` instances are simply rotated 360 degrees around the engine centre axis. This is not possible for the inlet and fan cowl curves if droop or scarf is added to the inlet, as defined in Figure 5.6. Therefore, additional instances of `InletCurve` and `CowlCurve` are created at the keel (bottom) of the nacelle. In combination with the instances at the crown (top), elliptic cross-sections are drawn and lofted to establish shells representing the complete inlet and cowl. Finally, all individual surfaces are sewn such that the nacelle can be considered as a single solid for subsequent geometric manipulations.

5.1.2. Short-Ducted Nacelle Design

To automate the overall design process as much as possible, engineering rules are implemented to provide initial estimates for the parameters defining the nacelle geometry. Results from the engine sizing are used in combination with guidelines from literature to fit the nacelle around the aero engine. In this section, the design rationale behind the nacelle geometry is discussed.

The shape of the inlet is rather critical since it has to provide an undisturbed airflow to the engine in a wide range of angles of attack, side-slip angles and mass flow ratios (A_∞ / A_{hi}). The parameters defining the shape

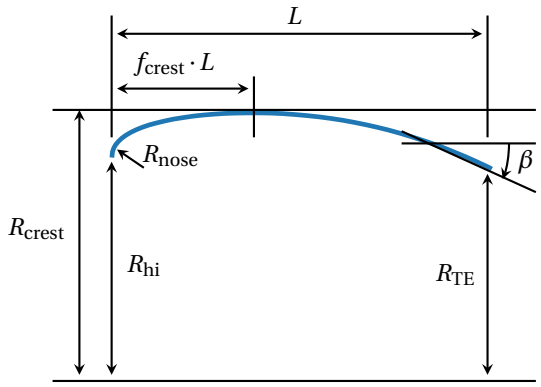

Figure 5.4: Parameterisation of the fan cowl shape

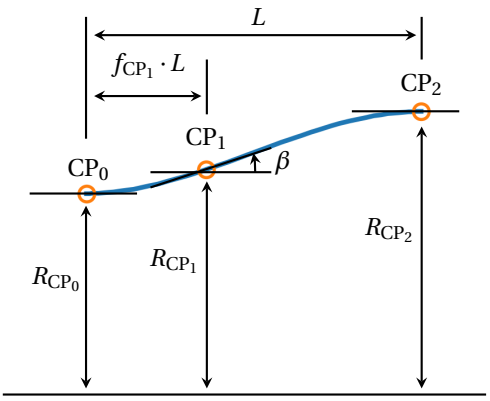

Figure 5.5: Parameterisation of a curve used in the exhaust ducts (orange circles represent the control points)

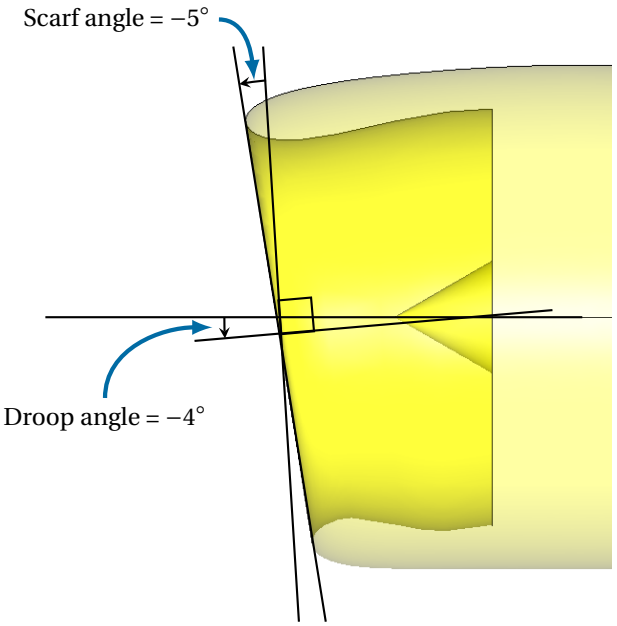

Figure 5.6: Illustration of droop and scarf angle applied to the inlet of a short-ducted turbofan nacelle, as defined by Stockman et al. [74]

of the inlet are the radii of the fan, the throat and the highlight sections, its length, and the internal nose leading edge radius. The radius of the fan is known from the engine sizing procedure.

The inlet acts as a diffuser to slow down the air in front of the fan in cruise conditions. The throat cross-sectional area is calculated from the take-off mass flow and a maximum axial Mach number of 0.8 to prevent a large drop in total pressure in this flight phase ([67], Figure 37.6). To ensure no separation occurs between the throat and the fan, while minimising the length, the wall angle (refer to Figure 5.7) between the throat and the fan is assumed to be six degrees, which is slightly less than the seven degrees specified by Chandavari and Palekar [75]. This angle and the difference in throat and fan radii determine the axial distance between the

throat and fan.

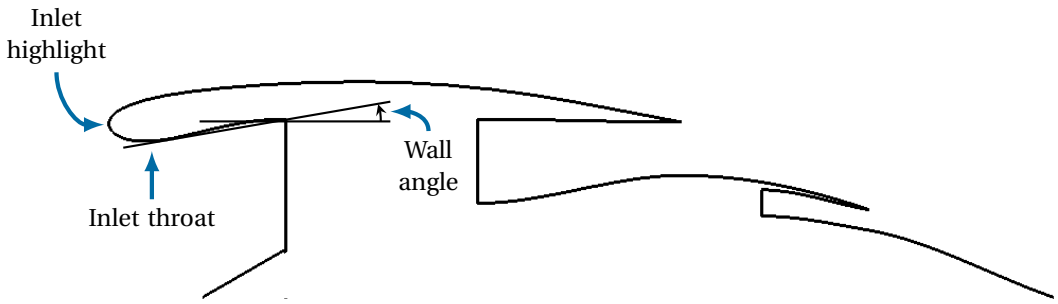

Figure 5.7: Anatomy of the inlet geometry

The radius of the highlight can be calculated from the throat radius by assuming a default contraction ratio A_{hi}/A_{th} of 1.25. This value leads to lower curvatures of the inside of the inlet lip, preventing separation during low speed flight at high mass flow ratios, and the associated total pressure losses [67]. However, if the aircraft has a relatively high transonic cruise Mach number (0.97-1.0), it is advised to lower the contraction ratio to avoid total pressure losses due to shocks at high velocities. The nose radii, as well as the axial distance between the highlight and the throat of the lip are by default related to the absolute difference between throat and highlight radii, but can be varied.

The aerodynamic shape of the fan cowl surface is mainly driven by the requirement to reduce local super-velocities and minimise the drag penalty of the podded installation. As indicated in Figure 5.4, the fan cowl typically has a crest point. It is assumed that this point lies above the fan casing, and that its thickness is determined by the fan diameter and an additional factor taking into account engine accessorises and structural elements. The default value of this thickness factor $R_{\text{crest}}/R_{\text{fan}}$ is taken to be 1.21 [9].

The length of the nacelle is computed from the required inlet and engine length. The core exhaust plane is placed at a distance of 50% of the LPT diameter behind the LPT exit [42]. Hence, the length of the inlet, plus engine, plus the latter distance result in the length of the nacelle without exhaust cone, called L_N. The length of the fan cowl (L_F) is typically 70 to 80% (f_N) of L_N [76]. Hence, the length of the core cowl is estimated by subtracting L_F from L_N. In general, it is advised to reduce the length of the parts immersed in jet velocities to decrease the scrubbing drag.

The outer radius of the bypass and the inner radius core exhaust faces are calculated according to Equations (5.7) and (5.8) [76]. The corresponding hub and tip radii can be retrieved from the respective nozzle areas determined in the design point analysis of the engines.

$$R_{\text{t, bypass\_ex}} = R_{\text{crest}} \cdot \left(1 - \frac{f_N^2}{3}\right) \tag{5.7}$$

$$R_{\text{h, core\_ex}} = 0.55 \cdot R_{\text{t, bypass\_ex}} \tag{5.8}$$

Certain nacelle design variables cannot be estimated from existing relations, but require an iterative approach including analysis steps. This subset containing for example the droop and scarf angles, and other angles specifying the local slope at the end of the surfaces, may be adapted according to aerodynamic results. The droop and scarf angles have to be set such that the intake highlight, indicated in Figure 5.7, is aligned with the local velocity during cruise [47], which in turn depends on the relative location of the inlet with respect to the wings. These lifting surfaces produce an upwash and downwash in their vicinity, which has to be determined by aerodynamic analyses.

To verify the validity of these rules, a nacelle is designed around the GE90 engine discussed in Section 4.5 and compared to the nacelle geometry presented by Rego et al. [16]. The dimensions of the latter are displayed in Figure 5.8. The model created by GTpy is shown in Figure 5.9, where the inlet droop is not included because

this is dependent on the installation location and has to be iterated upon. The dimensions are compared in Table 5.1. It can be seen that the nacelle dimensions are slightly overestimated when designed based on engineering rules, especially comparing the outlets of the core exhaust.

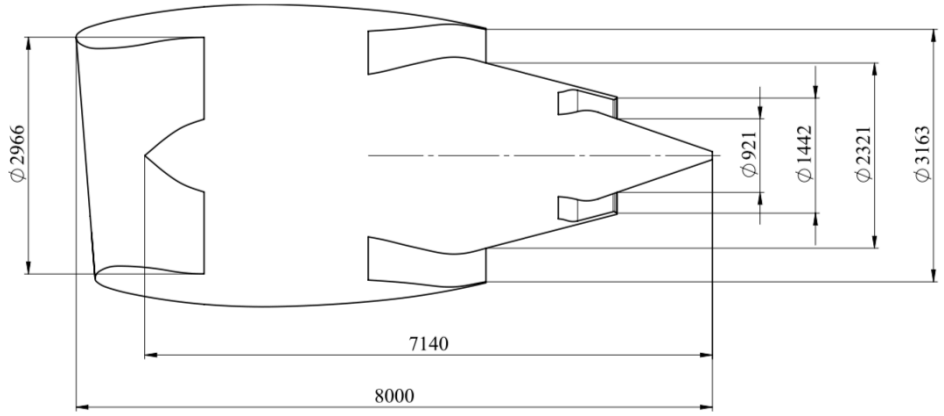

Figure 5.8: GE90-94B nacelle cross-section from literature (dimensions in mm) [16]

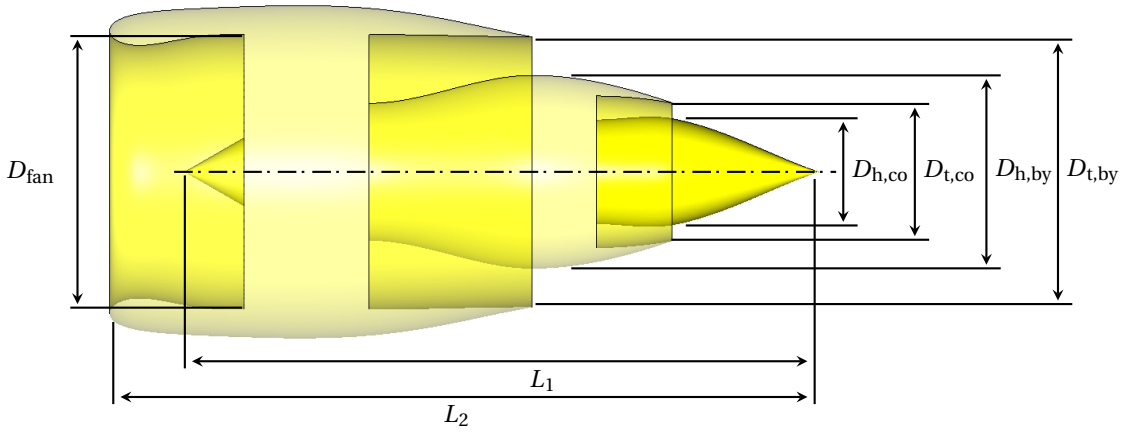

Figure 5.9: GE90-94B nacelle cross-section as predicted by the GTpy application

Table 5.1: Comparison of GE90 nacelle dimensions estimated by GTpy with values from literature [16]

Parameter	**ParaPy**	**Literature**	**Difference %**
D_{fan} [m]	3.222	2.966	+ 8.631
$D_{t,by}$ [m]	3.222	3.163	+1.865
$D_{h,by}$ [m]	2.466	2.321	+6.247
$D_{t,co}$ [m]	1.616	1.442	+12.067
$D_{h,co}$ [m]	1.246	0.921	+35.29
L_1 [m]	7.425	7.140	+3.992
L_2 [m]	8.307	8.000	+3.838

5.1.3. Nacelle Weight Estimation

The nacelle weight is estimated using the approach suggested by Water and Schairer [42]. In this method, the complex, non-axisymmetric nacelle shape is represented by two finite cylindrical surfaces, indicated by the thick, orange and blue rectangles in Figure 5.10. The orange cylinders represent the standard cowling fitted around the engine. The blue sections are parts of the nacelle which contain a thrust reversal system and/or nozzle built from heavier materials. For the fan cowl, the length of the blue section is assumed to be 50% of the bypass nozzle exit diameter. For the core cowl, the length of nozzle section is taken to be half of the low pressure turbine diameter. Phrased differently, $L_{\text{bypass\_ex}} = R_{\text{t, bypass\_ex}}$ and $L_{\text{core\_ex}} = R_{t,LPT}$.

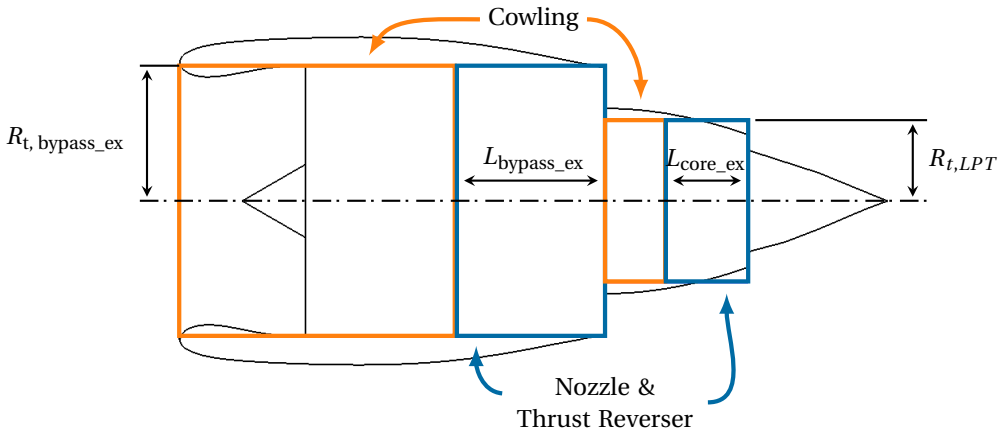

Figure 5.10: Simplified cylinder representation of nacelle employed for weight estimation

Water and Schairer suggest to multiply the surface areas of the cylinders by unit weight per area. For the regular cowling, i.e. not the thrust reverser or nozzle, a unit weight of 17.1 kg/m^2 is recommended. For the thrust reverser and hot exhaust nozzle, the unit weight is approximately 73.2 kg/m^2. These values are derived from a statistical analysis considering data from nine commercial turbofan engines of several manufacturers [42].

This preliminary weight estimation method is preferred over other empirical relationships since the weight is directly related to the diameter and length of the nacelle, and thus the bare engine itself. This allows to study the trend of increased nacelle weight with increased mass flow (related to thrust) and bypass ratio. Especially the relationship between the latter parameter and nacelle mass is of interest when very or ultra high bypass turbofan engines are investigated. Nevertheless, the mass values mentioned above may be outdated due to technological advances.

5.2. Pylon Design

Once the nacelle geometry is known and the nacelle is positioned and oriented, a pylon can be created to finally connect the engine installation with the airframe. The design of a pylon has to take into account the structural elements and systems it has to house, such as fuel and bleed air pipes [77]. Additionally, the pylon is often carefully shaped to minimise the aerodynamic interference between the nacelle and the aircraft [12, 47]. As discussed in the introduction of this chapter, in the current geometry model the pylon is a specialisation of the general `Wing` class. Although this does not allow for many local changes to the geometry, it simplifies the integration with the existing components in the current implementation of the MMG.

After the positioning of the nacelles, Oliveira et al. [47] suggest to firstly define the leading and trailing edge rails of the pylon. Based on the relative engine location with respect to the airframe, the leading and trailing edge segments are automatically drawn. This starts with the construction of the plane in which the engine centre line and rails lie, and thus the selection of the angle of attachment with respect to the engine top dead centre. If set to automatic, the application searches for the shortest possible connection. Alternatively, the user can select this angle manually. The difference between these two approaches is clarified in Figure 5.11.

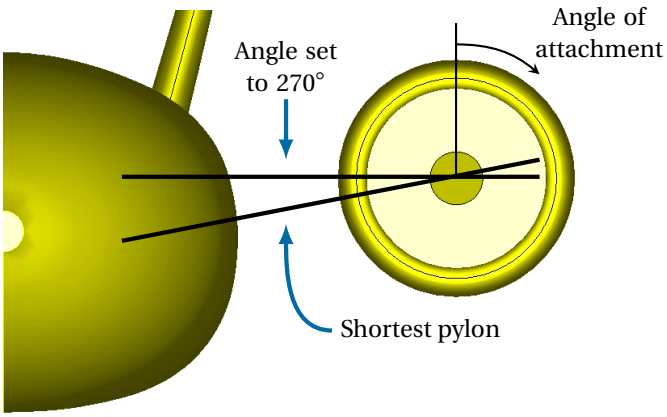

Figure 5.11: Definition of the pylon plane (thick black lines) in which the pylon leading and trailing rails are defined, as seen from the front of the aircraft

The tip leading and trailing edge points of the pylon have to be located within the nacelle solid. This is enforced to simplify the pylon-nacelle intersection in the current design stage and to simplify the meshing strategy, which is discussed in the next chapter. These tip points are defined as fractions of the engine length and maximum diameter, and are referred to as "attachment points". Once the pylon plane is built, these two points are located in that plane. Subsequently, two planes are created through these attachment points and perpendicular to the pylon plane. The intersection lines between these planes and the pylon plane form the leading and trailing edge rails of the pylon. By default, these planes are also orthogonal to the engine centre axis.

However, depending on the relative position of the engine with respect to the airframe, these planes may have to be rotated in order to cut the airframe. This for example occurs if the engine is placed in front of the wing. These rotations effectively add sweep to the leading and/or trailing edge of the pylon. This entire process, including a user set sweep angle on the trailing edge rail, is displayed in Figure 5.12 on the aft section of a fuselage.

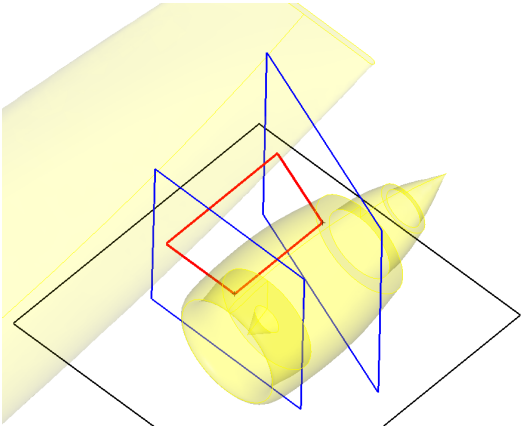

Figure 5.12: Creation of the pylon planform (red) by intersecting the leading and trailing edge planes (blue) with the pylon plane (black)

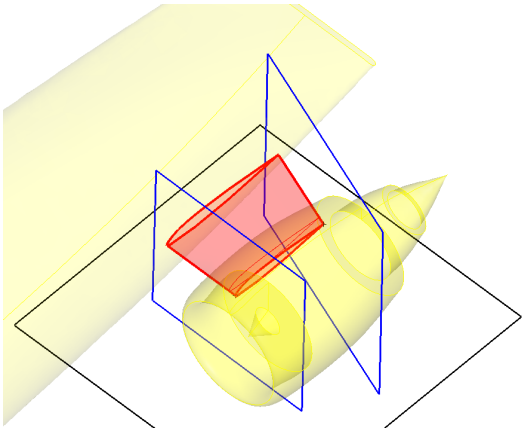

Figure 5.13: Creation of the pylon loft with airfoils (red)

If required, the designer can manually control the leading and trailing edge sweeps to obtain the desired pylon planform. For example, when a certain thickness to chord ratio (t/c) of the pylon cross-section is desired, the trailing edge can be swept to elongate the chord of the cross-section such that acceptable thickness ratio (t/c) is achieved [77]. Although the current geometry manipulation operations allow for the pylon to cut several faces of the nacelle, the aerodynamic analysis is currently limited to pylon shapes which only intersect with the fan cowl.

When the rails are completely defined by the intersections of the planes, the pylon shape can finally be lofted using airfoil definitions at the root and tip of the pylon, as presented in Figure 5.13. These cross-sectional profiles can be provided to the tool as a path referring to a file containing the airfoil coordinates. The definition of the airfoil coordinates can be used to apply local changes to aerodynamic shape. Although several measures are implemented to ensure that the pylon root and tip edges are completely surrounded by the geometries of the airframe and nacelle respectively, a manual inspection of the designer is recommended to prevent any problems when creating the complete aircraft solid.

At this stage, no sizing of the structural elements or other systems is implemented. Therefore, the weight of the pylon cannot be calculated accurately. For the sake of simplicity, the pylon is assumed to constitute 14% of the total powerplant installation weight [78]. This is a rudimentary estimation and the actual pylon weight is presumably different when installed on the wing instead of the fuselage. Furthermore, any additional structural mass required to strengthen the wing or fuselage locally is not taken into account since this is considered out of scope.

6

Multi-Disciplinary Analysis of the Integration

One of the reasons for selecting a Knowledge Based Engineering approach in the first place is that several design disciplines can be taken into account by creating dedicated reports (i.e. input files) for discipline specific analysis tools. The MMG performs an important role here since it can efficiently translate the aircraft geometry to a mesh, for example, according to programmed rules. Additionally, ParaPy software provides built-in capabilities to prepare geometries for commercial Computer Aided Engineering (CAE) software. In this chapter, the methodology to assess the impact of the engine installation on aerodynamics and noise is discussed.

Although more aspects are of interest for the integration problem, these disciplines were selected to define the most suitable solution in this preliminary design stage. Other integration aspects, such as the impact on the structural design, maintenance, safety or fuel system integration can be assessed qualitatively at this point, while the quantitative evaluation is left as a recommendation for future research.

6.1. Aerodynamic Analysis of the Engine Installation

The location, orientation and shape of the nacelles can have a direct influence on the forces and moments experienced by the aircraft [12, 47]. Although several specific aerodynamic effects are related to the installation of engines, as discussed in Section 2.5.1, here the overall effect on lift, drag and moments of the complete aircraft are of main interest. These can be used later to build aerodynamic databases for flight mechanics analysis. In this research, VSAERO is employed as aerodynamic analysis tool. In the following sections the modelling of the turbofans in VSAERO and the automatic mesh creation are discussed. Additionally, a mesh sensitivity study is included in Appendix C.

The reason for selecting VSAERO as aerodynamic analysis tool is threefold: firstly, an analysis of the entire aircraft, including control surfaces, is required to study the flight mechanics. Since such an analysis would require too much computational time when carried out with higher fidelity Computational Fluid Dynamic simulations, the panel method in VSAERO is preferred. The 3D panel code offers a trade-off between computational cost and accuracy [48]. Secondly, VSAERO has proven to be an efficient tool to study the engine installation in early design stages [79, 50]. Finally, the ParaPy software provides predefined functions to mesh geometrical objects and write VSAERO input files. These functionalities are employed in the research by Raju Kulkarni et al. [80] and Groot [48] for the airframe, and extended in this research to model the engines.

6.1.1. Aerodynamics of Podded Engines and Limitations of VSAERO

VSAERO offers a combination of a 3D potential flow method and integral boundary layer calculations where sources and doublets are placed on the surface of the object. The aim is to solve for the velocity potential Φ from which the local velocity components can be computed, as shown by Equation (6.1). Φ can rewritten as the sum of a freestream potential (ϕ_{ref}) and a perturbation potential ϕ. Since the methods in VSAERO assume that the flow is incompressible, irrotational and inviscid, except for thin boundary layers on the surface, the perturbation potential has to satisfy the Laplace's differential equation (Equation (6.2)).

$$\nabla\Phi = -\vec{V} \tag{6.1}$$

$$\nabla^2\phi = 0 \tag{6.2}$$

By adhering to the Laplace's equation, the velocity distribution over the geometry can be computed, which is in turn employed to determine the local pressure coefficients and the body forces. VSAERO can indeed take into account the changes in the velocity potential when nacelles are added in the vicinity of a wing or fuselage object. This may be of importance especially when the nacelle is placed under the wing, increasing the velocity on the pressure side of the local airfoil section and reducing the lift on the particular spanwise location.

Hence, it is expected that VSAERO can account for the impact due to the addition of relatively large nacelle bodies on the pressure coefficient distribution. Any loss or increase in lift, and its associated change in vortex drag is assumed to be taken into account by the aerodynamic analysis. Nevertheless, due to the assumptions made above, VSAERO cannot capture all effects related to the installation of podded engines, which were briefly discussed in Section 2.5.1.

However, once the local Mach increases above one, for example in transonic flight conditions, VSAERO cannot model the associated shock waves and drag. This effect is typically a driving factor in the design of the outer nacelle shape of transonic aircraft [81]. Hence, especially in cruise, the analysis conducted by VSAERO cannot account for local supersonic effects. Increasing the flight Mach number above 0.3 also invalidates the incompressibility assumption. In the current model set up, the compressibility effects are considered by applying the built-in Prandtl-Glauert correction which is recommended by Lednicer et al. [49] for propulsion system integration studies.

Boundary layer effects are considered by computing the development of the boundary layer along on-body streamlines on the surface of the aircraft and the fan cowl of the nacelles. The formation of the boundary layer is iterated upon by viscous iterations which follow the wake shape iterations. The estimated skin friction is included in the calculation of the total drag force. Nevertheless, separation of the boundary layer, due to an adverse pressure gradient or shock-wave interaction, cannot be captured. This includes spillage effects which may appear when engines are running in off-design or inoperative conditions, or when a shock wave interacts with the local boundary layer. Hence, at this stage, separation onsets and their consequences cannot be predicted.

Finally, since the jet plumes are modelled as closed wakes extending from the nozzles, as elaborated upon in the next section, the mixing or entrainment between the jets and the surrounding air is not accounted for, although such detailed effects are typically not of interest in the current design phase. However, the VSAERO analysis also does not simulate the separation on the after body of the fan and core nozzles, and the associated boat tail drag.

In conclusion, it is expected that the aerodynamic analysis with VSAERO is able to provide insight in the large scale impact the engine installations may have on the local pressure distributions, and hence the change in lift and moments on the aircraft. Only reduction in these parameters due to separation are not considered. Nonetheless, certain phenomena which may result in an increase in drag cannot be studied. Hence, it is recommended to employ higher fidelity aerodynamic analysis to investigate the above mentioned local effects further.

6.1.2. Modelling Engines and Nacelles in a 3D Panel Code

Once the aircraft geometry is completely modelled as a single solid in ParaPy, it can be prepared by the Multi-Model Generator for the analysis by VSAERO. This methodology has been developed in the research by Raju Kulkarni et al. [80] and Groot [48] and is extended in the current research to include engines. Once the solid model is created, the following steps have to be executed:

1. generating a structured mesh
2. translating the mesh into a geometry description which can be interpreted by VSAERO
3. impose boundary conditions on the nacelle inlet and outlet faces
4. constructing the wakes

The steps are implemented in the MMG such that they can be executed automatically without the need for human interaction to save time, allowing to analyse more configurations in a given timeframe [48]. The above steps, which are independent of aircraft configuration or engine location, are discussed separately in the next paragraphs.

Generating a Structured Mesh Since VSAERO employs a 3D panel method, the aircraft geometry has to be meshed with smaller individual panels. As discussed by Groot [48], it is advised to construct a fully structured mesh to minimise the computational time required by VSAERO. This requires the pylons and nacelles to be split into quadrilateral patches first, by folding curves over the 3D surfaces based on the intersection with the pylon. Figure 6.1 illustrates the creation of these so-called splitter curves over a nacelle installed on the side of the fuselage. The thin black edges originate from the complete aircraft solid, while the red lines are added to ensure all patches have four edges. The resulting split surface is presented in Figure 6.2. Note that for VSAERO analysis the bypass and core exhaust ducts are excluded, and the nacelle is closed at the exhaust faces. This is aspect is further elaborated upon later.

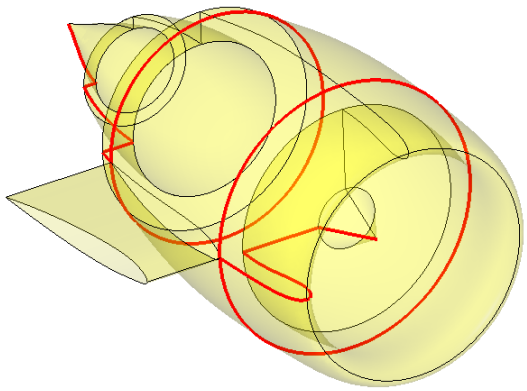

Figure 6.1: Example of splitter curves (red) drawn over the nacelle surfaces

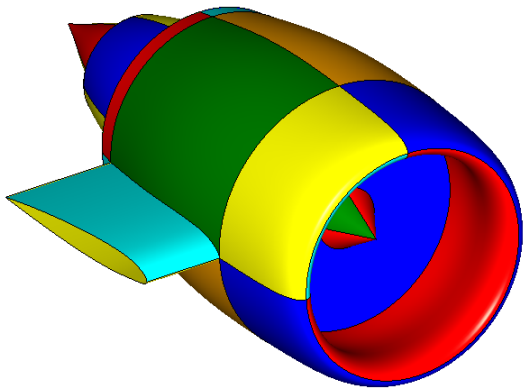

Figure 6.2: Example of nacelle and pylon components split into quadrilateral faces (patches)

The subsequent step is to identify all edges which need to have the same number of nodes and segments to ensure a structured mesh. To find such edge chains, similar to the approach for the airframe, a search algorithm is initiated at the apex point (in ParaPy a curve) of the exhaust cone which seeks the opposite edge on the current face. Since this opposite edge is a shared edge, the next face can be found. This approach of find the opposite edge and the subsequent face is repeated until the opposite edge is not shared any longer, which in case of the nacelle occurs on the spinner faces.

This procedure leads to longitudinal edge chains over the nacelle, of which one is shown in red in Figure 6.3. The exact same scheme is employed to find all circumferential chains, albeit with different initial edges. An example of a circumferential chain is highlighted in blue in Figure 6.3. This particular chain also includes the chordwise edges of the pylon such that an identical node distribution is applied.

The final step is to apply mesh controls to these edge chains to define the node distribution for each. For the pylon, the mesh is defined by the number of chordwise and spanwise points [48], allocated according to cosine and equidistant distributions in chordwise and spanwise directions respectively. The chordwise distribution is then also used on the edges of the nacelle which are located in the same edge chain.

The mesh on other nacelle patches is controlled by two parameters: the longitudinal pitch, expressed in number of points per unit length, and the radial angle pitch, which specifies the angle radial between mesh nodes

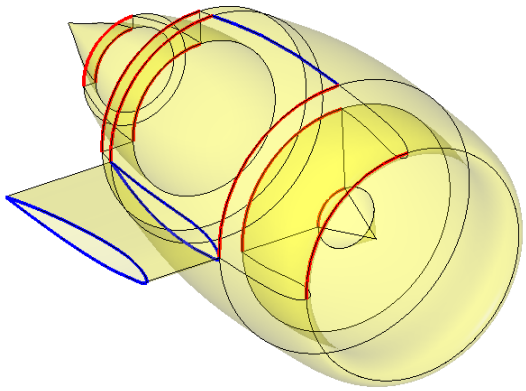

Figure 6.3: Illustration of longitudinal (red) and circumferential (red) edge chains

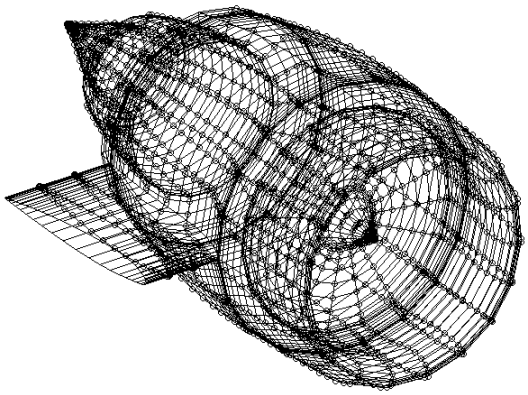

Figure 6.4: Example of meshed nacelle and pylon components

in circumferential direction as measured from the engine centre axis. The longitudinal nodes are placed employing a cosine distribution which is renewed on each patch. This cosine relation ensure that the leading and trailing edges of the nacelle patches have a finer distribution, and that the mesh matches with the refinements made for the pylon leading and trailing edges.

Although in reality the pylon often extends up to the core cowl or even the exhaust cone in longitudinal direction, in the current implementation only pylons cutting solely the fan cowl are supported. If the pylons intersected also with the core cowl, for example, additional splitter curves would have to be drawn from the bypass exhaust in chordwise and spanwise direction over the pylon to ensure that all patches have exactly four edges. Additionally, the chordwise splitter curve would have to continue over the airframe surface, possible intersecting with other components. This would increase the complexity of the meshing strategy, and hence it is decided to leave this for further consideration. A possible solution would be to employ an unstructured mesh on the pylon, such that the meshes on the airframe and nacelles are independent.

VSAERO Geometry Definition The aircraft geometry in VSAERO is built up of components, which in turn consist of patches and smaller panels. ParaPy functionalities allow to translate the mesh to a geometry definition which can be interpreted by VSAERO. Currently each half-wing and the fuselage define individual VSAERO components. Hence the rules for constructing the pylons were already implemented since they are instances of the general `Wing` class.

In this research a new turbofan component class is developed to include the engines in the geometry definition. The current solution is specifically constructed for short-ducted turbofan nacelles, taking into account patches on which a non-zero normal velocity is to be imposed, i.e. the fan inlet and exhaust faces. These faces are made up of a different type of VSAERO-patches to consider their influence on other patches, but the forces on these patches themselves are ignored in the force and moment summations. Additionally, the correct orientation of the patches is verified such that the patch normal vectors are pointing outwards.

Imposing Boundary Conditions on the Nacelle Inlet and Outlet Faces To model turbofan-nacelle installations using a potential flow solver, the open nacelle is closed by faces at the fan inlet and exhausts, i.e. the bypass and core exit planes. This allows to model a powered nacelle, as well as a flow-through model. This setup requires to specify non-zero normal velocities on the inlet and outlet faces to simulate the mass flow through the engine. For the mathematical model this is important since the Neumann boundary condition (Equation (6.3)) is different on the panels contained in these particular patches. On regular panels, the normal velocity V_N is assumed to be zero. On the engine inlets and outlets, V_N is set to a non-zero value.

$$\vec{n} \cdot \nabla \phi = -V_N \tag{6.3}$$

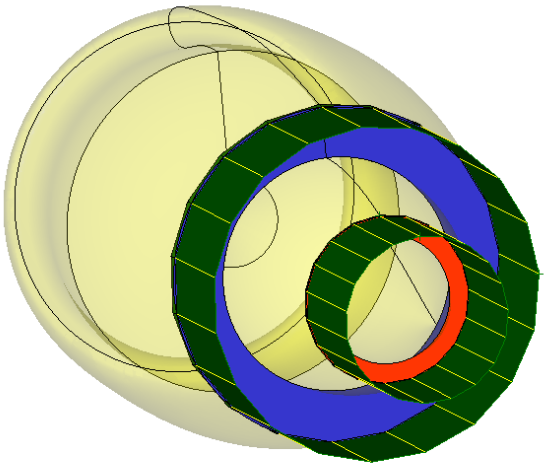

Figure 6.5: Initial shape of the wakes (green) extending from the bypass (blue) and core (red) exhaust faces as seen from the back of the nacelle

In the current research the normal velocities are set equal to the axial velocities computed by the engine performance analysis in GTpy and GSP at these stations. The thrust cannot be modelled correctly in VSAERO because the change in momentum produced by the engines cannot be completely captured when potential flow is assumed. Hence the effect on the local velocity and its respective effect on the body forces is of main interest. Any rotational velocity components introduced by the fan or turbomachinery components are also neglected.

Constructing the Wakes The final step is to construct the wakes behind the pylons and the nacelle elements. A wake is shed from the 3D geometry to represent the vorticity shed from the body. An initial wake geometry has to be specified but is iterated upon (i.e. relaxed) such that each wake panel is aligned with the local flow, $\vec{V} \cdot \vec{n} = 0$, and the pressure on either side is equal since the wake cannot be loaded.

A prediction for initial wake shape of pylons has already been created since they are instances of the existing `Wing` class, but the wakes of the engines have to be constructed automatically. Two closed wakes, resembling cylindrical surfaces, are placed at the outer radii of the bypass and core exhaust faces, as displayed in Figure 6.5. Note that the wakes in the figure are shortened for visual purposes and normally extend up to several times the wingspan in freestream direction.

Closed wakes are selected to account for the difference in total pressure inside these wakes. For each wake, the ratios between inner velocity and outer velocity with respect to the reference velocity have to be specified. For the bypass and core exhaust wakes the inner velocities ratios are identical to the ones specified on the respective exhaust planes. For the core wake the outer velocity is then equal to the inner velocity of the bypass wake, while the outer velocity of the bypass wake is assumed to be equal to the reference velocity. Although the latter premise may not be entirely correct depending on the location of the engines, the differences were found to be negligible, although it is advised to inspect this when a new aircraft configuration or engine location is chosen.

6.1.3. Validation

To ensure that the automatic meshing approach and the modelling of the engines as described above leads to accurate predictions, the NASA Common Research Model (CRM) wing-body (WB) and wing-body-nacelle-pylon configuration (WBNP) is modelled in ParaPy and simulated using VSAERO. Through-flow nacelles are added to the wing and fuselage which had already been constructed previously. In this validation case. the velocities on the in- and outlet planes are user-specified instead of being determined by GTpy. The configuration is shown in Figures 6.6 and 6.7. Since the exact parametric definition of the nacelle geometry is not available, the nacelle and pylon are adapted to resemble the large-scale geometries provided for the 6th AIAA CFD Drag Prediction Workshop [1].

Both the configuration without nacelles (WB) and including nacelles (WBNP) are tested to compare the differences. For each geometry the reference point is located at (x=33.66 m, y=0 m, z=4.52 m), while the moment is calculated around the approximate quarter chord point of the mean aerodynamic chord at x=31.99 m as indicated in Figure 6.7. The reference chord length, surface area and span are set to 7.005 m, 383.69 m^2 and 29.38 m respectively [1]. The simulations in VSAERO are completed at a Mach number of 0.70 and a Reynolds number of 5.0 million, corresponding to wind tunnel runs 39 and 69 in the NASA Langley National Transonic Facility (NTF).

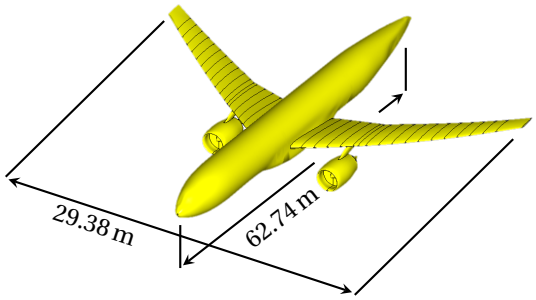

Figure 6.6: ParaPy model of the NASA CRM WBNP configuration

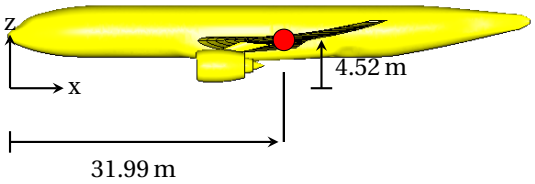

Figure 6.7: Overview of NASA CRM configuration with reference point indicated in red

The polars obtained through wind tunnel tests are compared to the aerodynamic data from VSAERO analysis in Figures 6.8a and 6.8c. The drag coefficient appears to be predicted rather well, including the increase in drag due to the nacelles. The moment coefficient is underestimated for both configurations for a given lift coefficient. Also for the wing-body layout, the slope is positive in the case of the VSAERO results, opposite to what is expected from wind tunnel data. However, this can be expected if the reference point is chosen close to the aerodynamic centre, where, according to its definition, the moment should not vary with angle of attack.

Similar differences in the lift and moment polars have been observed in other studies of the Common Research Model. Rivers et al. [82] examined the influences of the wing twist and support system on the wind tunnel results. Since the model was built as a 1-g, wind-on condition instead of the 0-g, wind-off, the wing twisted differently than expected during the tests. The ParaPy model considered here assumes a fixed twist with varying angle of attack [48], while in the wind tunnel model the local twist varied with the flow conditions.

Additionally, correction factors for the coefficients are proposed to account for effect of the support arm. The impact of these corrections ($\Delta C_L = -0.0243$, $\Delta C_D = -0.00336$, $\Delta C_M = +0.0435$) is indicated in Figures 6.8b and 6.8d. Although these improve the prediction of the lift and pitching moment coefficients, the drag is underestimated. Nonetheless, this is in fact expected for both configurations since VSAERO cannot take into account wave and interference drag at high subsonic conditions.

Furthermore, it is noticed from the detailed VSAERO results that in certain cases the outer lip of the nacelle inlet produces a force in forward direction. This is associated to the strong suction on the highlight of the nacelle. Lednicer et al. [49] mention a similar peak in negative pressure coefficient and attribute this effect to the use of the Prandtl-Glauert correction for compressibility effects. This may be one of the reasons why the drag coefficient is underestimated.

[1] URL `https://aiaa-dpw.larc.nasa.gov/Workshop6/DPW6-geom.html` [Accessed on 19 September 2019]

In conclusion, the current implementation of the methods described in the previous sections can be employed to study the influence of the turbofan installations on the aerodynamics of the aircraft. However, it is advised to limit the use to relatively small angles of attack. In the case of the CRM model, VSAERO is only able to provide accurate predictions for angles of attack up to six degrees. Moreover, certain drag components are not considered by VSAERO.

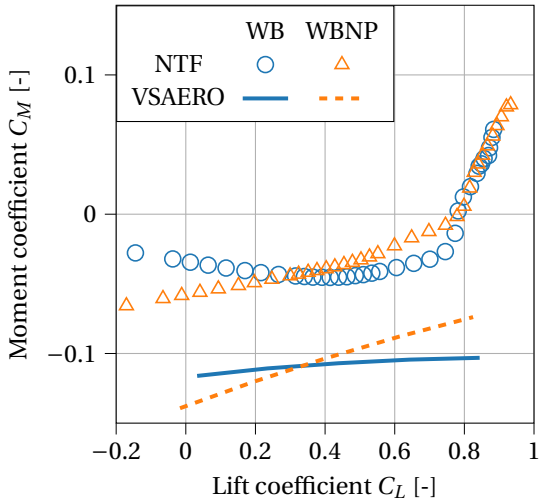

(a) Lift and moment comparison

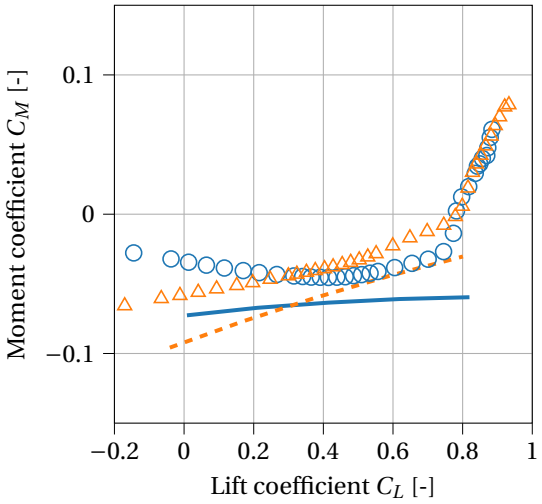

(b) Lift and moment comparison, corrected for support

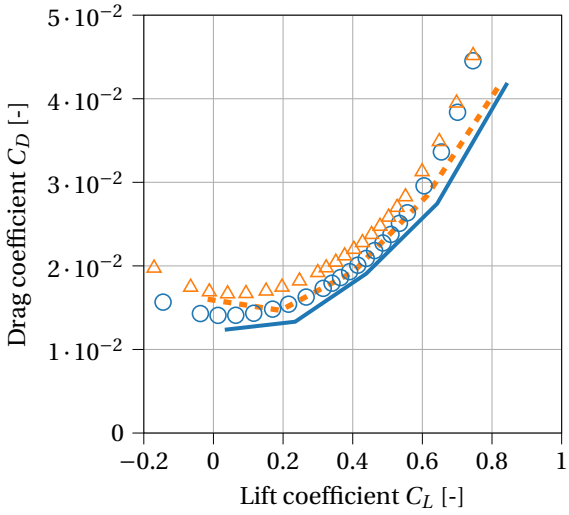

(c) Lift and drag comparison

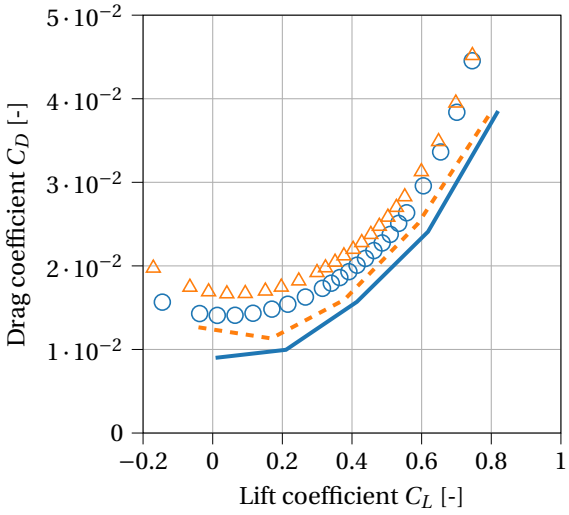

(d) Lift and drag comparison, corrected for support

Figure 6.8: Comparison of NASA CRM NTF wind tunnel data [2] and results obtained through VSAERO, without (a, c, e) and with corrections (b, d, f) for the support arm (Mach=0.70, Reynolds number= 5.0 million)

[2] URL `https://commonresearchmodel.larc.nasa.gov/experimental-data/` [Accessed on 27 September 2019]

6.2. Data Generation to Support Noise Modelling

Since the engines perform a rather dominant role in noise production of the entire aircraft, especially during take-off [52], it is recommended to include them in the preliminary noise analyses. In the PARSIFAL project, a different partner is studying the perceived noise around the aircraft in various flight conditions. The current propulsion integration tool allows to produce the necessary inputs for the noise models by Heidmann (fan and compressor noise) and Stone (jet noise) which are implemented by the PARSIFAL partner.

These parameters consist of geometry specific variables such as liner lengths and exhaust diameters, and operating point dependent parameters such as temperature rises and rotational velocities. The latter can be obtained at any in point in the flight envelope by making use of the GSP connection. An overview of the produced input data is provided in Tables 6.1 and 6.2.

Table 6.1: Input parameters for the Heidmann noise model of the fan element (The Variable? column indicates whether the parameter changes with operating conditions)

Parameter	Variable?
Number of rotor blades	No
Number of stator blades	No
Rotor-Stator-Spacing (RSS)	No
Design relative tip Mach	No
Inlet liner length	No
Static temperature rise	Yes
Total temperature rise	Yes
Mass flow	Yes
Tip Mach number	Yes
Relative tip Mach number	Yes
Rotational speed	Yes

Table 6.2: Input parameters for the Stone noise model of the exhaust elements (The Variable? column indicates whether the parameter changes with operating conditions)

Parameter	Variable?
Core exhaust velocity	Yes
Core static exhaust temperature	Yes
Core total exhaust temperature	Yes
Core exhaust density	Yes
Core exhaust outer diameter	No
Core exhaust outer annulus height	No
Bypass exhaust velocity	Yes
Bypass static exhaust temperature	Yes
Bypass total exhaust temperature	Yes
Bypass exhaust density	Yes
Bypass exhaust outer diameter	No
Bypass exhaust outer annulus height	No

Since the complete analysis including other aircraft noise sources is the subject of a separate work package in the PARSIFAL project, the exact methods and results are not discussed in this report. However, in subsequent iterations, the results from this noise analysis can be taken into account to, for example, reconsider the assumed liner lengths of the nacelles, the engine design parameters and the location of the engines. It is also recommended to assess the cabin noise, especially when the engines are installed on the fuselage.

7

Experiments

The methods and tools described in the previous three chapters can be applied to any aircraft configuration modelled by the MMG. In this research however, the Prandtlplane studied in the PARSIFAL project is of main interest. In this chapter, the results from three experiments are discussed. This analysis work is conducted to test the newly developed tools and their connections to external analysis software, while also exploring the design space of engine cycles and installation opportunities of the box-wing airframe.

The first experiment focuses on the relation between key engine design variables and the mass of the complete installation. Secondly, the aerodynamics of wing-mounted engines is compared to results obtained for engines installed on the fuselage and the aircraft without engines. Finally, the influence of engine design variables on the forces and moments acting on the aircraft is examined.

The PARSIFAL MS1 configuration is employed throughout this chapter. This intermediate design is detailed in Appendix D while its reference values are summarised in Table 7.1. The position of the reference point with respect to the aircraft configuration is shown in Figure 7.1. Preceding performance analyses led to the engine design requirements specified in Table 7.2. All engine models developed in this chapter are designed for the cruise operating point from this table.

Table 7.1: Reference values employed in aerodynamic analyses of PARSIFAL MS1 aircraft

Reference Parameter	**Value**	**Unit**
Surface Area (S_{ref})	266.70	m^2
Span (b)	36.00	m
Mean Aerodynamic Chord Length (MAC)	4.31	m
Moment Reference Point (x,y,z)	(23.37, 0.00, 3.10)	(m, m, m)

Table 7.2: Design requirements assumed for a single PARSIFAL engine

Operating Condition	**Net Thrust** [kN]	**Altitude** [m]	**Mach** [-]	ΔT_{ISA} [K]
Cruise	33.00	11000.0	0.79	0.0
Take-off	180.00	0.0	0.0	15.0

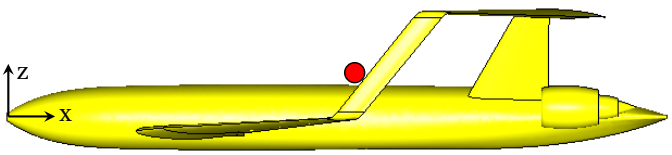

Figure 7.1: Overview of aircraft configuration with moment reference point

7.1. Engine Design Parameters Versus Installation Weight

The variation in cycle design variables is considered in this section. Recent engine developments have shown an increase in bypass ratio and overall pressure ratio to improve fuel consumption. However, this comes at the cost of increased engine size and mass. Additionally, also the nacelle and pylon have to be adapted accordingly and are expected to become heavier. In Figure 7.2, the TSFC and installed mass of 42 engines are plotted for varying BPR and OPR, adhering to the requirements from Table 7.2 and keeping the TIT constant at 1430 K. In the installed mass, the weight of a single engine and nacelle are included. The weight of the pylon is left out in this analysis since it is merely a factor of the aero engine mass.

Although both design parameters increase the mass (the OPR through heavier compressor cases, and the BPR because of larger fan and low pressure turbine components), it can be concluded that the overall installation weight is more sensitive to an increase in BPR than a change in OPR. The fact that the BPR is driving the outer dimensions of the engine is clarified by Figure 7.3.

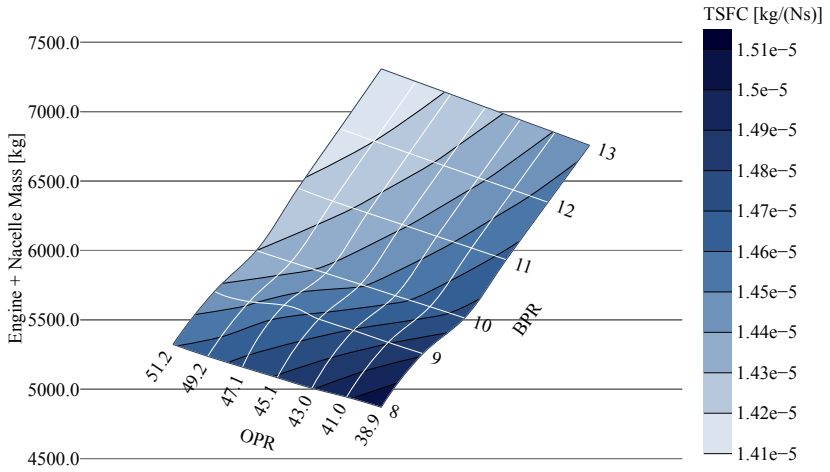

Figure 7.2: Effect of bypass ratio and overall pressure ratio on TSFC in cruise and installation mass (TIT=1430 K)

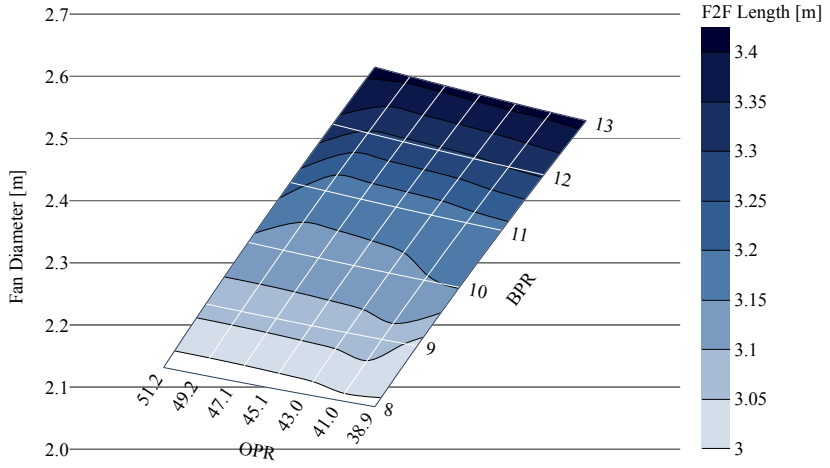

Figure 7.3: Effect of bypass ratio and overall pressure ratio on the flange-to-flange (F2F) length of the engine and its fan diameter (TIT=1430 K)

The logarithmic sensitivity of the installation mass with respect to BPR varies approximately between 0.55 and 0.77, while the sensitivity to OPR is limited to 0.42 for the currently implemented engineering rules and studied intervals. Nevertheless, both variables can have a similar impact on TSFC. Hence, from this perspective, it appears to be more valuable to focus on increasing the OPR parameter rather than the BPR.

In Figure 7.4, the same analysis as in Figure 7.2 is shown but considering a lower TIT in the cruise reference point. The contour lines are located differently, but most remarkably, the installation mass increased for all cases. Although the turbine inlet temperature does not have a direct effect on the nacelle or engine mass, a lower temperature at the design point requires more mass flow for a fixed thrust. Hence, the engine diameter has to be enlarged, and thus the overall installation becomes heavier.

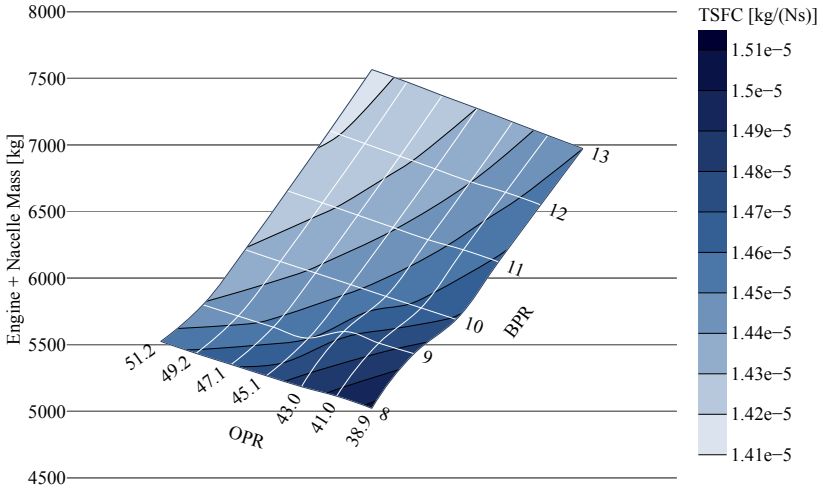

Figure 7.4: Effect of bypass ratio and overall pressure ratio on TSFC in cruise and installation mass (TIT=1400 K)

Hence, from a mass perspective, it appears to be better to maximise the turbine inlet temperature. Increasing the TIT further may necessitate the inclusion of cooling flows which are omitted in the current model for the sake of simplicity. However, maximising this temperature does not necessarily lead to the best thrust specific fuel consumption, as illustrated in Figure 7.5. Depending on the OPR, an optimal TIT exists which minimises the TSFC, although the differences with surrounding TIT values appear to be limited.

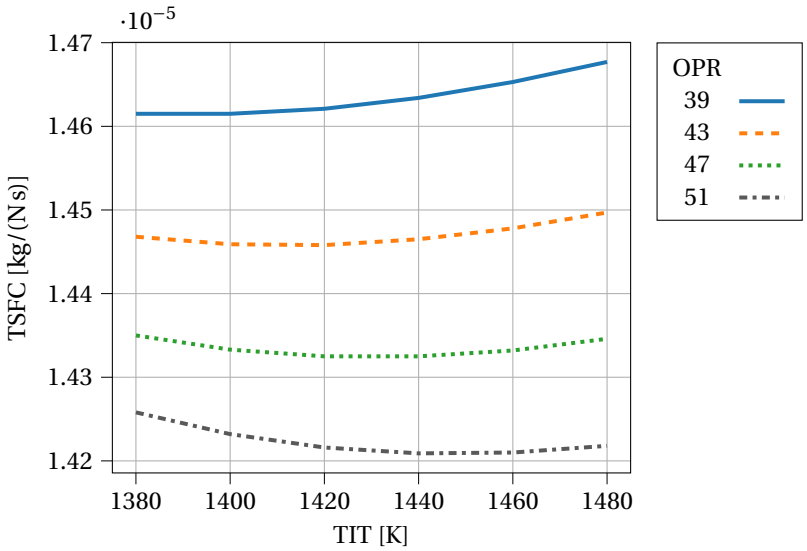

Figure 7.5: Variation in TSFC due to TIT and OPR at the cruise design point (BPR=11)

Hence, in conclusion, it is observed that increasing the OPR instead of the BPR at first sight both improves the fuel consumption, while increments in OPR have a smaller negative effect on the installation weight. Additionally, the installation mass can be lowered by increasing the turbine inlet temperature, while for a given BPR and OPR, an optimal TIT can be selected to reduce the TSFC. These observations are made considering a fixed design thrust requirement and an outer fan pressure ratio which is minimised for a set of OPR, BPR and TIT. These considerations are taken into account when proposing a propulsion system in Chapter 8.

7.2. Fuselage Versus Wing Installation

In the second experiment, the installation on the rear wing of the box-wing aircraft is compared to the installation on the aft fuselage section. These two different installations are displayed Figures 7.6 and 7.7. The change in aircraft aerodynamic coefficients is studied with respect to the aircraft without engines. This comparison was for example not possible during the study by de Klerk [4] in 2010 since the VSAERO preprocessor was limited to the installation on the fuselage. The use of the Multi-Model Generator in this research allows to efficiently adapt the geometry and opens the door for more creativity in early design stages.

To make a comparison of purely the aerodynamic effects, the moment reference point (as specified in Table 7.1) is kept at the same location for all three cases, while for an actual aircraft the moments around the centre of gravity would also be influenced by the shift in the centre of gravity due to engine positioning. The aircraft is tested at a Mach number of 0.79 and a Reynolds number of 25.7 million (approximate cruise conditions) for angles of attack between -2 and 6 degrees. The engine installed in both cases is characterised by a BPR of 11, and OPR of 43 and a TIT of 1430 K.

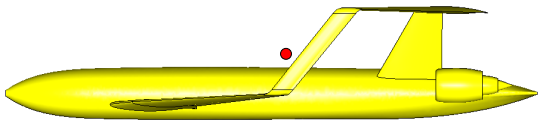

Figure 7.6: Engines installed on the fuselage of the MS1 configuration for the experiment discussed in Section 7.2 (red dot indicates moment reference point)

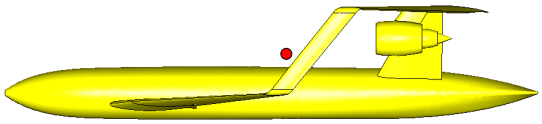

Figure 7.7: Engines installed on the rear wings of the MS1 configuration for the experiment discussed in Section 7.2 (red dot indicates moment reference point)

The results are presented in Figures 7.8 and 7.9. It can be seen that installing the engines on the rear wing has a larger effect than attaching the engines to the fuselage. Both integration types have a negative effect on the overall lift for a given angle of attack. The decrease in lift, and hence the larger moment, can be attributed to a downwash caused by the forward wing and/or local interference with the vertical tail. This negative induced angle of attack on the nacelles and pylon is confirmed by studying the streamlines in the neighbourhood of the engine, as displayed in Figure 7.11.

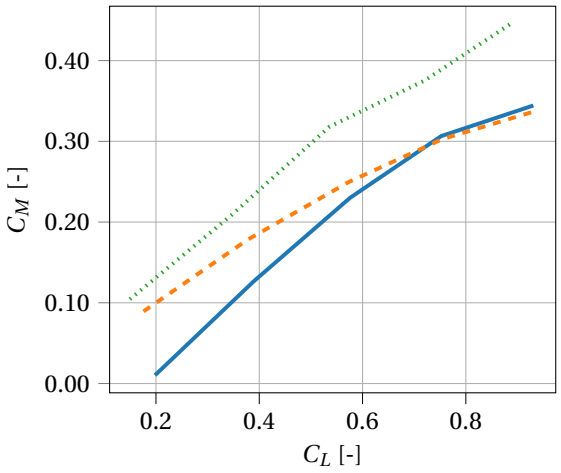

Figure 7.8: Lift and moment coefficients for two potential engine positions

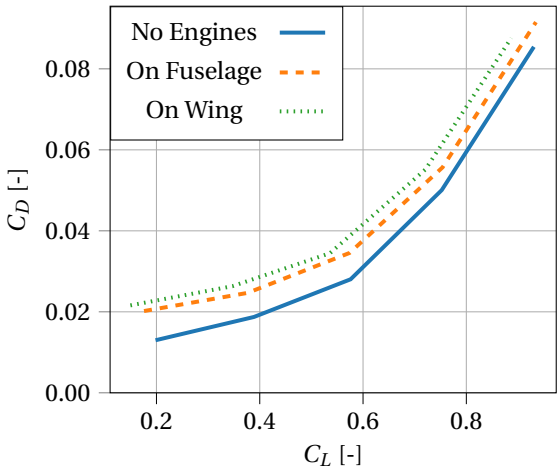

Figure 7.9: Lift and drag coefficients for two potential engine positions

For the on-wing installation, the aerodynamic flow around the rear wing is disturbed and a decrease in lift on the aft wing is observed which is caused by increased velocity on the pressure side of the wing. This decreases the pressure on this side, leading to the overall drop in lift force. The pressure distribution on the pressure side for the three cases is compared in Figure 7.10. Additionally, this makes the lift produced by the front more dominant in the calculation of the moment coefficient, increasing the pitch up tendency of the aircraft. Both engine locations cause an increase in drag, as expected, although this difference appears to be rather large (up to approximately 50%). This unexpected large increase is further discussed in following section.

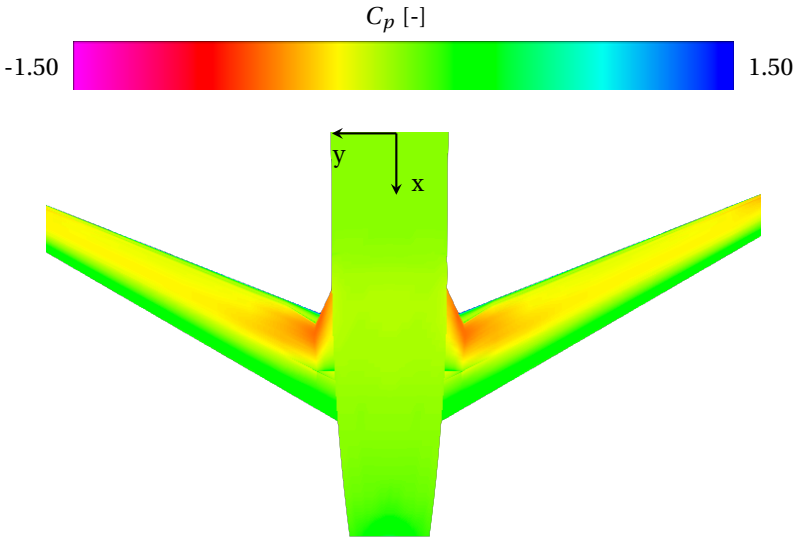

(a) Pressure coefficient distribution for the aircraft without engines

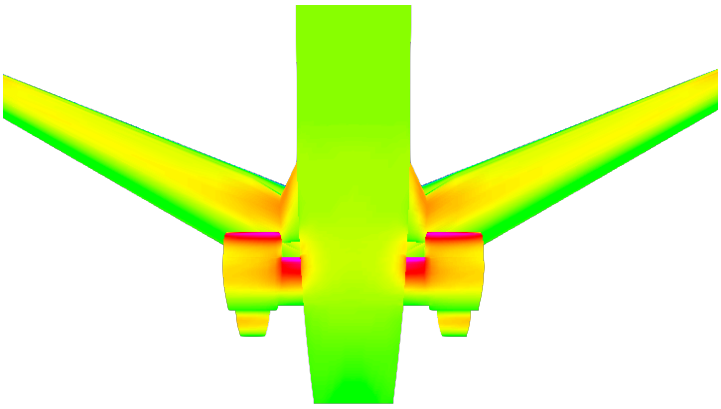

(b) Pressure coefficient distribution for the aircraft with engines installed on the fuselage

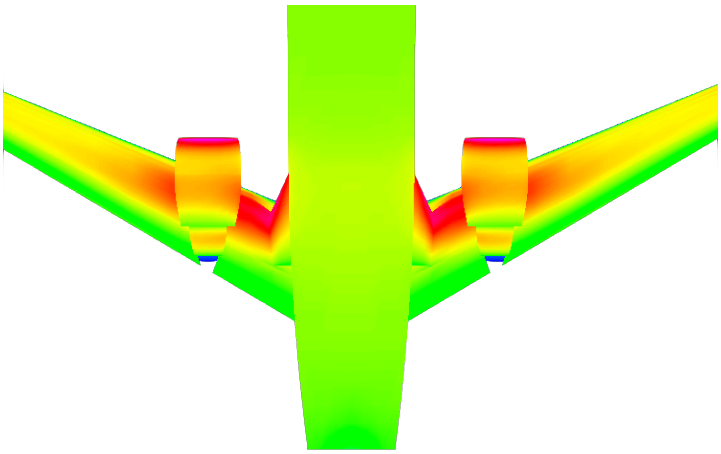

(c) Pressure coefficient distribution for the aircraft with engines installed under the rear wing

Figure 7.10: Pressure coefficient distribution on the pressure (bottom) side of the rear wing, as seen from the bottom of the MS1 configuration

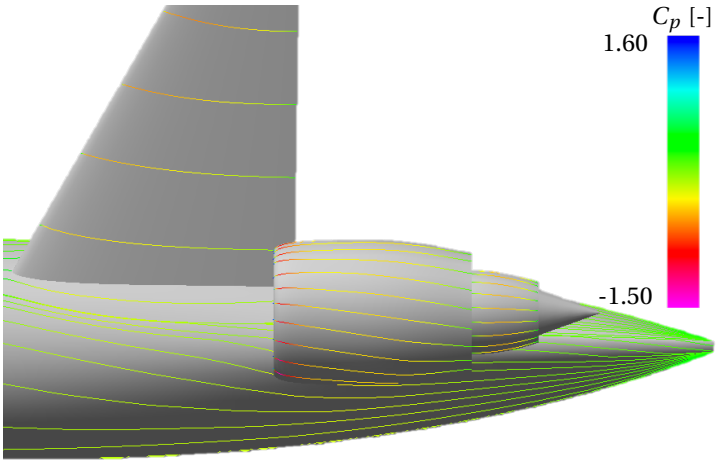

Figure 7.11: Streamlines on the aircraft near the engine installation with BPR=10 and OPR=43 (colours represent local pressure coefficient C_P)

7.3. Engine Design Parameters Versus Aerodynamic Penalties

In this experiment, it is tested whether developments in engine technology can be captured by the aerodynamics analysis. For this particular study, the engines are installed on the rear section of the fuselage, close to the vertical tail structure. Figures 7.12 and 7.13 present the change in aerodynamic force and moment coefficients at two distinct Mach numbers for engines with varying BPR and overall pressure ratio, but designed for the same reference thrust. The data of the aircraft with engines is here compared to the aerodynamic data of the aircraft without pylons or nacelles. Although the lift and moment coefficients show a slight trend with varying BPR, the drag coefficients appear to increase, decrease and increase again.

Nonetheless, the data presented in Figures 7.12 and 7.13 shows no consistent trend with OPR and BPR, while the negative influences are expected to grow clearly with increasing nacelle size, and thus BPR. Although the coefficients vary within limited ranges, it appears that in its current implementation, the aerodynamic analysis does not capture the sensitivities of aerodynamic forces with respect to engine size correctly. Upon further research of the automatic nacelle design and automated meshing, no evident issues were observed. At this point it is concluded that although VSAERO allows to study preliminary the flow around the propulsion system (see for example Figure 7.11), the quantitative results should be considered critically, especially if they are employed in flight mechanics models.

Since the use of VSAERO appears to be able to provide a reasonable estimate of the effect of the nacelles on the lift and moment coefficients, as discussed in Section 6.1.3, the cause of these sensitivity issues here is unknown at the moment. Two reasons are currently expected to have an impact on the sensitivity of the results:

1. In this analysis, the nacelles are modelled with powered engines for which the normal velocities on the inlet and exhaust planes are calculated with the GTpy and GSP tools. The VSAERO results show to be susceptible to small changes in these specified velocities. Therefore, a possible solution would be to model the engine installations as flow-through nacelles in this design stage, as is often done in wind tunnel experiments for example. In this manner, the effects of changing nacelle diameters and lengths can still be captured, without taking into account subtle changes in velocities due to different BPR and OPR values.

2. The position of the engines on the aft fuselage produces a strong local interaction with the fuselage in the simulations, as can be seen from a more detailed study of the VSAERO output files. The most aft patches of the fuselage for example produce a forward drag component in certain conditions. An important factor here is the lateral mesh distribution on the fuselage, which also affects the geometry definition of the wake. A similar study to the one specified in this section, but with the conventional NASA CRM layout and engines placed under the wing rather than on the fuselage, revealed that the fluctuation in results can be reduced. Hence, the formation of the wake on the fuselage and its interac-

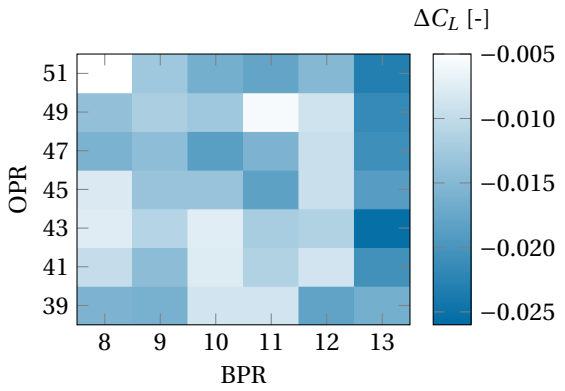

(a) Difference in aircraft lift coefficient

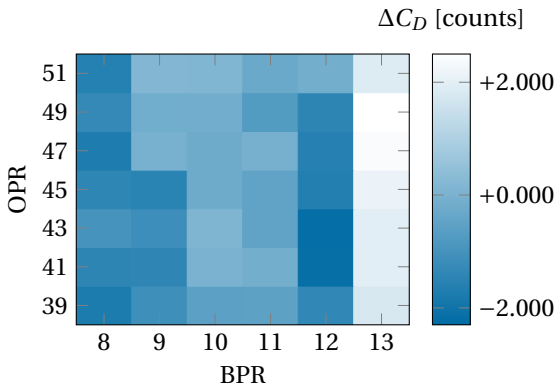

(b) Difference in aircraft drag coefficient

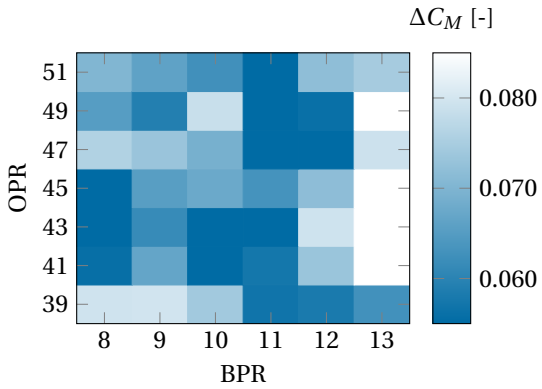

(c) Difference in aircraft pitch moment coefficient

Figure 7.12: Change in force and moment coefficients in cruise (Mach=0.30, Reynolds number= 27.5 million, angle of attack=0 deg) for engines installed on the rear fuselage for varying BPR and OPR

tion with the wakes extending from the engines may be further investigated.

Unexpected trends can especially be observed when studying the change in drag in Figures 7.12b and 7.13b. In the low Mach condition, both positive and negative variations are found, while in the high Mach case the differences are all positive, but for some combinations of OPR and BPR the drag of the aircraft is increased by almost 50%. Although it is anticipated that the drag prediction could not be accurate due to the limitations of VSAERO, these values cannot be considered to be precise in either case.

Therefore, it is suggested to calculate the difference in drag due the engine installations with simpler, empirical relationships in the current development stage, as discussed in Appendix F of Torenbeek [17]. These relationships account for the change in the profile drag and additional engine related drag components. However, these simplifications do not consider the position of the engines with respect to the airframe, and thus vortex induced and interference drag are not considered. By using this method and the nacelle geometry from the MMG, the variation in drag due to OPR and BPR is shown in Figure 7.14, considering a reference wing area of 266.7 m^2.

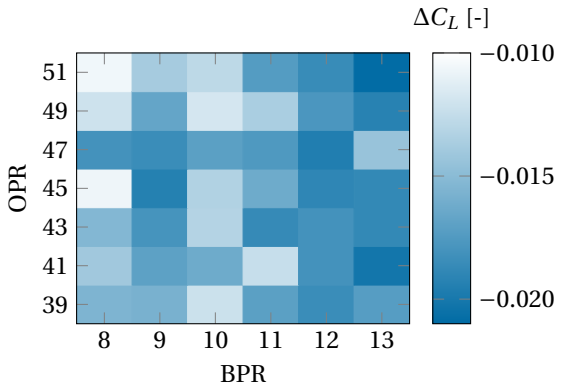

(a) Difference in aircraft lift coefficient

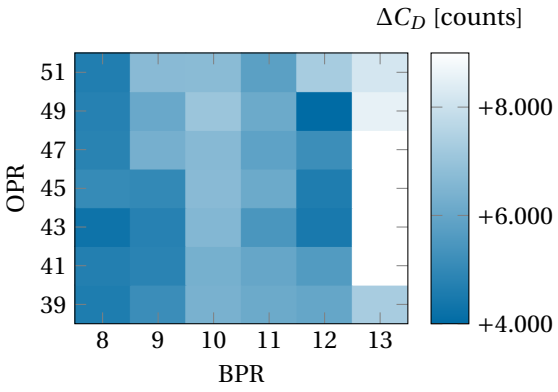

(b) Difference in aircraft drag coefficient

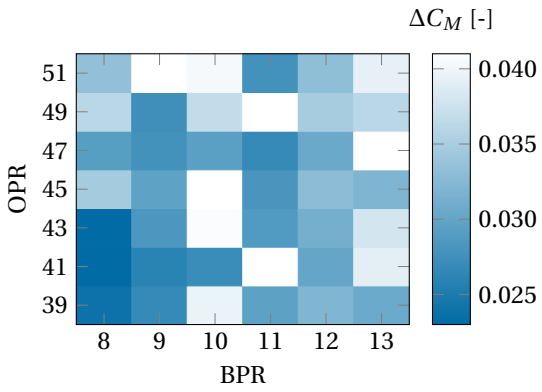

(c) Difference in aircraft pitch moment coefficient

Figure 7.13: Change in force and moment coefficients in cruise (Mach=0.79, Reynolds number= 25.7 million, angle of attack=0 deg) for engines installed on the rear fuselage for varying BPR and OPR

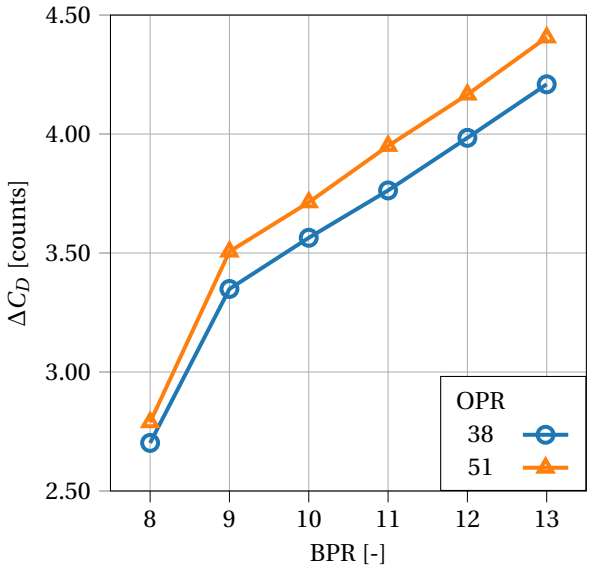

Figure 7.14: Change in drag due to the addition of two engines with varying BPR and OPR, using methods described in Appendix F of Torenbeek [17]

8

PARSIFAL Propulsion System

Considering the analysis work completed in Chapter 7 and the engine design requirements gathered in Table 7.2, a preliminary engine solution for the current PARSIFAL MS1 configuration is proposed. In the current requirement specification, no bleed air and/or power needs are taken into account. Similar to the study completed by de Klerk [4], it is advised to install two engines on the airframe. The two, large engines are able to provide sufficient thrust, while minimising complexity and costs [4].

Based on the considerations from Section 7.1, it is advised to increase the OPR while possibly limiting the bypass ratio. The latest turbofan development programmes, such as the LEAP-1A and PW1000G, feature a bypass ratio of approximately 11 [1]. Research by Hall and Crichton [52] indicates that ultra high bypass ratio engines may require a variable exhaust system (or other system) to obtain a low fan pressure ratio in take-off conditions with a sufficient margin to the surge line to meet noise reduction goals.

Hence, in the current research a BPR of 11 is selected to work within the currently available technology level. However, the achievable OPR level is expected to increase in the following years. The new GE9X engine aims at a maximum pressure ratio of 60, employing compressor technology capable of delivering a pressure ratio of 27, while limiting its BPR to 10 [2]. Taking this constraint and the developments regarding OPR into account, the analysis Figures 7.2 and 7.5 can be further refined. The results are presented in Figures 8.1 and 8.2.

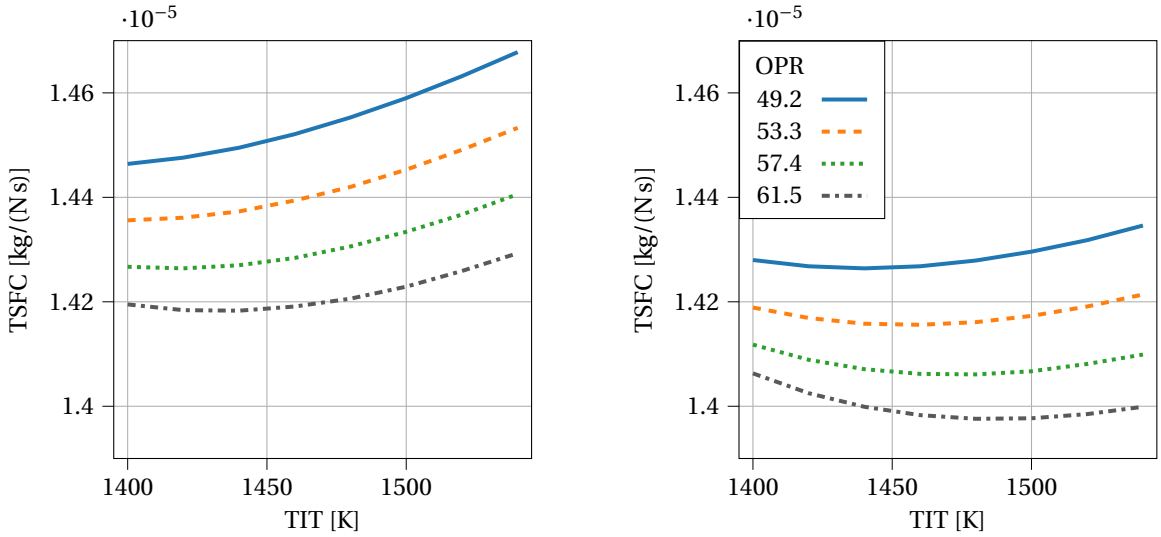

(a) Variation for BPR=9

(b) Variation for BPR=11

Figure 8.1: Variation in cruise TSFC with turbine inlet temperature and overall pressure ratio

[1] URL https://www.safran-aircraft-engines.com/commercial-engines/single-aisle-commercial-jets/leap [Accessed on 15 November 2019]

[2] URL https://www.geaviation.com/commercial/engines/ge9x-commercial-aircraft-engine [Accessed on 15 November 2019]

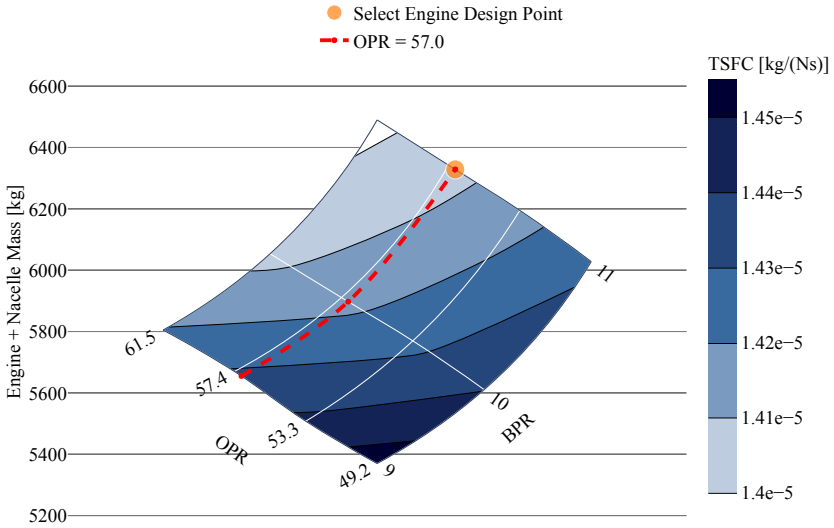

Figure 8.2: Carpet plot showing the selected engine design point (TIT=1480 K)

By comparing Figure 8.1a and Figure 8.1b, it can be seen that the bypass ratio still has a strong effect on the thrust specific fuel consumption. Since the highest pressure ratio of 60 is to be reached at top-of-climb, the design cruise OPR is set to 57. According to Figure 8.1b, a turbine inlet temperature of 1480 K further minimises TSFC. Raising this temperature compared to the analysis in Chapter 7 also decreases the mass flow required, hence reducing the mass. Considering these parameters, the optimal outer fan pressure ratio is equal to 1.57.

The expected thrust specific fuel consumption is summarised and put in perspective in Table 8.1. The difference in thrust with the other two engines shows that the considered PrandtlPlane may indeed require a tailored engine cycle. Additionally, the change in TSFC, which is independent of engine size, shows the improvement in fuel consumption due to the assumed technology level.

Table 8.1: Performance of suggested engine in comparison with in-service engines (FN in kN, TSFC in mg/(Ns)) [83, 20]. The differences (Δ) are with respect to the newly proposed PARSIFAL engine.

	PARSIFAL		**CFM56-5B4**		**GE90-85B**	
Operating Point	**FN**	**TSFC**	**FN** (Δ%)	**TSFC** (Δ%)	**FN** (Δ%)	**TSFC** (Δ%)
Cruise	33.00	14.01	22.24 (-32.6)	15.40 (+9.921)	77.85 (+135.8)	15.30 (+9.208)
Take-Off	180.0	7.027	120.1 (-33.28)	9.6 (+36.62)	376.8 (+109.3)	8.300 (+18.12)

The chosen design point is highlighted in Figure 8.2. The result is an aero engine with a total mass of 4783 kg where the mass of individual modules is summarised in Table 8.2. The dimensions shown in Figure 8.3. Possibly including a geared fan may decrease this weight by making the the low pressure turbine smaller. However, since the weight relation for such a layout is only validated with one engine, a design point selection for this configuration is recommended for further research.

Although this engine is capable of delivering 193 kN of net thrust at standard SLS conditions, which is more than the 180 kN specified in Table 7.2, it is recommended to re-visit this take-off requirement since the engine may not be able to provide 180 kN of thrust in high and hot-day take-offs, if these are expected in the desired flight missions. This study of such effects, as illustrated in Figure 8.4, is simplified by the integration of the GSP software. In addition, it is suggested to use the top-of-climb point as reference point once it is known since it will possibly result in a larger engine. Then the TOC point can be employed to size the engine aerodynamically, the maximum efficiency is desired at cruise, and the engine mechanical design can be driven by the take-off requirement [52].

Table 8.2: Mass breakdown of the PARSIFAL aer engine

Component / Module	**Mass** [kg]	**Percentage of Total** [%]
Fan	1244	26.01
Low Pressure Compressor	283	5.92
High Pressure Compressor	515	10.77
Combustor	231	4.83
High Pressure Turbine	485	10.13
Low Pressure Turbine	1124	23.5
Accessories + Other	901	18.84
Total	4783	

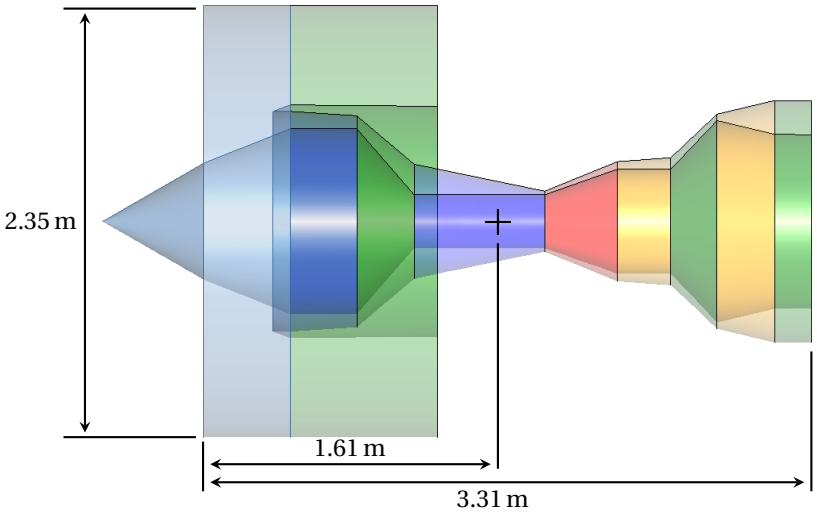

Figure 8.3: PARSIFAL aero engine dimensions with centre of gravity

The engine geometry from above is surrounded by the nacelle design shown in Figure 8.5. The dimensions are gathered in Table 8.3. The engines are installed on the fuselage close to the vertical tail as shown in more detail in Appendix D. The vertical position is selected such that the thrust vector acts through the airframe's centre of gravity, while the longitudinal location is set such that the engine's centre of gravity is aligned with the rear spar of the vertical tails (70% of the chord). The lateral location is determined such that the pylon has span of approximately 0.25 times the maximum nacelle diameter [77].

Table 8.3: Dimensions of nacelle fitted around PARSIFAL aero engine

Parameter	**Value** [m]
D_{fan}	2.35
$D_{\text{t,by}}$	2.32
$D_{\text{h,by}}$	1.62
$D_{\text{t,co}}$	1.15
$D_{\text{h,co}}$	0.89
L_1	5.74
L_2	6.40

The fuselage installation is suggested based on the brief comparison performed in Section 7.2. It is expected that if the engines are to be placed on the rear wing, the aerodynamic design may have to be adapted to overcome the decrease in lift due to the propulsion system. Additionally, since the rear wing is structurally attached to the vertical tail, the loads acting on the engines and the rear wing have to be transferred through the vertical tails to the fuselage. This requires a different structural design of the vertical tail compared to

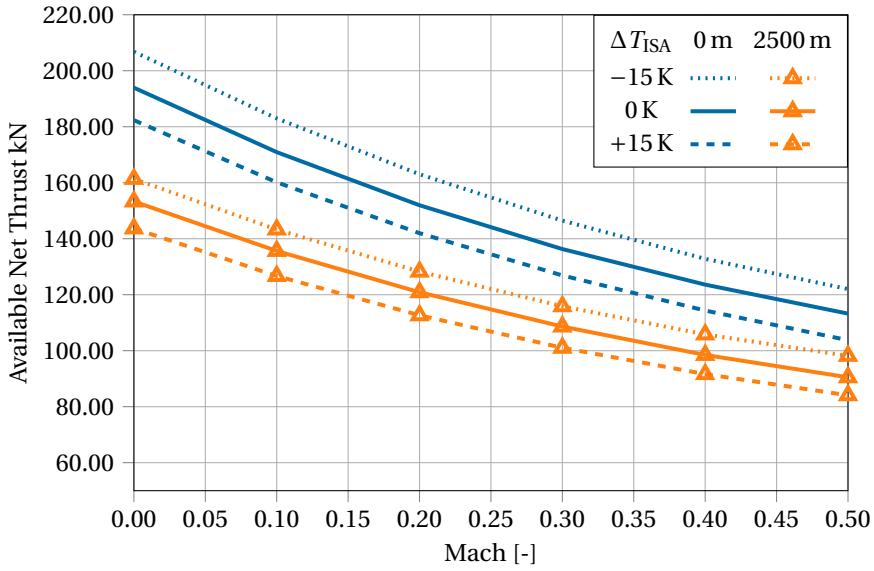

Figure 8.4: Thrust lapse rates for varying altitude and ground temperature

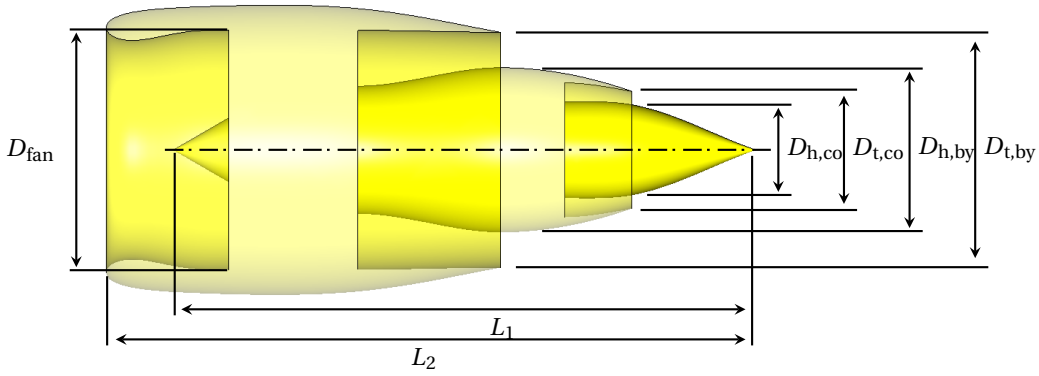

Figure 8.5: Nacelle fitted around PARSIFAL aero engine

conventional configurations and the effect on the weight of the overall structure cannot be captured at this stage.

For this integration, the powerplant mass, including two engines, two nacelles and two pylons, amounts to a total of 13 676 kg for two engines. A detail of this mass distribution is provided in Table 8.4. If the centre of mass of the airframe without engines is assumed to be located at 21.88 m from the nose in maximum take-off weight condition (110 410 kg) without engines, then the position and weight of the engine installation suggested in this chapter causes this location to shift towards the tail by approximately 23.34 m. The difference in x-location amounts to 33.88% of the mean aerodynamic chord.

Table 8.4: Mass distribution of propulsion system installation

	Mass [kg]	**Number**	**Total [kg]**
Aero Engine	4783	2	9566
Nacelle	1385	2	2770
Pylon	670	2	1340
			13676

9

Conclusions and Recommendations

The aim of the research presented in this report was to apply a Knowledge Based Engineering approach towards the design, integration and analysis of the propulsion system in a preliminary design phase. The methods are set up independently from the aircraft configuration, allowing them to be employed for a study of the engine integration on box-wing aircraft. In this chapter an overview of the completed work is provided and conclusions are drawn from the research by reflecting back on the initial research questions. Moreover, recommendations are made for further research utilising the newly acquired tools, as well as for new developments extending the methodology.

Conclusions

The research was triggered by the need for a propulsion system tailored for the aircraft configuration studied in the PARSIFAL project. In addition, the need for tools which are sensitive to changes in top level requirements aligns with the recommendations made by de Klerk [4] to employ more advanced design methodologies to examine the integration of engines as a multi-disciplinary problem. Hence, it was decided to employ a KBE approach, including the use of the in-house Multi-Model Generator. This technology facilitates the efficient storage and execution of engineering rules to size components and to automate repetitive tasks such as manipulating the product geometry.

Since the inclusion of the propulsion discipline in the MMG and the overall design framework was new, it was decided to build a separate tool called GTpy which focuses on a physics-based approach towards turbofan design. Subsequently, the engine geometry can be joined with the aircraft model in the MMG. From this integrated model, input files for discipline specific analyses, such as aerodynamics (VSAERO), engine performance (GSP) and flight mechanics (PHALANX), can be created.

The preliminary engine design, as carried out by GTpy, is initiated by the component-based specification of the engine in a CPACS input file. To support this object-oriented definition, a toolspecific element was introduced to the standard format. The advantage of using CPACS is that it simplifies the communication between independently built analysis tools which target distinct disciplines. Hence, the information produced by GTpy, such as an engine performance deck, can be communicated with the flight mechanics tool by writing and reading the necessary data from preallocated slots in the CPACS structure.

Once the engine cycle and requirements are fixed, the engine can be automatically sized for the required thrust. To analyse the engine model in more detail and to carry out off-design simulations, the model can be translated into an XML format which can be interpreted by GSP. The provided GSP API is called from GTpy to immediately obtain the 0D performance of the engine for various conditions. The results from the design and off-design steps are utilised to build a preliminary geometry of the flowpath and to determine the approximate mass of turbofan engines. These aero engine design steps are verified and validated with publicly available data of the General Electric GE90 engine.

The nacelle is parameterised using a convenient set of design variables, for which values are computed based on the engine flowpath and knowledge based rules from literature. However, to fully define the aerodynamic shape, the intuitive parameters are transformed to a CST parameterisation which results automatically in smooth contours. Based on the relative location of the nacelle with respect to the airframe, the pylon is

automatically constructed by exploiting the CAD operations built into ParaPy. The key is to first define the leading and trailing edge segments of the pylon, which are then used as guides for lofting the outer shape.

Having a fully integrated product model, the geometry can be prepared for an aerodynamic analysis by VSAERO. To this extent, the geometry is translated to a body of smaller, individual panels on the surface. In this research, the methods for automatic meshing are extended to include the nacelles. The engines are modelled by specifying non-zero normal velocities on their inlet and outlet faces, and by instantiating closed wakes from the exhaust edges.

In a validation with the NASA Common Research model it was shown that VSAERO is capable of modelling the lift and moment coefficients accurately, while the drag coefficient appeared to be underestimated. Nevertheless, the latter was expected since the 3D panel code cannot capture all drag components. In this research the figures of merit are limited to immediate forces and moments acting on the aircraft, although the velocity and pressure distribution over the 3D model are available for inspection.

Once the individual methods were implemented and validated, a series of experiments was conducted to test the connected tools and to explore the design space the Prandtlplane offers. Firstly, the influence of engine design parameters on the thrust specific fuel consumption and installation mass was analysed. It appears that especially the overall pressure ratio is a valuable design parameter since it decreases the fuel consumption of the engine, while having a smaller influence on the mass of the installation than the bypass ratio.

Subsequently, the effects on lift, drag and pitching moment due to engine installations on the rear wing and aft fuselage were compared. It can be observed that the fuselage position has the least overall effect in contrast to the airframe without engines. For the fuselage mounted engines, the overall lift is reduced due to a downwash acting on the nacelles, increasing the pitch up moment. In case of the wing-mounted configuration, the nacelles disturb the flow around the aft wing, which has a larger negative effect on the lift produced by this wing.

The last experiment attempted to retrieve the effects of engine design choices, such as BPR and OPR, on the aerodynamic forces and moments when installed on the fuselage close to the vertical tail structure. The implementation including the MMG greatly simplifies the process of changing geometries and adapting the mesh accordingly. However, it is concluded that in the current implementation, the VSAERO analysis does not show consistent trends, but rather results including noise. A specific reason for these irregularities was not identified at the time of writing. Improvements can possibly be made by considering flow-through nacelles instead of powered models, and by further reviewing the local interactions on rear section of the fuselage.

In response to research question two, which aims at a propulsion system design and integration tailored to the PARSIFAL aircraft, a limited exploration of the design space is completed. It is recommended to tailor the engine cycle using the design variables specified in Table 9.1, where indeed the bypass ratio is limited to currently available values, while the overall pressure ratio has been increased taking into account further developments. Two engines are installed on the PARSIFAL aircraft, near the vertical tails to minimise the interference with the wing system, while also eliminating the need for additional structural elements.

Table 9.1: PARSIFAL aero engine design variables

Design Parameter	**Value**
BPR [-]	11.00
OPR [-]	57.00
FPR [-]	1.57
TIT [K]	1480.00

Research question three considered the sensitivity of the methodology to varying design requirements. Altering the requirements and design choices clearly has a logical impact on the aero engine and nacelle geometries and on the weight estimations. From the experiments carried out in this research, it is concluded that the current implementation of the design methods indeed allows to react to variable inputs as expected and can thus also react to findings from other disciplines. Nonetheless, it has to be recognised that the aerodynamic results do not respond as expected to variations in design variables. Therefore, it is advised to review these results critically, since such irregularities may further propagate in the results of other disciplines relying on the aerodynamic data.

Due to the above mentioned irregularities in the VSAERO results and time constraints, the effect of the chosen engine cycle on other aircraft performance parameters, such as fuel weight, handling characteristics, etc., could not be evaluated in the current project. Nevertheless, the proposed engine design can be introduced into other work packages of the larger PARSIFAL research project. Following up on the findings from other work packages, the implemented tools allow to update the engine design and integration accordingly.

Recommendations

The currently implemented tools should also be employed to assess other installation locations, such as the lower, front wings for example. However, in this research only the aerodynamic forces and moments were considered as figures of merit. Since the coupling between engine deck produced by GTpy and the PHALANX flight mechanics tool has already been implemented, the aerodynamic data can be used to perform flight mechanics analyses.

The latter are expected to provide better insight in the overall aircraft performance by, for example, carrying out a mission analysis leading to the total fuel consumption, or by investigating the influence of the propulsion system on the control and stability derivatives. Specifically, the trim drag in cruise can be evaluated and provided as an input to GTpy to iterate on the required thrust at this design point. Such metrics would also allow to highlight the missions in which the Prandtlplane has a distinct advantage over conventional layouts. However, to be able to iterate on all disciplines in a MDAO framework in a robust manner, the noise in the VSAERO results first has to be reduced.

Additionally, the following research topics and further developments are suggested:

1. It would be interesting to study the effect of higher bypass engines (BPR > 11) on aircraft performance. Although the current implementation is set up in a general manner, it is recommended to verify the implemented design rules for higher values of bypass ratio. For example, variable exhaust systems may be required, as described by Hall and Crichton [52], to obtain satisfactory engine operation while reducing the noise production.
2. Since the geometries of the nacelles and pylons are available, ParaPy functions can be employed to create meshes for higher fidelity aerodynamic analysis, such as Euler codes or RANS simulations. Although an analysis of the entire aircraft may be too computationally expensive, at least the local effects can be further examined with improved accuracy.
3. Certain aspects of integration are not yet considered, such as the structures and aero-elasticity disciplines. Especially for box-wing aircraft, installing the engines on the rear wing potentially has an impact on the weight of the vertical tail and the deformation of the wing system.
4. The mechanical design of the engines can be further extended, facilitating a hybrid [43] or a full component-based [18] weight estimation of turbofan engines. However, it is expected that the validation of such methods may be troublesome, and therefore it has to be weighed against the increase in accuracy.
5. Also engine emissions perform an important role for the future aircraft concepts, since the goal is to further reduce the negative effect on global warming [26]. This can possibly be taken into account by built-in methods provided by GSP which were not activated in this research. These methods model the composition of the exhaust gases. Furthermore, costs can be included to have a more complete picture in optimisations for example.
6. As discussed in Section 4.1 and Appendix A, use is made of the CPACS format and a dedicated toolspecific section is proposed. However, in the author's opinion it would be helpful to include a component-based definition of engines in the standard CPACS format, similar to the setup for complete aircraft. This would allow to store more key design variables and performance parameters such as efficiencies.

The newly developed and validated GTpy tool, and the integration with the in-house Multi-Model Generator can also be employed in future aircraft design research projects with varying objectives. Applications to consider the propulsion discipline in a preliminary design stage were not yet included in the Design Engineering Framework described in Section 2.6 and Chapter 3. Although in this Thesis project the focus lied on the PARSIFAL PrandtlPlane configuration, the tools are developed with a broader range of applications and aircraft configurations in mind.

Bibliography

[1] International Air Transport Association (IATA), "Airport of The Future," https://www.iata.org/whatwedo/ops-infra/airport-infrastructure/documents/aof_brochure_02.pdf, 2017.

[2] Cipolla, V., Frediani, A., Abu Salem, K., Picchi Scardaoni, M., Nuti, A., and Binante, V., "Conceptual design of a box-wing aircraft for the air transport of the future," *2018 Aviation Technology, Integration, and Operations Conference*, AIAA, Atlanta, Georgia, 2018, p. 3660. doi:10.2514/6.2018-3660.

[3] McMasters, J., Paisley, D., Hubert, R., Kroo, I., Bofah, K., Sullivan, J., and Drela, M., "Advanced Configurations for Very Large Subsonic Transport Airplanes," Tech. Rep. NASA CR-198351, National Aeronautics and Space Administration (NASA) and Boeing Commercial Airplane Group, 1996.

[4] de Klerk, J., "Design and integration of a propulsion system for the PrandtlPlane," Master's thesis, Delft University of Technology (TU Delft), 2010.

[5] Lange, R., Cahill, J., Bradley, E., Eudaily, R., Jenness, C., and MacWilkinson, D., "Feasibility Study of The Transonic Biplane Concept for Transport Aircraft Application," Tech. Rep. LG74ER0077 / NASA-CR-132462, Lockheed-Georgia Co. / NASA, 1974.

[6] Schiktanz, D., and Scholz, D., "Box Wing Fundamentals - an Aircraft Design Perspective," *Deutscher Luft- und Raumfahrtkongress*, Bremen, 2011, pp. 601–615.

[7] Barnstorff, K., "New Ideas Sharpen Focus for Greener Aircraft," https://www.nasa.gov/topics/aeronautics/features/greener_aircraft.html, Jan 2012.

[8] Mattingly, J. D., Heiser, W. H., and Pratt, D. T., *Aircraft Engine Design*, 2nd ed., AIAA, Reston, Virginia, 2002. doi:10.2514/4.861444.

[9] Jenkinson, L., Simpkin, P., and Rhodes, D., *Civil Jet Aircraft Design*, Arnold, London, 1999. doi:10.2514/4.473500.

[10] Heidebrecht, A., Stańkowski, T., and MacManus, D., "Parametric Geometry and CFD Process for Turbofan Nacelles," *ASME Turbo Expo 2016: Turbomachinery Technical Conference and Exposition*, ASME, Seoul, 2016, p. V001T01A033. doi:10.1115/GT2016-57784.

[11] Stankowski, T. P., MacManus, D. G., Robinson, M., and Sheaf, C. T., "Aerodynamic Effects of Propulsion Integration for High Bypass Ratio Engines," *Journal of Aircraft*, Vol. 54, No. 6, 2017, pp. 2270–2284. doi:10.2514/1.C034150.

[12] Berry, D. L., "The Boeing 777 Engine/Aircraft Integration Aerodynamic Design Process," *19th Congress of the International Council on Aeronautical Sciences (ICAS)*, AIAA, Anaheim, California, 1994, pp. 1305–1320.

[13] La Rocca, G., and van Tooren, M., "Enabling distributed multi-disciplinary design of complex products: a knowledge based engineering approach," *Journal of Design Research*, Vol. 5, No. 3, 2007, pp. 333–352. doi:10.1504/JDR.2007.014880.

[14] Walsh, P. P., and Fletcher, P., *Gas turbine performance*, 2nd ed., Blackwell Science Ltd, Oxford, 2004. doi:10.1002/9780470774533.

[15] Turner, M. G., "Full 3D Analysis of the GE90 Turbofan Primary Flowpath," Tech. Rep. NASA/CR-2000-209951, National Aeronautics and Space Administration (NASA), 2000.

[16] Rego, L., Avallone, F., Ragni, D., Casalino, D., and van der Velden, W., "Free-Stream Effects on Jet-Installation Noise of a Dual-Stream Engine," *25th AIAA/CEAS Aeroacoustics Conference*, 2019, p. 2491. doi:10.2514/6.2019-2491.

[17] Torenbeek, E., *Synthesis of Subsonic Airplane Design*, Delft University Press and Kluwer Academic Publishers, Dordrecht, 1982.

[18] Onat, E., and Klees, G. W., "A Method to Estimate Weight and Dimensions of Large and Small Gas Turbine Engines," Tech. Rep. NASA-CR-159481, National Aeronautics and Space Administration (NASA), 1979.

[19] Greitzer, E. M., Bonnefoy, P. A., de la Rosa Blanco, E., Dorbian, C. S., Drela, M., Hall, D. K., Hansman, R. J., Hileman, J. I., Liebeck, R. H., Lovegren, J., Mody, P., Pertuze, J. A., Sato, S., Spakovszky, Z. S., Tan, C. S., Hollman, J. S., Duda, J. E., Fitzgerald, N., Houghton, J., Kerrebrock, J. L., Kiwada, G. F., Kordonowy, D., Parrish, J. C., Tylko, J., Wen, E. A., and Lord, W. K., "N+3 Aircraft Concept Designs and Trade Studies. Volume 2: Appendices - Design Methodologies for Aerodynamics, Structures, Weight, and Thermodynamic Cycles," Tech. Rep. NASA/CR-2010-216794/VOL2, National Aeronautics and Space Administration (NASA), 2010.

[20] IHS Markit, "General Electric GE90," *Jane's Aero-Engines*, IHS Markit, 2018.

[21] York, M. A., Hoburg, W. W., and Drela, M., "Turbofan Engine Sizing and Tradeoff Analysis via Signomial Programming," *Journal of Aircraft*, Vol. 55, No. 3, 2018, pp. 988–1003. doi:10.2514/1.C034463.

[22] Ostrower, J., "Boeing narrows 737 Max engine fan size options to two," `https://www.flightglobal.com/news/articles/boeing-narrows-737-max-engine-fan-size-options-to-tw-361438/`, Aug 2011.

[23] Prandtl, L., "Induced Drag of Multiplanes," Tech. Rep. NACA-TN-182, National Advisory Committee for Aeronautics (NACA), 1924.

[24] La Rocca, G., "Knowledge Based Engineering Techniques to Support Aircraft Design and Optimization," Ph.D. thesis, Delft University of Technology (TU Delft), 2011.

[25] Airbus, *Global Networks, Global Citizens 2018-2037*, 5th ed., Airbus S.A.S., Blagnac Cedex, 2018.

[26] The High Level Group on Aviation Research, "Flightpath 2050 Europe's Vision for Aviation," , 2011. doi:10.2777/50266, URL `http://ec.europa.eu/transport/modes/air/doc/flightpath2050.pdf`.

[27] IHS Markit, "Airbus A320," *Jane's All The World's Aircraft: Development & Production*, IHS Markit, 2019.

[28] IHS Markit, "Airbus A330," *Jane's All The World's Aircraft: Development & Production*, IHS Markit, 2019.

[29] Demasi, L., Dipace, A., Monegato, G., and Cavallaro, R., "Invariant Formulation for the Minimum Induced Drag Conditions of Nonplanar Wing Systems," *AIAA Journal*, Vol. 52, No. 10, 2014, pp. 2223–2240. doi:10.2514/1.J052837.

[30] Frediani, A., Cipolla, V., Abu Salem, K., Binante, V., and Picchi Scardaoni, M., "On the preliminary design of PrandtlPlane civil transport aircraft," *7th European Conference for Aeronautics and Space Sciences (EUCASS)*, Milan, 2017, p. 546. doi:10.13009/EUCASS2017-546.

[31] Spaeth, A., "Onboard Lufthansa's First Airbus A320neo Flight," `https://airwaysmag.com/traveler/lufthansa-first-airbus-a320neo-flight/`, Jan 2016.

[32] Kok, H., Voskuijl, M., and van Tooren, M., "Distributed Propulsion Featuring Boundary Layer Ingestion Engines for the Blended Wing Body Subsonic Transport," *51st AIAA/ASME/ASCE/AHS/ASC Structures, Structural Dynamics, and Materials Conference*, AIAA, Orlando, Florida, 2010, p. 3064. doi:10.2514/6.2010-3064.

[33] Rosenblum, A., and Pastore, R., "The Jets of the Future," `https://www.popsci.com/technology/article/2012-04/jets-future`, May 2012.

[34] Lockheed Martin ERA Team, "Lockheed Martin ERA N+2 Advanced Vehicle Concept Results," , Jan 2012. Meeting presentation.

[35] Jemitola, P. O., and Fielding, J. P., "Box Wing Aircraft Conceptual Design," *28th International Congress of The Aeronautical Sciences (ICAS)*, Brisbane, 2012, pp. 570–579.

[36] Andrews, S. A., and Perez, R. E., "Comparison of box-wing and conventional aircraft mission performance using multidisciplinary analysis and optimization," *Aerospace Science and Technology*, Vol. 79, 2018, pp. 336–351. doi:10.1016/j.ast.2018.05.060.

[37] Bartel, M., and Young, T. M., "Simplified Thrust and Fuel Consumption Models for Modern Two-Shaft Turbofan Engines," *Journal of Aircraft*, Vol. 45, No. 4, 2008, pp. 1450–1456. doi:10.2514/1.35589.

[38] Svoboda, C., "Turbofan engine database as a preliminary design tool," *Aircraft Design*, Vol. 3, No. 1, 2000, pp. 17–31. doi:10.1016/S1369-8869(99)00021-X.

[39] Reitenbach, S., Krumme, A., Behrendt, T., Schnös, M., Schmidt, T., Hönig, S., Mischke, R., and Mörland, E., "Design and Application of a Multidisciplinary Predesign Process for Novel Engine Concepts," *Journal of Engineering for Gas Turbines and Power*, Vol. 141, No. 1, 2018, p. 011017. doi:10.1115/1.4040750.

[40] Drela, M., "Simultaneous Optimization of the Airframe, Powerplant, and Operation of Transport Aircraft," *2nd Aircraft Structural Design Conference*, Royal Aeronautical Society, London, 2010, pp. 1644–1671.

[41] Seitz, A. F., "Advanced Methods for Propulsion System Integration in Aircraft Conceptual Design," Ph.D. thesis, Technische Universität München, 2012.

[42] Water, M. H., and Schairer, E. T., "Analysis of Propulsion System Weight and Dimensions," Tech. Rep. NASA-TM-X-73199, National Aeronautics and Space Administration (NASA), 1977.

[43] Lolis, P., Giannakakis, P., Sethi, V., Jackson, A. J., and Pilidis, P., "Evaluation of aero gas turbine preliminary weight estimation methods," *Aeronautical Journal*, Vol. 118, No. 1204, 2014, pp. 625–641. doi:10.1017/S0001924000009404.

[44] Hoheisel, H., "Aerodynamic Aspects of Engine-Aircraft Integration of Transport Aircraft," *Aerospace Science and Technology*, Vol. 1, No. 7, 1997, pp. 475–487. doi:10.1016/S1270-9638(97)90009-2.

[45] Rubio Pascual, B., "Engine-Airframe Integration for the Flying-V," Master's thesis, Delft University of Technology (TU Delft), 2018.

[46] Christie, R., Heidebrecht, A., and MacManus, D., "An Automated Approach to Nacelle Parameterization Using Intuitive Class Shape Transformation Curves," *Journal of Engineering for Gas Turbines and Power*, Vol. 139, No. 6, 2017, pp. 062601–062601–9. doi:10.1115/1.4035283.

[47] Oliveira, G., Trapp, L. G., and Puppin-Macedo, A., "Engine-Airframe Integration Methodology for Regional Jet Aircrafts with Underwing Engines," *41st Aerospace Sciences Meeting and Exhibit*, AIAA, Reno, Nevada, 2003, pp. AIAA 2003–934. doi:10.2514/6.2003-934.

[48] Groot, R., "Stability & control derivatives prediction for box wing aircraft configurations," Master's thesis, Delft University of Technology (TU Delft), 2019.

[49] Lednicer, D., Tidd, D., and Birch, N., "Analysis of a Close Coupled Nacelle Installation using a Panel Method (VSAERO) and a Multigrid Euler Method (MGAERO)," *19th Congress of the International Council of the Aeronautical Sciences*, Vol. 19, AIAA, Anaheim, California, 1994, pp. 2409–2409.

[50] Clark, D., Maskew, B., and Dvorak, F., "The Application of a Second Generation Low-Order Panel Method - Program 'VSAERO' - to Powerplant Installation Studies," *22nd Aerospace Sciences Meeting*, AIAA, Reno, Nevada, 1984, p. 122. doi:10.2514/6.1984-122.

[51] Tejero, F., Robinson, M., MacManus, D. G., and Sheaf, C., "Multi-objective optimisation of short nacelles for high bypass ratio engines," *Aerospace Science and Technology*, Vol. 91, 2019, pp. 410–421. doi:10.1016/j.ast.2019.02.014.

[52] Hall, C. A., and Crichton, D., "Engine Design Studies for a Silent Aircraft," *Journal of Turbomachinery*, Vol. 129, No. 3, 2007, pp. 479–487. doi:10.1115/1.2472398.

[53] Berton, J. J., "Noise Reduction Potential of Large, Over-the-Wing Mounted, Advanced Turbofan Engines," Tech. Rep. NASA/TM-2000-210025, National Aeronautics and Space Administration (NASA), Cleveland, Ohio, 2000. doi:10.13140/RG.2.1.1373.9608.

[54] Early, K., "Propulsion Airframe Integration Design, Analysis and Challenges Going into the 21st Century," *22nd Congress of International Council of the Aeronautical Sciences (ICAS)*, Harrogate, 2000, pp. 6103.1–11. doi:10.1017/S0001924000064010.

[55] Cedar, R., Forrester, J., and Yokoyama, K., "Integrated Aircraft Engine Design - The Implementation of the Master Model Concept At GE Aircraft Engines," *24th International Congress of the Aeronautical Sciences (ICAS)*, Yokohama, 2004, pp. 2004–6.4.2.

[56] Elmendorp, R. J. M., "Synthesis of Novel Aircraft Concepts," Master's thesis, Delft University of Technology (TU Delft), 2014.

[57] Heidmann, M. F., "Interim Prediction Method for Fan and Compressor Source Noise," Tech. Rep. NASA-TM-X-71763, National Aeronautics and Space Administration (NASA), 1979.

[58] Stone, J. R., "Interim Prediction Method for Jet Noise," Tech. Rep. NASA-TM-X-71618, National Aeronautics and Space Administration (NASA), 1974.

[59] van Gent, I., and La Rocca, G., "Formulation and integration of MDAO systems for collaborative design: A graph-based methodological approach," *Aerospace Science and Technology*, Vol. 90, 2019, pp. 410–433. doi:10.1016/j.ast.2019.04.039.

[60] Nagel, B., Böhnke, D., Gollnick, V., Schmollgruber, P., Rizzi, A., La Rocca, G., and Alonso, J. J., "Communication in Aircraft Design: Can We Establish a Common Language?" *28th International Congress Of The Aeronautical Sciences (ICAS)*, Brisbane, 2012, pp. ICAS2012–1.9.1.

[61] Visser, W. P., "Generic Analysis Methods for Gas Turbine Engine Performance: The development of the gas turbine simulation program GSP," Ph.D. thesis, Delft University of Technology (TU Delft), 2015.

[62] Kurzke, J., and Halliwell, I., *Propulsion and Power: An Exploration of Gas Turbine Performance Modeling*, Springer, Cham, 2018. doi:10.1007/978-3-319-75979-1.

[63] Hall, E. J., Delaney, R. A., Lynn, S. R., and Veres, J. P., "Energy Efficient Engine Low Pressure Subsystem Aerodynamic Analysis," *34th AIAA/ASME/SAE/ASEE Joint Propulsion Conference and Exhibit*, Cleveland, Ohio, 1998, p. 3119.

[64] Suzuki, M., and Kuno, N., "Research & Development of Two-stage Fan Component in HYPR Project," *31st AIAA/ASME/SAE/ASEE Joint Propulsion Conference and Exhibit*, San Diego, California, 1995, p. 2344.

[65] Plencer, R. M., "Plotting Component Maps in the Navy/NASA Engine Program (NNEP) – A Method and Its Usage," Tech. Rep. NASA-TM-101433, National Aeronautics and Space Administration (NASA), 1989.

[66] Csank, J., May, R. D., Litt, J. S., and Guo, T., "Control Design for a Generic Commercial Aircraft Engine," *46th AIAA/ASME/SAE/ASEE Joint Propulsion Conference & Exhibit*, AIAA, Nashville, Tennessee, 2010, pp. 6.2010–6629.

[67] Obert, E., *Aerodynamic design of transport aircraft*, IOS press, 2009.

[68] IHS Markit, "CFM International CFM56," *Jane's Aero-Engines*, IHS Markit, 2019.

[69] Pini, M., "Axial Turbines," , 2019. Turbomachinery - AE4206 (lecture slides).

[70] Nicolai, L. M., and Carichner, G. E., *Fundamentals of Aircraft and Airship Design*, Vol. 1, AIAA, Reston, Virginia, 2010. doi:10.2514/4.867538.

[71] Kozaczuk, K., "Engine nacelles design–Problems and challenges," *Proceedings of the Institution of Mechanical Engineers, Part G: Journal of Aerospace Engineering*, Vol. 231, No. 12, 2017, pp. 2259–2265. doi:10.1177/0954410017706993.

[72] Bartoli, N., Lefebvre, T., Dubreuil, S., Panzeri, M., d'Ippolito, R., Anisimov, K., and Savelyev, A., "Robust Nacelle Optimization Design investigated in the AGILE European project," *2018 Multidisciplinary Analysis and Optimization Conference*, Atlanta, Georgia, 2018, p. 3250. doi:10.2514/6.2018-3250.

[73] Kulfan, B., and Bussoletti, J., ""Fundamental" Parameteric Geometry Representations for Aircraft Component Shapes," *11th AIAA/ISSMO Multidisciplinary Analysis and Optimization Conference*, Portsmouth, Virginia, 2006, p. 6948. doi:10.2514/6.2006-6948.

[74] Stockman, N. O., Yates, D. E., and Crum, T. S., "Nacelle inlet for an aircraft gas turbine engine," , Oct 1991. US Patent 5,058,617.

[75] Chandavari, V., and Palekar, S., "Diffuser Angle Control to Avoid Flow Separation," *International Journal of Technical Research and Application*, Vol. 2, No. 5, 2014, pp. 16–21.

[76] Torenbeek, E., and Berenschot, G., "De berekening van het omspoeld gonderoppervlak van enkel- en dubbelstroom straalmotoren voor civiele vliegtuigen," *Technische Hogeschool Delft, Vliegtuigbouwkunde, memorandum m-445*, 1983.

[77] Vos, R., and Melkert, J. A., "Wing and Propulsion System Design," , 2019. AE1222-II Aerospace Design and Systems Engineering Elements I (lecture slides).

[78] Torenbeek, E., *Advanced Aircraft Design: Conceptual Design, Analysis and Optimization of Subsonic Civil Airplanes*, John Wiley & Sons, Chichester, 2013.

[79] Lord, W. K., and Zysman, S. H. a., "VSAERO Analysis of a Wing/Pylon/Nacelle Configuration," *AIAA/ASME/SAE/ASEE 22nd Joint Propulsion Conference*, AIAA, Huntsville, Alabama, 1986, p. 1523.

[80] Raju Kulkarni, A., Varriale, C., Voskuijl, M., La Rocca, G., and Veldhuis, L., "Assessment of Sub-scale Designs for Scaled Flight Testing," *AIAA AVIATION Forum*, Dallas, Texas, 2019, pp. AIAA–2019–3089. doi:10.2514/6.2019-3089.

[81] Robinson, M., MacManus, D. G., and Sheaf, C., "Aspects of aero-engine nacelle drag," *Proceedings of the Institution of Mechanical Engineers, Part G: Journal of Aerospace Engineering*, Vol. 233, No. 5, 2019, pp. 1667–1682. doi:10.1177/0954410018765574.

[82] Rivers, M. B., Hunter, C. A., and Campbell, R. L., "Further Investigation of the Support System Effects and Wing Twist on the NASA Common Research Model," *30th AIAA Applied Aerodynamics Conference*, New Orleans, Louisiana, 2012, p. 3209. doi:10.2514/6.2012-3209.

[83] Roux, É., *Turbofan and turbojet engines: database handbook*, Éditions Élodie Roux, Blagnac, 2007.

A

CPACS Data Model for Aircraft Design with Propulsion Systems

As discussed in Chapter 3, the aircraft and engine design are stored in the CPACS data model [60] to be able to employ the propulsion specific tools in a collaborative framework. In this appendix, the use of this data model is elaborated upon, in particular for the generation of engine models in GTpy.

The hierarchical architecture presented in Figure A.1 shows how the PARSIFAL aircraft including engines can be defined using the CPACS format. Firstly, an aircraft model is created (indicated with uID "PARSIFAL") which, among wings and fuselages, is built up of engines. These engines represent the installed instances of a certain engine type on the aircraft. Here the physical location of the engines is provided, as well the engine type (defined by the engineUID element) and the uID of the component to which the engine is attached, in this case the "cpacs_engine_pylon".

The engine pylons are defined separately in the aircraft model. An engine pylon element must contain the uID of the aircraft element it is connected to, here the "fuselage", but can also include specific design variables of the pylon. The inclusion of enginePylon elements clarifies that the engines are installed in a podded fashion.

On the same level as the aircraft definition, the engines element allows for different engine models to be prescribed in the CPACS structure. From the aircraft element, these engines can be accessed through their unique identifiers (here "cpacs_engine"). Each engine in the engines element is isolated from the aircraft, and hence does contain the physical location since it can be instantiated multiple times in the same aircraft. Engine specific information such as mass, take-off thrust, and engine deck maps can be stored here.

However, the current CPACS format does not provide the necessary slots to define the engine in a component-based manner, similar to the aircraft. Therefore, a toolspecific format is suggested in Figure A.2. The gtpyUID in an engine element refers to the engine definition in GTpy, as indicated by the blue arrow. Multiple engines can be defined in the GTpy element by specifying the operating points (i.e. requirements) and its components. Currently, all element types, except for the inlet, can be repeated and are therefore given unique identifiers. For each component, its performance parameters at the design point, geometry variables and its position with respect to other components has to be specified as can be seen in Figure A.3. Both required and optional inputs have to be specified through one single file.

The designer can fixate the engine cycle and thus the chain of components by enumerating the component inlet and outlet stations in the config elements. The order of the component elements in the XML file does not matter since GTpy can automatically configure the engine based on the station numbers. This feature, where the order is not important, is key in MDAO workflows where the files writers do not have to write the elements in a prescribed sequence.

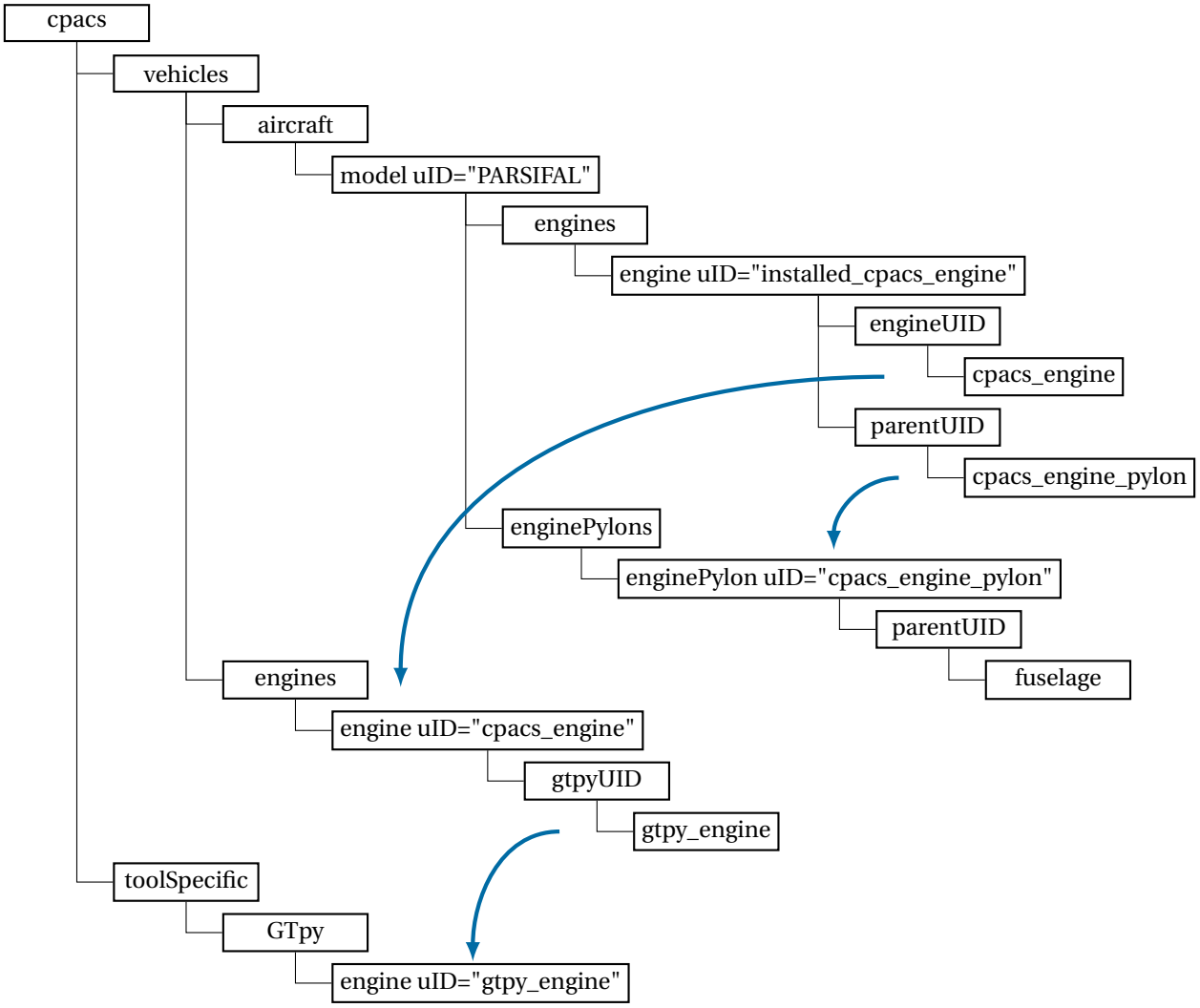

Figure A.1: Definition of an aircraft including engines in the CPACS data model. Blue arrows indicate references to other elements in the tree where the uID is used as key.

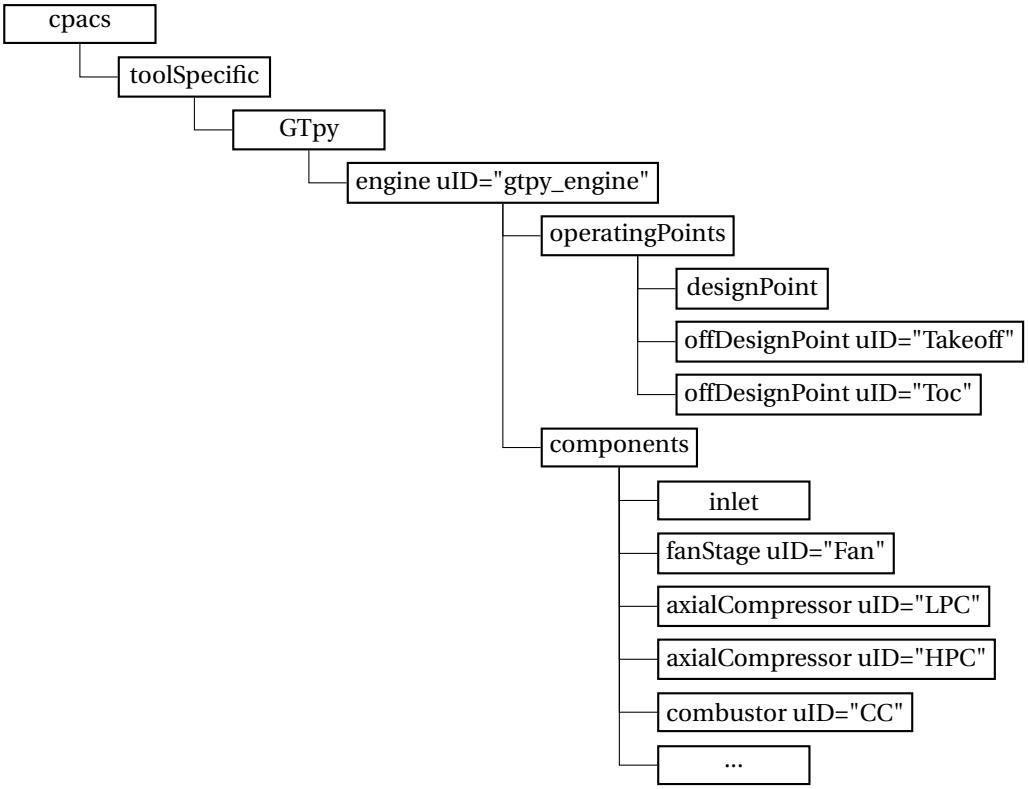

Figure A.2: Hierarchical data format implemented in the XML input file

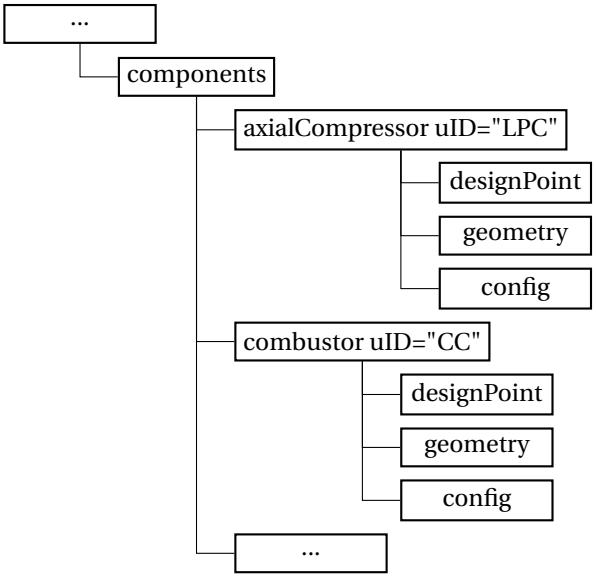

Figure A.3: XML data format of a single component in an engine definition

B

Input Data for the GE90 Validation Case

The conditions and data presented in Tables B.1 and B.2 [1] are adopted to model the General Electric GE90 engine for verification and validation purposes.

Table B.1: Design requirements assumed for the GE90 engine model

Operating Condition	**Net Thrust** [N]	**Altitude** [m]	**Mach** [-]	$\Delta T_{\mathbf{ISA}}$ [K]
Cruise	77850.0	10670.0	0.8	0.0
Take-off	376800.0	0.0	0.0	15.0

Table B.2: Design parameters assumed to model the GE90 at design point (cruise) [21, 19]

Component	**Parameter**	**Value**	**Unit**
Inlet	Total pressure loss ΔP_T	0.980	-
Fan	Bypass Ratio BPR	8.50	-
	Core total pressure ratio Π_{core}	1.58	-
	Bypass total pressure ratio Π_{bypass}	1.58	-
	Core polytropic efficiency $\eta_{\text{pol, core}}$	0.915	-
	Bypass polytropic efficiency $\eta_{\text{pol, bypass}}$	0.915	-
Low Pressure Compressor	Total pressure ratio Π	1.26	-
	Polytropic efficiency η_{pol}	0.910	-
High Pressure Compressor	Total pressure ratio Π	20.0	-
	Polytropic efficiency η_{pol}	0.900	-
Combustor	Total pressure loss ΔP_T	0.950	-
	Combustion efficiency η_{comb}	0.990	-
	Outlet temperature $T_{T,\text{out}}$	1430	K
High Pressure Turbine	Polytropic efficiency η_{pol}	0.930	-
	Mechanical efficiency η_{mech}	0.990	-
	Power Offtake	522	kW
Low Pressure Turbine	Polytropic efficiency η_{pol}	0.930	-
	Mechanical efficiency η_{mech}	0.990	-
Bypass Duct	Total pressure loss ΔP_T	0.990	-
Core Duct	Total pressure loss ΔP_T	0.990	-
Bypass Convergent Nozzle	Thrust coefficient C_x	0.986	-
Core Convergent Nozzle	Thrust coefficient C_x	0.986	-

[1] URL `https://janes.ihs.com/AeroEngines/Display/jae_0735-jae_#` [Accessed on 15 January 2019]

C

Nacelle Mesh Sensitivity Study

In addition to the validation completed in Section 6.1.3, the NASA CRM configuration with nacelles and pylons is employed to conduct a sensitivity analysis of the mesh density. Here the focus lies on the two parameters defining the mesh on the nacelle surfaces, as described in Section 6.1.2, rather than the mesh on the wings and fuselage. The latter has been studied in the research by Groot [48]. In this section the NASA CRM aircraft (WBNP) is tested at a Mach number of 0.7, an angle of attack of 3 degrees and a Reynolds number equal to five million.

To briefly rehearse, the number of nodes in the longitudinal (i.e. freestream) direction is controlled by the longitudinal pitch specified as the number of nodes per metre along the curved edges of the nacelle patches. In radial direction, the number of nodes is determined by the angle between them, measured from the engine centre line. Hence the number of radial nodes will be equal to the integer number closest to 360 divided by this radial angle.

Figures C.1 to C.4 show how the lift and moment coefficients vary with these mesh controls, both absolute and relative to the presumed most accurate prediction. Overall, it can be concluded that the longitudinal pitch has limited influence on the overall lift coefficient of the aircraft, while it may impact moment and drag coefficients. However, increasing the pitch from 15 to 20 nodes per metre increases the computational time by 13% while the improvement in accuracy is limited. Therefore, a longitudinal pitch between 10 and 15 nodes per metre is advised.

Regarding the effect of radial angle mesh control parameter, as displayed in Figures C.3 and C.4, it can be deduced that this parameter appears to have a small effect on the summary of forces and moments. Nevertheless, the cylindrical shape of the nacelle still has to be captured, and therefore it is not recommended to increase the angle above 30 degrees. Note that in Figures C.3 and C.4 a smaller radial angle leads a to a finer mesh with more panels.

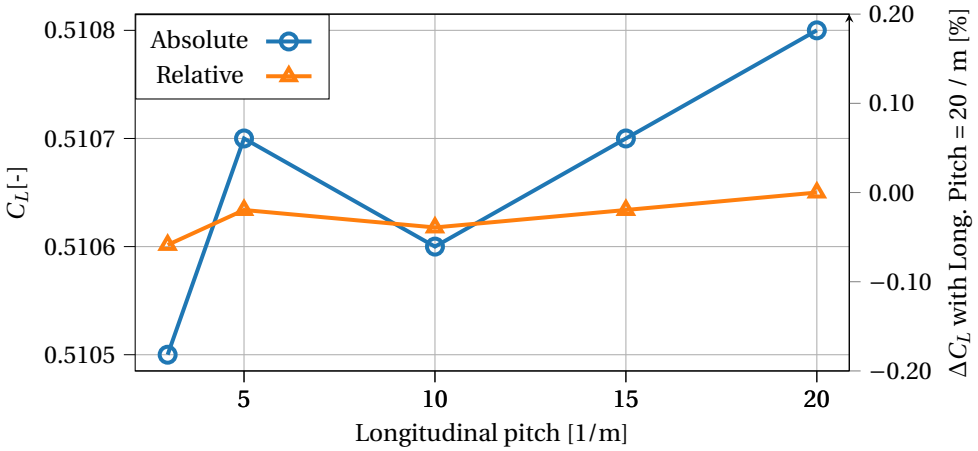

Figure C.1: Variation in lift coefficient with longitudinal pitch control

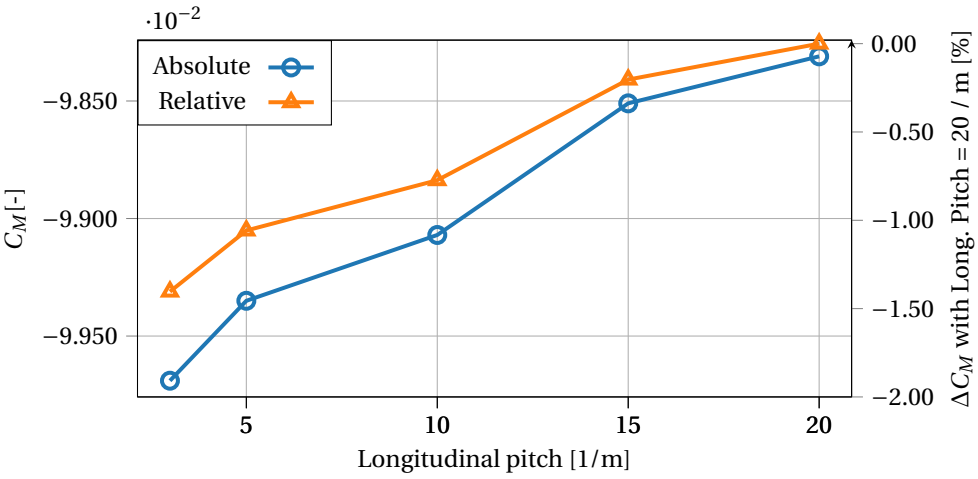

Figure C.2: Variation in moment coefficient with longitudinal pitch control

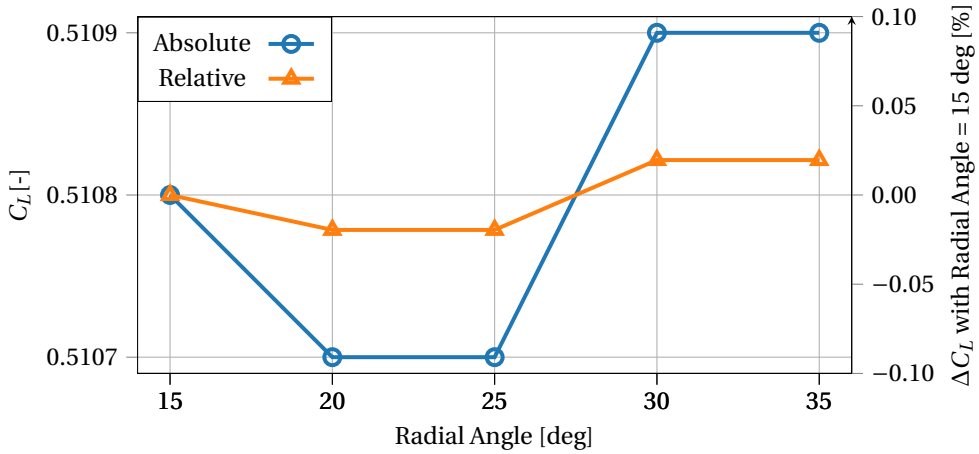

Figure C.3: Variation in lift coefficient with radial angle control

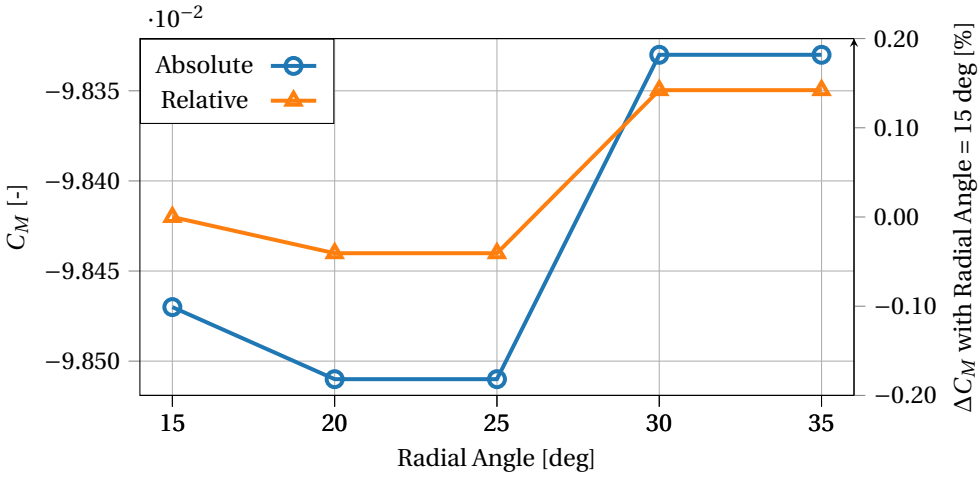

Figure C.4: Variation in moment coefficient with radial angle control

D

PARSIFAL MS1 Configuration

This appendix presents the PARSIFAL MS1 configuration which is employed in the analysis work in Chapters 7 and 8. The locations of the engines shown here are the ones proposed for the PARSIFAL project. Figures D.2 to D.4 present the major dimensions of the aircraft in its current configuration. The aircraft is characterised by a fuselage cross-section similar to an oval and two vertical tails, on which the rear wing is placed. The front and rear wings are joined by connecting elements. On these elements the suction side from the rear wing becomes the pressure side on the front wing, and thus the camber reverses on these side wings to obtain butterfly-like lift distribution.

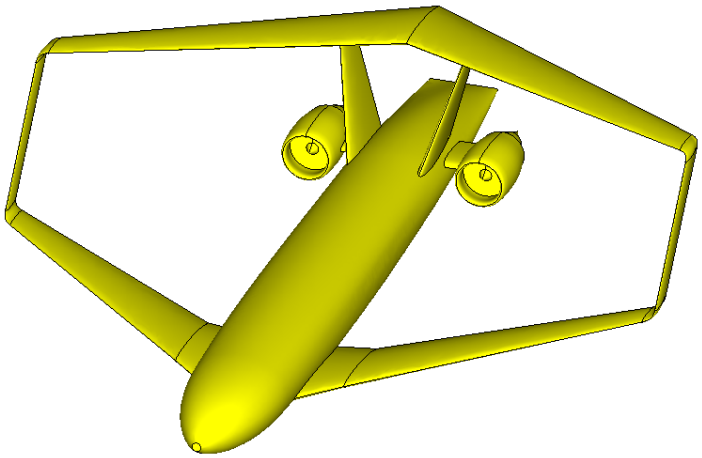

Figure D.1: Isometric view of the MS1 configuration

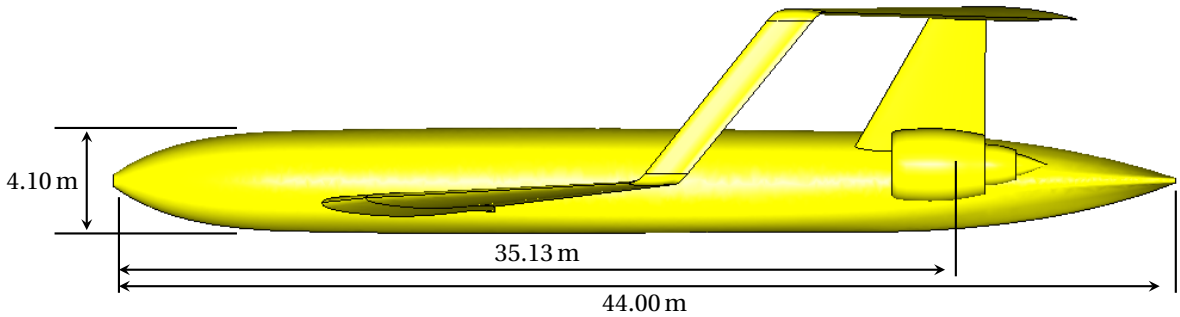

Figure D.2: Port side view of the MS1 configuration

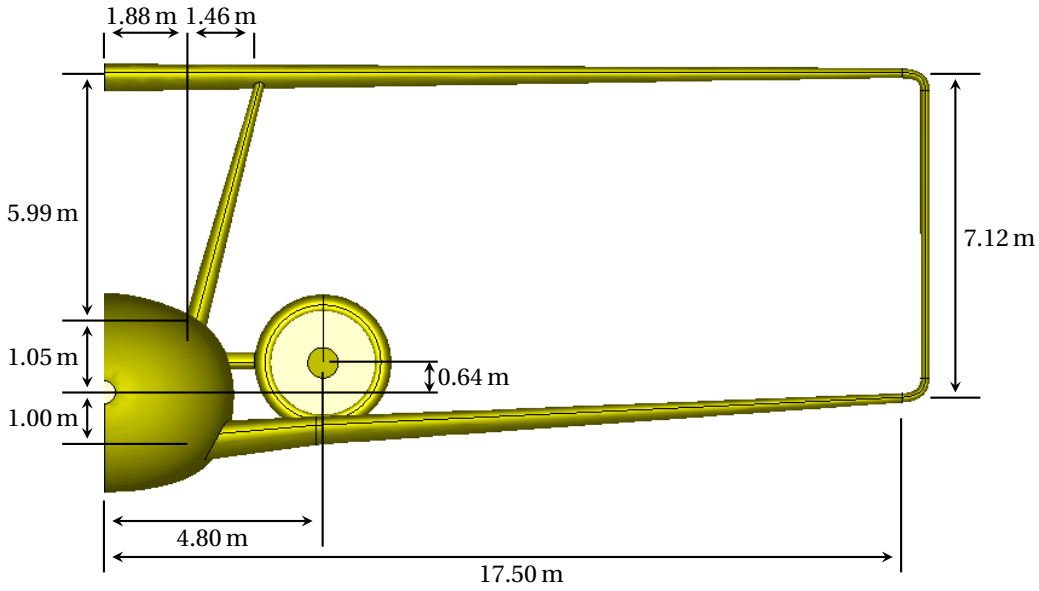

Figure D.3: Front view of the MS1 configuration

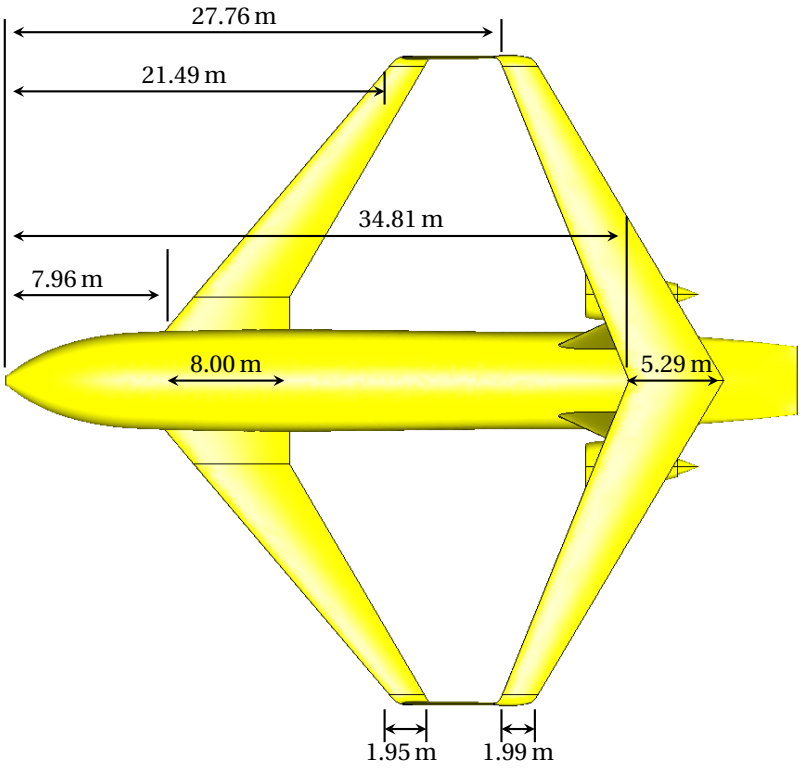

Figure D.4: Top view of the MS1 configuration